

DATE ISSUED APR 14 1984

ORNL/Sub-7676/4

ORIGINAL  
MASTER COPY

RESEARCH SUPPORT FOR PLASMA DIAGNOSTICS  
ON ELMO BUMPY TORUS-

DEVELOPMENT OF A MULTICHANNEL HALL-PROBE  
BASED DIAMAGNETIC DIAGNOSTIC INSTRUMENT  
AND OBSERVATION AND MODELING  
OF EBT ELECTRON RINGS

Kenneth H. Carpenter  
and  
Robert H. Booker

October 1983

 *Department of*  
**ELECTRICAL ENGINEERING**  
ELECTROMAGNETICS



---

**University of Missouri-Rolla**

---

Printed in the United States of America  
Available from  
National Technical Information Service  
U.S. Department of Commerce  
5285 Port Royal Road  
Springfield, Virginia 22161  
NTIS Price Codes: Printed Copy: A06; Microfiche: A01

This report was prepared as an account of work sponsored by the United States Government. Neither the United States nor the Department of Energy nor any of their employees, nor any of their contractors, subcontractors, or their employees, makes any warranty, express or implied, or assumes any legal liability or responsibility for the accuracy, completeness or usefulness of any information, apparatus, product or process disclosed, or represents that its use would not infringe privately owned rights.

RESEARCH SUPPORT FOR PLASMA DIAGNOSTICS  
ON ELMO BUMPY TORUS -  
DEVELOPMENT OF A MULTICHANNEL HALL-PROBE  
BASED DIAMAGNETIC DIAGNOSTIC INSTRUMENT  
AND OBSERVATION AND MODELING  
OF EBT ELECTRON RINGS

by

Kenneth H. Carpenter

and

Robert H. Booker

Department of Electrical Engineering  
University of Missouri-Rolla  
Rolla, Missouri 65401

October 1983

Report prepared by University of Missouri - Rolla  
under subcontract number 7676/X01

for

OAK RIDGE NATIONAL LABORATORY  
Oak Ridge, Tennessee 37830

operated by  
UNION CARBIDE CORPORATION  
for the

US DEPARTMENT OF ENERGY  
Contract No. W-7405-eng-26

## ABSTRACT

Use of multiple Hall effect probes is a cost effective way to observe diamagnetic fields from the hot electron rings in the Elmo Bumpy Torus device at several locations simultaneously. A special diagnostic instrument has been developed having six Hall probe channels with the sensitivity and stability needed for the diamagnetic measurements. The instrument uses an AC carrier system with isolation transformers located remotely from the instrument and near the probe locations. Details of instrument design as well as operating instructions for it are included in this report.

Diamagnetic data taken with the Hall probe instrument has confirmed earlier data with regard to electron ring centering in the EBT cavities, but anomalies have been observed with regard to the rings' radial extents.

The computer code implementing the current sheet model used for electron ring diamagnetic data analysis has been generalized to allow surface current densities to vary along the toroidal extent of the model ring. A derivation has been carried out to show that the approach to drift current effects used in the current sheet model is consistent with tensor pressure MHD models.

The ferromagnetic resonance (YIG) magnetometer, which was used earlier to observe electron ring diamagnetic fields, has been evaluated for ability to measure small fluctuations in large magnetic fields. Such use is limited to frequencies of fluctuations less than the resonant line width of the YIG crystal in the field probe; typically up to 3 MHz fluctuations can be observed.

## FORWARD

This report covers the work performed during the period October 1, 1982, to September 30, 1983, under Basic Agreement No. 7676, Project Authorization No. X01, a subcontract from Union Carbide Corporation to the University of Missouri. This is the final report under this Project Authorization for this time period. The work was performed by the Principal Investigator, Dr. Kenneth H. Carpenter, with assistance from Mr. Robert H. Booker. Dr. Carpenter is a Professor in the Department of Electrical Engineering of the University of Missouri - Rolla, and Mr. Booker was a Graduate Research Assistant in that department.

## ACKNOWLEDGEMENTS

The authors wish to thank the members of the EBT Experimental Group of the Fusion Energy Division of Oak Ridge National Laboratory for their guidance, assistance, and hospitality during the carrying out of the research described in this report.

## TABLE OF CONTENTS

	PAGE
ABSTRACT. . . . .	ii
FORWARD . . . . .	iii
ACKNOWLEDGEMENTS. . . . .	iv
I. INTRODUCTION. . . . .	1
II. DIAMAGNETIC DIAGNOSTIC INSTRUMENT DEVELOPMENT . . . . .	3
Preliminary tests of Hall effect probes on EBT. . . . .	3
Development of the UMR Hall Effect Diamagnetic Diagnostic Instrument . . . . .	4
III. EBT RING DIAMAGNETIC DIAGNOSTIC DATA. . . . .	7
Data acquisition and reduction methods. . . . .	7
Analysis of diamagnetic data taken in March 1983. . . . .	9
Analysis of diamagnetic data taken in July 1983 . . . . .	12
Analysis of diamagnetic data taken in August 1983 . . . . .	14
IV. FURTHER STUDIES IN RING MODELING. . . . .	19
Equivalence of diamagnetic currents of a plasma as derived from single particle kinetics and MHD tensor pressure . . . . .	19
Generalized computer simulation for a current sheet model . . . . .	23
Correction to values calculated for ring center offset. . . . .	24
Limitations of diamagnetic measurements . . . . .	24
V. USE OF A FERROMAGNETIC RESONANCE MAGNETOMETER FOR OBSERVATION OF HIGH FREQUENCY FIELD FLUCTUATIONS. . . . .	26
REFERENCES. . . . .	27

	PAGE
APPENDIX A. UMR Hall Effect Diamagnetic Diagnostic Instrument Reference Manual and Operating Instructions. . . . .	29
APPENDIX B. FORTRAN Sources for FWP and FPR Data Analysis. . . . .	51
APPENDIX C. FORTRAN Source Codes for EBT Ring Current Sheet Models . . . . .	58
APPENDIX D. Corrected Pages for ORNL/Sub-7676/3. . . . .	82
APPENDIX E. Abstract from Master's Thesis. . . . .	92
APPENDIX F. Abstracts of Papers Presented at 1982 APS-DPP Meeting. . . . .	93

RESEARCH SUPPORT FOR PLASMA DIAGNOSTICS ON ELMO BUMPY TORUS -  
DEVELOPMENT OF A MULTICHANNEL HALL-PROBE BASED DIAMAGNETIC DIAGNOSTIC  
INSTRUMENT AND OBSERVATION AND MODELING OF EBT ELECTRON RINGS

## I. INTRODUCTION

Characterization of the hot electron rings and the correlation of ring parameters with other plasma parameters is one of the significant areas of investigation for the EBT experiment. Diamagnetic diagnostics for the rings has a limited but important roll in this investigation. We have been developing diagnostic instrumentation and ring models to be used in this effort. Our work prior to October 1982 has been reported previously.<sup>1,2,3</sup> This report presents the results of our efforts during the 1983 (federal) fiscal year.

During the past year our work has included several separate areas related to ring diagnostics. A major portion of the effort was spent on evaluating Hall probes as a diagnostic for ring magnetic fields and then developing and testing a multichannel, Hall probe based, ring diagnostic instrument. Along with the testing of the Hall probe instrument a sizeable amount of data was taken for EBT rings, and the appropriate interfacing to the EBT computer data acquisition system was obtained and the necessary software developed for data reduction. Section II; below, describes the Hall probe instrument development while the detailed operation instructions and circuit schematics are given in Appendix A. Reduced data from the test of the Hall probe instrument are given and discussed in Section III, and data reduction program listings are given in Appendix B.

The current sheet model<sup>4</sup> has been used extensively for data analysis. Further insights into it have been gained by calculations showing the drift current effect utilized is in agreement with MHD theory. This is discussed in Section IV. A more general ring simulation computer program has been written, and a listing of it is given in Appendix C. An error in algebraic sign on one term in an earlier ring simulation subroutine caused several values reported in our

1982 report<sup>3</sup> to be in error. We have produced corrected pages for this report and they are given in Appendix D.

The work done in previous years on the YIG magnetometer<sup>2,3</sup> has been extended to include measurement of high frequency (up to 3 MHz) magnetic field fluctuations. The results are described in Section V and the abstract of a Master's thesis<sup>5</sup> written on this topic is given in Appendix E.

Finally, abstracts of papers based on work under subcontract and presented at the 1982 Annual Meeting of the APS Division of Plasma Physics are given in Appendix F.

This work has brought the diamagnetic diagnostic tools and theory to the point where they can be used in correlation with other diagnostics to build a description of EBT ring structure. This will be the goal of our efforts in the following year.

## II. DIAMAGNETIC DIAGNOSTIC INSTRUMENT DEVELOPMENT

After making a number of observations of EBT ring diamagnetic fields using the YIG magnetometer, it became apparent that it would be necessary to measure diamagnetic fields at several points simultaneously in order to obtain the desired information.<sup>6</sup> Thus a study was undertaken to find a simple, reliable, cost effective way to make multiple field measurements. The YIG magnetometer had proven reliable and had the advantage of an inherent self calibration. However, it is a complex and expensive instrument that could not be expanded to multiple channels without considerable development effort and/or capital cost. Single pickup loops with flux integrators are straightforward, but have sensitivity and noise problems, as encountered in earlier use,<sup>7</sup> and they only provide field averages over relatively large volumes. Hall effect probes appeared attractive, but there were concerns over their stability and performance in the EBT environment. A preliminary test of a single Hall probe on EBT gave good results, indicating that a satisfactory multichannel instrument could be developed. Thus such an instrument was designed, constructed, and tested - the details are given in the following.

### Preliminary tests of Hall effect probes on EBT

A preliminary test of a Hall effect probe in measuring EBT ring diamagnetic fields was made by using an F. W. Bell model 620 Hall Effect Gaussmeter with a model HFT-6000C25 transverse probe. This probe - Gaussmeter combination is "precalibrated" to a higher precision than the standard reference magnets. For added precision, the output signal was read on a HP3490A digital voltmeter instead of using the meter on the Bell 620. Bench tests showed stability to 0.05 Gauss in both a 1 KG reference magnet and in a zero Gauss chamber for time periods of several minutes. This is quite adequate for observation of diamagnetic signals on plasma turn-downs.

The Hall probe was mounted on the midplane access port cover outside (large major radius) of EBT cavity E3 with 1/4 inch of styrofoam

between the EBT wall and the probe for thermal insulation. A battery - potentiometer combination was placed in series with the output signal from the F. W. Bell model 620, which was located in the EBT control room (the 50 ft leads to the Hall probe passing through the lead wall via the observation port). The potentiometer was adjusted to null out the signal due to the average magnetic field and the resulting incremental signal was observed on a Soltec strip chart recorder set for 10 mV full scale (corresponding to 10 Gauss). With EBT in operation a slow drift was observed in the Hall signal which stabilized after about 30 minutes. This was apparently due to the change in temperature of the probe environment. The total field reading of 689 to 685 Gauss at this probe location was reasonable for the 7250 A generator currents used. A noise level of about 0.1 G peak to peak was observed, presumably due to generator current fluctuations (although generator fluctuations have been observed at significantly higher levels on other occasions). A ring diamagnetic field of 1.68 G was easily observed on a plasma turn-down. The styrofoam insulation lengthened the thermal time constant sufficiently that no thermal problems interfered with the before - after field observations on plasma turn-down, although a slow drift occurred when the plasma was changed.

This preliminary test indicated that a Hall probe ring diagnostic could be successfully operated on EBT. Thus development of a multichannel instrument was undertaken.

#### Development of the UMR Hall Effect Diamagnetic Diagnostic Instrument

To observe all possible ring symmetries one would have to observe the diamagnetic field at six points (top-bottom, front-back, left-right). Also, six simultaneous field measurements appeared to be adequate for studies of field versus toroidal length or other linear array applications. Hence it was decided to construct a six channel Hall effect incremental Gaussmeter. In addition, to allow for (off line - not real time) generator fluctuation compensation it was decided to include generator current fluctuation amplifiers in the same chassis. This instrument was designed, built, and tested at UMR during the winter

of 1983 and then tested at EBT and further improved and tested, culminating in the instrument installed at EBT for permanent use in August 1983.

The Hall instrument design had to meet a number of criteria. The instrument requires accurate output signals with a resolution of 0.01 G or better, and calibration capabilities for different probes to yield six identical channels. Long cable runs to the probes are required. Long term stability and low noise performance are needed at relatively low cost per channel. After considering a DC amplifier design using chopper stabilized operational amplifiers it was determined that an AC carrier system would be required to give the required stability and noise performance. With the AC system, remote transformer coupling was chosen to allow the long cable runs from the instrument to EBT to be done with conventional coaxial lines rather than special (expensive) Hall probe extension cables. F. W. Bell flexible axial Hall probes were chosen for use with this system over custom made probes for sake of convenience, repeatability, and ease of testing. Details of the circuit design of the six channel instrument and the rationale behind it are given in the instrument Reference Manual, which is included in Appendix A to this report.

The four generator fluctuation compensation amplifiers would not have been needed if the data acquisition system included 16 bit analog to digital converters with 0.1 second conversion time. However, the converters available with sufficiently high sampling rates could only achieve 12 bit precision. Since the fluctuations that produce errors in the diamagnetic signal are on the order of 0.1 to 10 A out of 7250 A, 12 bit resolution (1 out of 4096) is not enough. For each generator shunt signal a gain of 20 was provided along with an adjustable DC offset voltage to null the average signal. The resulting incremental generator current signals could then be sampled at the same time as the Hall probe incremental signals and a compensation made for the generator current fluctuations in the data reduction process.

Appendix A contains the operating instructions and the reference

manual for the instrument, and these should be studied before using the instrument if optimum results are to be obtained.

### III. EBT RING DIAMAGNETIC DIAGNOSTIC DATA

In the process of testing the Hall effect Gaussmeter instrumentation we have observed the EBT ring diamagnetic fields (and fluxes, using the standard flux pickup loops) for a number of plasma conditions in three separate time periods. The first data taking was done in March, 1983, with subsequent sessions in July and August. Primary data was recorded on strip charts in each case, along with simultaneous digital data acquisition using the 32 channel LeCroy CAMAC data loggers (the "FWP and "FPR" diagnostics in the EBT data base). New digital data analysis computer programs were required, and these are described in the following. Interpretation of the data by means of the current sheet model led to some surprising results for each of the sessions; however, lack of repeatability leaves open the question of their real significance. These will be discussed in the following for each data taking session in turn.

#### Data acquisition and reduction methods

Digital data acquisition was accomplished for each experimental session by using the CAMAC LeCroy data loggers. The software to acquire the data from the CAMAC system into the EBT data base was written by Brian Peterson.<sup>8</sup> The diagnostic designations in the data base are "FWP" and "FPR" which refer to "fast perpendicular energy" and "fast pressure", respectively. The "fast" adjective is due to the ability to sample data from a 10 Hz to several kilohertz rate in contrast to the 1 to 10 Hz rate for the other "machine condition" diagnostics. For the Hall effect instrumentation tests, 1024 point samples were taken at a rate of 20 Hz, which provided ample time to observe a plasma ring turn-down along with a sufficient sample rate for the signal bandwidth. While FWP and FPR programs were primarily intended to sample the corresponding 24 EBT cavity values, each data logger has 32 channels so the unused channels were available for the Hall probe signals and the generator fluctuation signals.

Data acquisition for the Hall probes was somewhat different for the three sessions. During the March experimental data taking only four Hall probes were available, so the Hall signals and the four generator fluctuation signals from the UMR Hall Effect Diamagnetic Diagnostic instrument were placed in channels 25-32 of the FWP diagnostic, and the FPR diagnostic was not used. The data acquisition program was run on a PDP-11/34 computer, and transfer time from CAMAC to the data base was excessive. During the July runs the data acquisition was the same as for March, but the data base access software on the PDP-10 had been changed. In August, six Hall probes were used so the six Hall probe signals were acquired in channels 27-32 of FWP while the generator fluctuation signals were acquired in channels 29-32 of FPR. In addition, the data acquisition program was now run on the VAX-11/780 computer, which reduced waiting time between plasma turn-downs significantly.

The data taking procedure was the same in all cases. First the Hall instrument was connected and calibrated with probes in place. With the probes installed on EBT, files were taken into the data acquisition system as each of the four generators was separately incremented by 10 to 50 A (with no plasma present). This provides the calibration needed to eliminate the effects of generator fluctuations in the Hall probe signals placed in the data base for plasma turn-downs. Then for each plasma condition studied a controlled increase in pressure from the initial value to a C-mode value ( $\approx 20 \times 10^{-6} \text{T}$ ) was made over a time interval of around 10 seconds. The data loggers were triggered near the beginning of the pressure increase with approximately 20 S of both pre- and post trigger data acquired. This provides for averaging the sampled data over "before" and "after" ring turn-down by the data analysis programs.

Data analysis was made in each case by examining the strip chart recorded Hall probe signals. Programs were then written to access the EBT data base, average "before" and "after" signals and take their differences, and then write out files containing these diamagnetic

signals (and generator shunt signals) for further analysis. This preliminary digital data reduction program had to be rewritten for each data taking session due to changes in the data base and the way the data was acquired. The most recent version is capable of examining data from all three sessions. A listing of the FORTRAN for this program, titled FWPDWN, is given in Appendix B.

#### Analysis of diamagnetic data taken in March 1983

Data taken during March, 1983, using the UMR Hall Effect Diamagnetic Diagnostic instrument was difficult to interpret for two reasons. First, the probes were placed on EBT cavity E3, which is in a diamagnetically unsymmetrical environment due to cavity E2 having no 28 GHz power. Second, at this first major test of the instrument, only one flexible axial Hall probe was available, so the other three Hall probes used were two types of transverse probe and one rigid axial probe. While every effort was made to calibrate these different probes accurately, they undoubtedly had different temperature coefficients, and the axial and transverse reference magnets could not be compared for relative accuracy.

Data acquired for "baseline" EBT-S operation - 100 KW @ 28 GHz for ion gauge pressures from 4 to 15 x 10<sup>-6</sup>T with error field compensation currents optimally adjusted - were given exhaustive study, both from the strip charts and the EBT digital data base. Resulting values of Hall signal, converted to Gauss and corrected for generator current fluctuations, are shown plotted versus the flux loop signals for cavity E3 and versus the S4 ion gauge pressure in Figs. 1 and 2.

The plots of Hall probe signals versus flux loop signals are qualitatively similar to those obtained for YIG magnetometer signals versus flux loop signals. However, the four Hall probe field measurements were obtained simultaneously for each plasma turn-down while only one YIG field measurement could be made for each turn-down. The Hall probe signals are approximately linear with flux loop signal for smaller signals (which implies constant ring geometry), while the

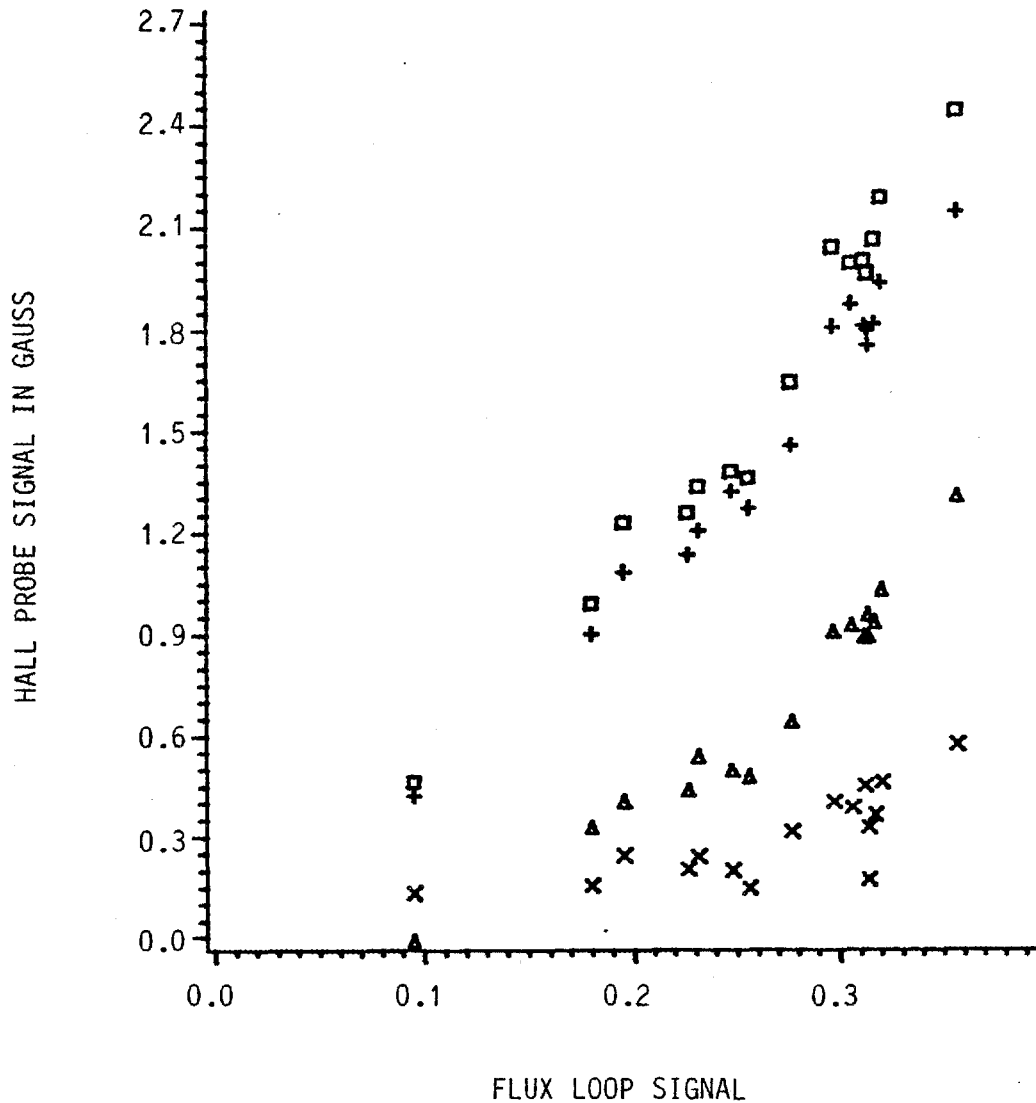


Fig. 1. Diamagnetic data for EBT-S electron rings obtained during March 1983 testing of UMR Hall Effect Diamagnetic Diagnostic instrument. Hall probe signals are shown versus flux pickup loop (perpendicular energy) signals for Hall probes mounted on cavity E3 at cavity center in the large major radius position (triangles), in small major radius position (squares), at the top of the cavity (pluses), and at a position 9 cm left of center at the major radius position (X's). Data points correspond to plasma turn-downs made by increasing pressure to a C-mode value starting with stable T-mode conditions for different cold gas ion gauge pressures. Other conditions are for nominal T-mode operation of 100 KW, 18 GHz heating and 7250 A generator currents.

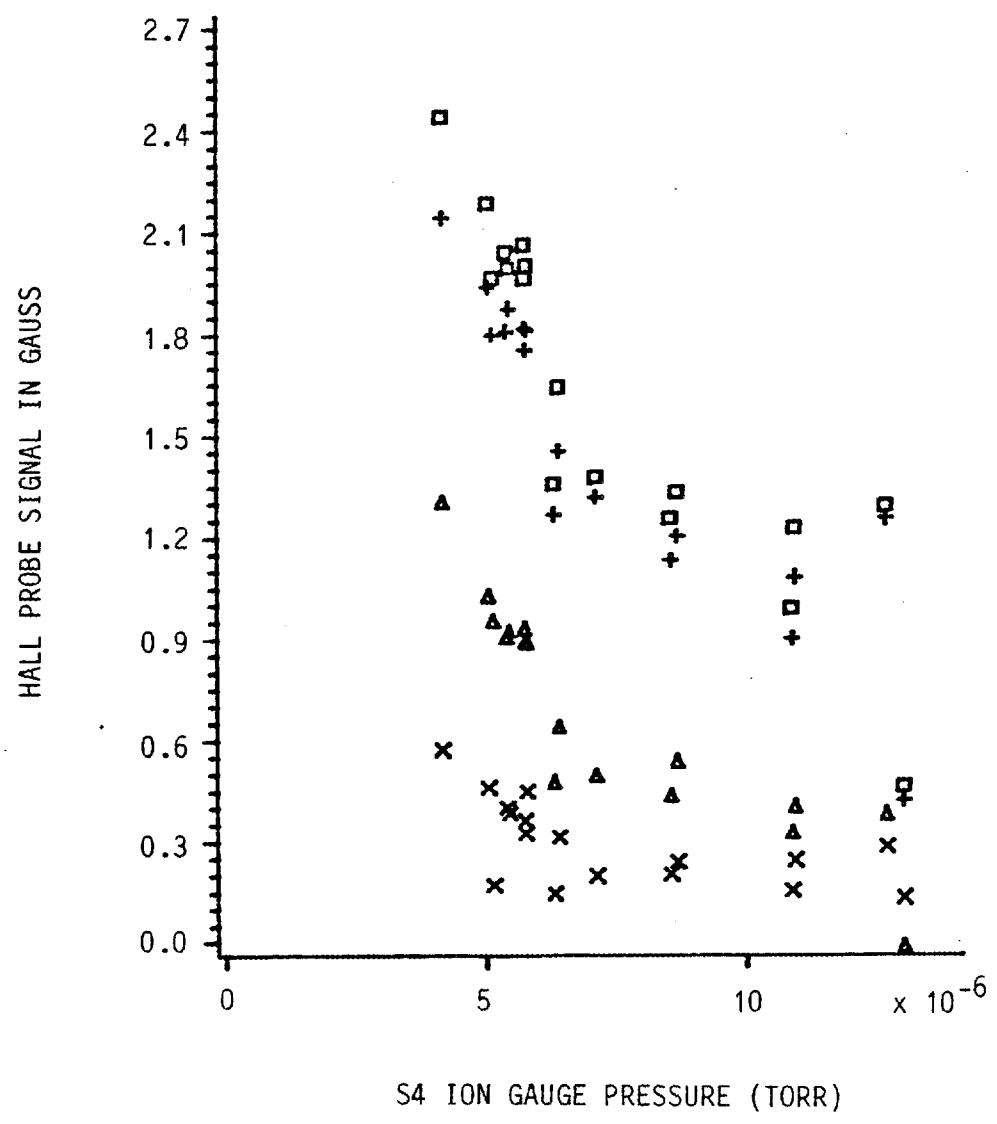


Fig. 2. Same data as Fig. 1, but plotted versus cavity S4 ion gauge pressure.

Hall signals rise faster than the flux loop signals for large signals.

The plots of Hall probe signals versus pressure show the typical T-mode shape. Note that the data points corresponding to a pressure of  $12.7 \times 10^{-6} \text{T}$  are for 145 KW 28 GHz power rather than 100 KW which was the nominal power for all the other points. (The 28 GHz power on March 16 was pulsed at low duty cycle on top of the 100 KW base power level for a net average power of approximately 112 KW. Data points made March 17 were for CW conditions. There are no apparent differences in diamagnetic data from the two days.)

The plots of field ratios versus pressure, shown in Fig. 3, are the ones raising the questions. The ratio of the field at the small major radius position to that at the large major radius position was found to be in the range 1.2 to 1.4 for the data from the YIG magnetometer taken during plasma turn-downs made in March and May 1982.<sup>9</sup> This ratio can be understood in terms of an axisymmetric ring model having the rings' centers displaced slightly towards the small major radius position from the cavity center. The current sheet model for the rings predicts the field at the top edge of the cavity to be approximately the mean of the values at small and large major radius positions ("inside" and "outside"). This holds true even if there is no ring in one of the neighboring cavities. The value of 1.1 for the inside/top field ratio observed with the Hall probes (and shown on the plot) is thus in good agreement with the YIG magnetometer data (which was obtained with the YIG probes on cavities W5 and W4). However, an axisymmetric ring with 1.1 for the inside/top field ratio should give a value of 1.2 for inside/outside field ratio, not the range of 2 to 3 that was observed with the Hall probes. We cannot account for this in terms of instrumentation error, even though a different type of probe was used in the large major radius position. To explain these ratios one would need a non-symmetrical ring in cavity E3 under 28 GHz excitation. However, we were unable to duplicate this observation of high inside to outside field ratios during the July measurements, so there most likely was an undetected instrumentation error during March for the channel measuring the field at the large major radius position.

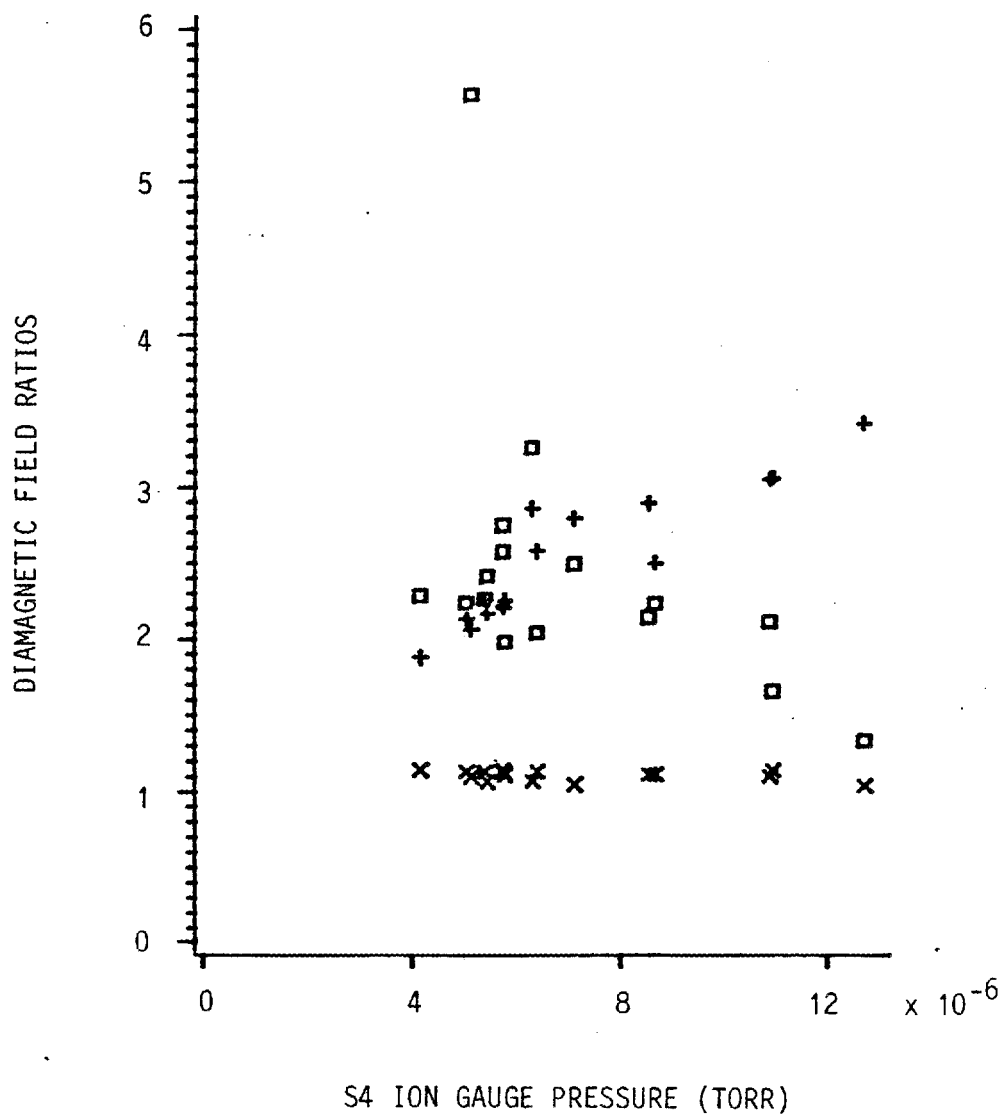


Fig. 3. Diamagnetic data of Fig. 2 displayed as ratios of Hall probe signals. Pluses are for ratios of field at cavity center and small major radius position to field at large major radius. Squares are for ratios of field at cavity center and large major radius to fields 9 cm left of center. X's are for ratios of field on center at small major radius position to field at top of cavity.

Analysis of diamagnetic data taken in July 1983

The July experimental sessions using the UMR Hall Effect Diamagnetic Diagnostic instrument led to no new insights into the EBT rings, but did clear up questions raised earlier and provided answers to some questions concerning the instrumentation itself. Diamagnetic data was obtained with Hall probes mounted on EBT cavity E3 in both EBT-I and EBT-S modes of operation. The Hall probes were then moved to cavity W4 and data taken with and without ICRH power applied in W3. The data has not yet received the exhaustive, automated analysis given to that taken in March, but strip chart and digital data have been examined to establish the results needed for further development.

During the July measurements the same four Hall probes were used as in March but their locations were changed to allow checks for possible errors due to different probe characteristics. In order to separate the effects of radiation and conductive heating on the probes, the flexible axial probe was placed inside a 1/4 inch cylindrical lead shield, the rigid axial probe was placed inside 1/4 inch of styrofoam insulation, and these two were mounted to read equivalent fields - just to the right and left of center at the large major radius midplane access port surface on cavity E3. When operating with around 40 KW @ 18 GHz in EBT-I mode (5000 A generator current) the strip chart signals from these two probes were practically identical - the amplitude of variation from the flexible probe being about 5% greater - corresponding closely to the difference in calibration of the two signals in terms of magnetic field. When 100 KW @ 28 GHz, EBT-S mode was employed the two probe signals still tracked each other nearly identically. However, thermal drift over long time intervals was different with the probe in the lead shield drifting more rapidly. (For example, at one point in time the drift on the probe in the lead shield was twice that of the one in styrofoam for a time interval of approximately 3.5 minutes.) Thus it was concluded that the lead shield provided no advantage and all subsequent probe mountings were insulated with styrofoam from the EBT cavity wall.

In March, the x10 transverse probe had been placed in the location having the two axial probes in July. The signals from the probe at the large major radius position in March had appeared unusually low, leading to the speculation of a non-symmetrical ring due to the non-symmetrical environment in E3. In July this speculation was tested by, first, independently turning off 18 GHz power to E3 and E2. The results were signals that had nearly the same ratios of small major radius fields increment to that at large major radius for all combinations of power to E2 and E3. The ratio for all power off together was 1.33, for power to E3 off with E2 left on was 1.33, and for power to E3 off with power to E2 off earlier was 1.53. Second, a repetition of the March cases for EBT-S operation (no 28 GHz power to E2) yielded corresponding ratios of 1.37 and 1.33 for typical high energy ring turn-downs. Thus we concluded that the values of 2 to 3 obtained for this ratio in March were due to a problem with the data from the x10 probe, which was at the large major radius position in March.

The conclusion that the x10 probe data was in error in March was supported by the fact that the x10 probe gave difficulty in July also. It gave a noisy signal at all times, and gave readings significantly lower than a x1 axial probe placed at the same location simultaneously (when the probes were transferred to cavity W4). These lower signal values were obtained during EBT operation even with the calibration with the reference magnet taken into account. The suspected problem in the instrumentation was a high resistive section or connection in one of the cables and/or a noisy IC amplifier. The system was corrected for the August data taking session, and the x10 probe was no longer used but a set of (as nearly as possible) identical, flexible, axial probes was used instead.

The observations of diamagnetic fields on W4 with ICRH turned off and on in W3 yielded data qualitatively similar to that produced by ring turn-downs from pressure increases for EBT-S operation. In EBT-I operation the field signals had an overshoot and the flux signal decreased while field signals increased. This behavior corresponded to what had been seen before with regard to flux loop signals about the

torus with ICRH in one cavity. (The raw data for this case is in files A0090.FWP through A0092.FWP in the EBT data base for anyone wishing to examine it in detail.) Note, however, that 18 KW ICRH was being fed to W3 while only 44 KW of 18 GHz fed the entire torus. This undoubtedly led to the ring in W3 being much different than in W4 or W5, and hence the incremental changes in diamagnetic fields in W4 due to ring changes in W3 would not be expected to look like those from a ring turn-down in all cavities.

#### Analysis of diamagnetic data taken in August 1983

The data taking session carried out in August 1983 using the UMR Hall Effect Diamagnetic Diagnostic instrument provided the most complete set of data for ring symmetries for typical EBT-S conditions to that date. While the symmetries were as seen in earlier data, the data from off center probes did not agree with simple current sheet model predictions. These results are discussed below.

All six channels of the instrument were equipped with Hall probes, which were mounted on small and large major radius positions in the central midplane on cavity W4, on the top-center of W4, on left and right of center at large major radius (front) of W4, and on the top of W6 (for cavity to cavity comparison). In addition, the left of center probe was also moved to W3 for experiments with ICRH power to W3. Five of the probes were flexible axial type while one was rigid axial. All were of nearly equal sensitivity and calibrated in the same axial reference magnet. (The reference magnet used suffered from poor repeatability of readings on multiple probe insertions, however, which limits relative calibration accuracy to several percent.) All were thermal shielded from the EBT cavity with styrofoam. The Hall probe signals were placed in channels 27-32 of the "FWP" diagnostic while the generator current fluctuation signals were placed in channels 29-32 of "FPR". The six Hall probe signals were also monitored using a strip chart recorder, and data analysis done to date has used the strip charts. (Computer analysis, when implemented, will allow correction for generator current fluctuations - but these did not appear severe during

the August data taking. Hall probe signals were quite low noise.) For these conditions ratios were formed from the Hall probe signals for comparison to values from the current sheet model. Three of these ratios are shown in Fig. 4 versus ion gauge pressure. We note from the figure that there is little variation of the ratios with pressure. Mean values of the ratios employing pressures of  $5$  to  $9 \times 10^{-6}$ T are:

ratio of field at small major radius position to field at large major radius position in central midplane

$$1.3 \pm 0.1$$

ratio of field at small major radius to field at top of cavity

$$1.06 \pm 0.03$$

ratio of field at 9.5 cm right or left of cavity center (in horizontal midplane at large major radius position)

$$-0.12 \pm 0.04$$

(Note: the  $\pm$  uncertainties only include the scatter of the data with pressure. They do not include calibration or other systematic errors.)

The 1.3 value for back to front field ratio agrees with data taken a year earlier using the YIG magnetometer<sup>3</sup> as well as with some of the earlier Hall probe results. It is consistent with the current sheet model and a plasma offset toward the torus center from the geometrical center of the cavity - as also predicted from single particle drift surfaces in the vacuum magnetic field.

The ratio of 1.06 of back to top field values is somewhat low compared to the current sheet model which would yield a value near 1.15 for a back to front ratio of 1.3. This is not a large discrepancy, however, considering the relative calibration uncertainties between probes.

The ratio of fields 9.5 cm off center to the central field presents a problem. From the data, these off center probes, which measure only single field components - approximately the toroidal ones, were obviously placed near the point where the field becomes purely radial. However, the current sheet model, using the usual assumptions for ring radius and thickness, will not give 9.5 cm as the location for the

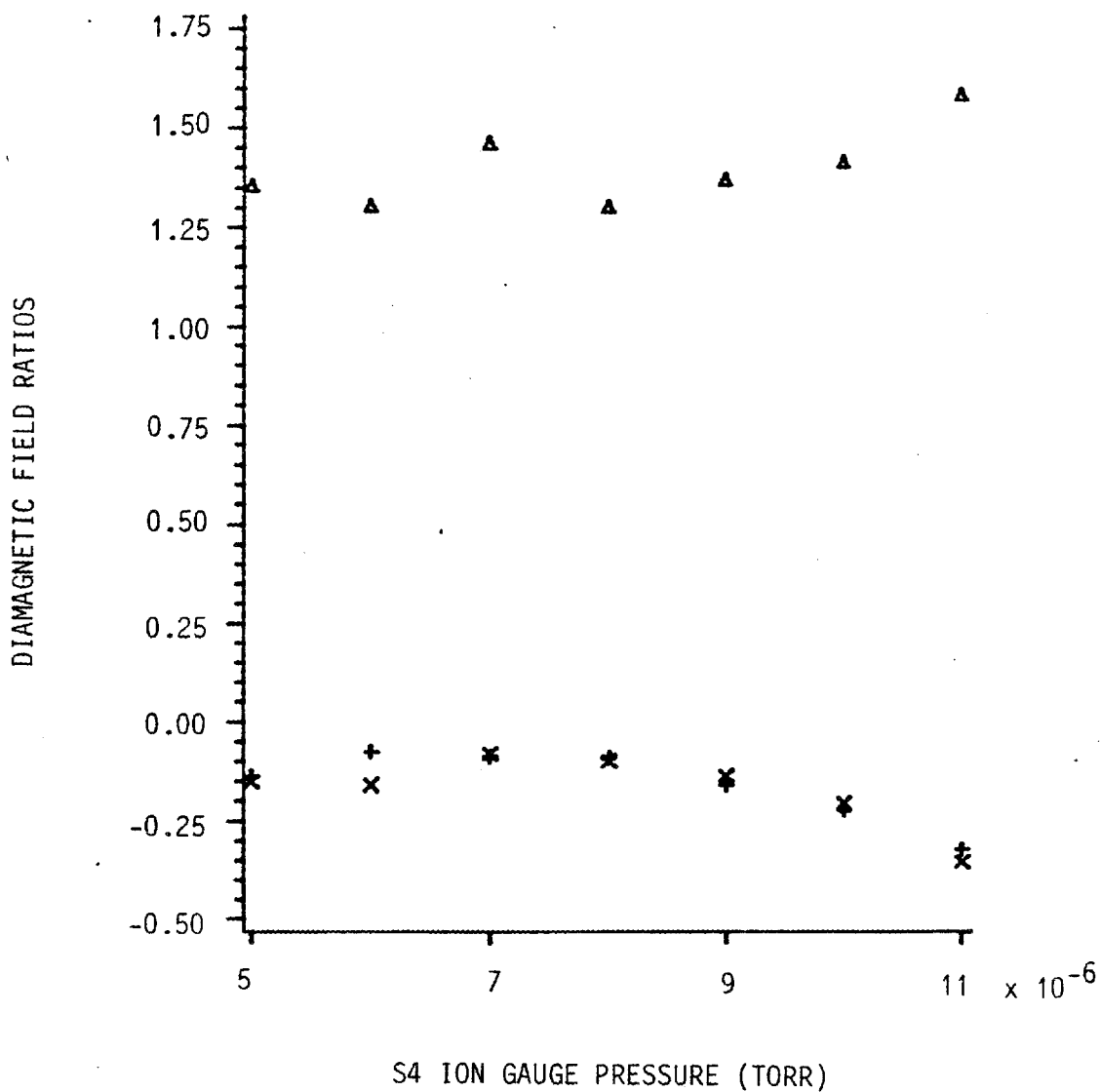


Fig. 4. Ratios of diamagnetic fields due to EBT-S electron rings at different locations on cavity W4 versus cold gas pressure from ion gauge on cavity S4. Fields were obtained using the Hall effect instrument and identical Hall probes. Nominal plasma conditions of 100 KW @18 GHz power and 7250 A for generator current for confining field were used. Points plotted are values of field at large major radius position at cavity center in horizontal midplane divided into fields located:

Pluses : 9.5 cm right of center at large major radius  
 X's : 9.5 cm left of center  
 Triangles: rear of cavity (small major radius position)

toroidal field null point for any assumption of ring toroidal extent. This is shown by the curves of Fig. 5. It is necessary to assume that a ring component exists near the cavity wall in order to reproduce the results for the off center field observations, as is shown in Fig. 6.

At the next data taking opportunity, additional readings will be made at other off center locations to provide more details for analysis of this phenomenon. One final note on this subject - a ring component near the EBT cavity wall couples much more strongly to the probes than one further removed. Hence the fraction of ring energy required in this component to produce the observed off center fields is not large.

The observations made with ICRH power into cavity W3 were qualitatively similar to those made in July. We note that turning ICRH on with EBT-S operation increased the diamagnetic signals in the probes on cavity W4 but decreased the signal in the probe on W3. More detailed analysis of the ICRH effects remains to be done.

Finally, we observed that the field at the top of W4 differed from the field at the top of W6 in an almost random manner on the different ring turn-downs. The field at the top of W6 ratioed to that at the top of W4 gave values of 0.84, 1.22, 0.59, 0.71, 0.84, 0.80, 1.03 for pressures of 5, 6, 7, 8, 9, 10, 11 x 10<sup>-6</sup>T respectively. While there are any number of possible causes for this, e.g., power distribution or gas distribution variations, the significant fact is that it is only a rather poor approximation to assume all the EBT rings are identical.

While a large amount of data has been acquired during the development of the UMR Hall Effect Diamagnetic Diagnostic instrument, the need still exists for systematic investigation of the rings to determine symmetries, and, in correlation with other diagnostics, geometry under the many possible conditions of operation of EBT. Now that the basic instrument is available, with careful probe placement and calibration, it should be possible to obtain the needed data expeditiously in the future.

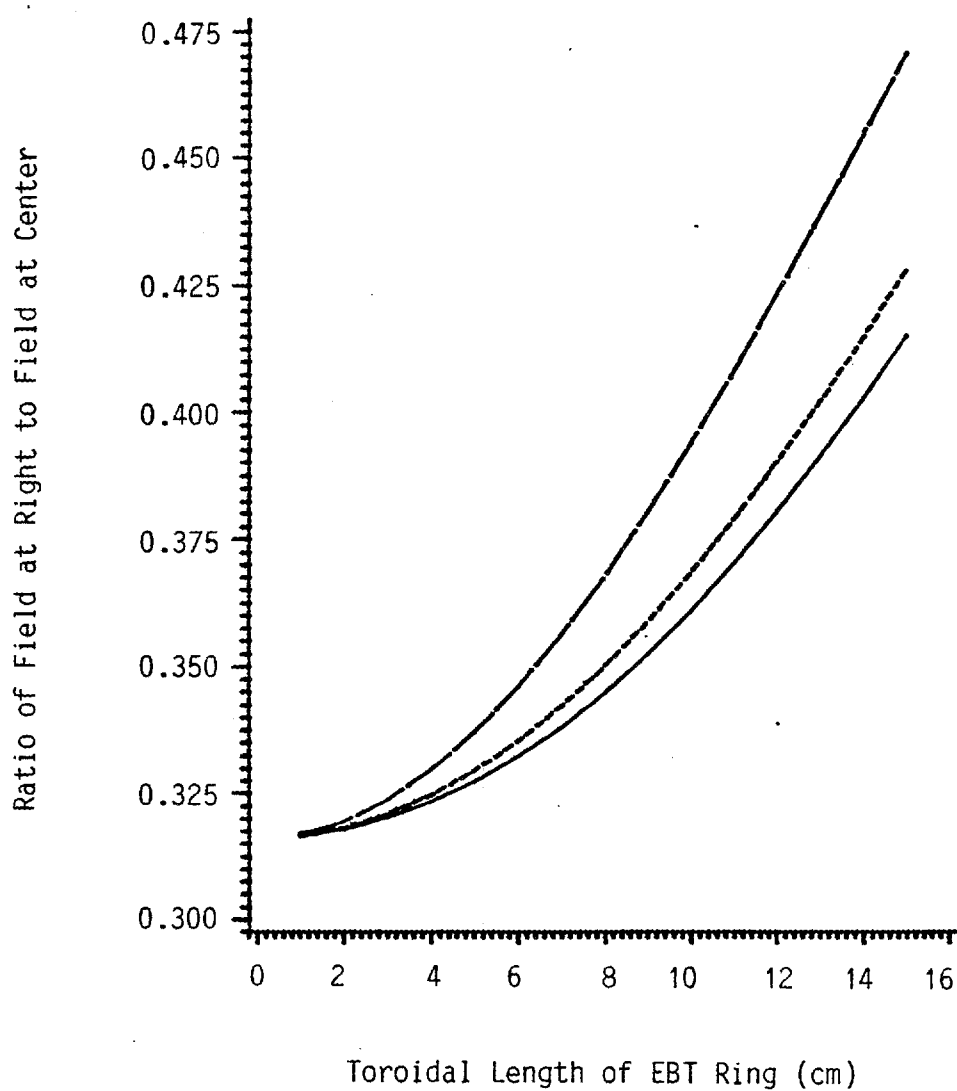


Fig. 5. Ratios predicted by the current sheet model for EBT electron ring diamagnetic field 9 cm left or right of cavity center at large major radius position to that on cavity center, versus toroidal length of model rings. Toroidal lengths are measured between half maximums for surface current density. Current sheets are assumed to be located at 2nd harmonic resonance position in vacuum field and to be separated by 3 cm. Solid curve is for a uniform surface current density. Dashed curve is for a parabolic current density variation with length; dotted curve is for a Gaussian current density variation.

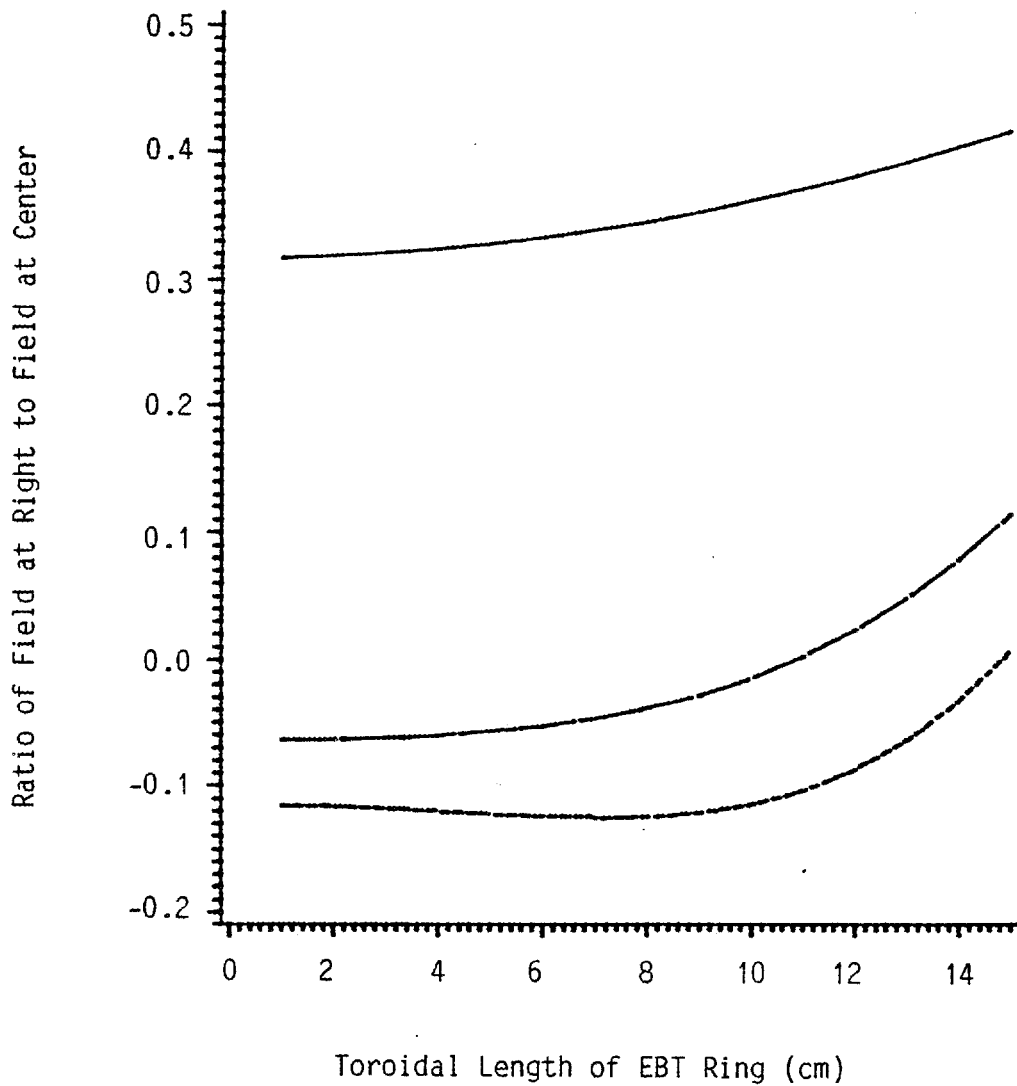


Fig. 6. Ratios predicted by the current sheet model for EBT electron ring diamagnetic field 9 cm left or right of cavity center at large major radius position to that on cavity center, versus toroidal length of model rings. Solid curve is for nominal ring parameters of 3 cm thickness located at 2nd harmonic resonance. Dashed curve is for a thick ring extending from near the 2nd harmonic resonance to the cavity wall. Dotted curve is for a ring 5 cm thick with outside edge at cavity wall. Actual case is presumed to be a superposition of solid and dashed curves with weights chosen to give zero crossing for lengths near 10 to 12 cm.

#### IV. FURTHER STUDIES IN RING MODELING

A simple current sheet model<sup>4</sup> has been used for analysis of the ring diamagnetic data. Some questions have been raised as to the adequacy of this model. In an attempt to answer the question of adequacy of the model in regard to calibration of the flux pickup loop signals in terms of ring energy, a bumpy cylinder MHD equilibrium was studied earlier.<sup>10</sup> Recently we have carried out a derivation which shows the equivalence of the treatment of electron diamagnetism in the current sheet model and MHD equilibrium approach. This is presented below. The current sheet model using a surface current density that is constant along the length of the cylindrical sheet is obviously not realistic. We have extended the computer code for calculation of ring fields from the model to allow other surface current distributions. We also have corrected a sign error in a subroutine used in the earlier calculations assuming constant surface current density, and the results of this correction are noted below. Finally, we give a simple derivation of the fact that diamagnetic measurements alone cannot determine ring geometry.

#### Equivalence of diamagnetic currents of a plasma as derived from single particle kinetics and MHD tensor pressure

Numerical calculations with a 2-D, tensor pressure MHD equilibrium code give values for calibration of flux pickup loop signals in terms of ring energies reasonably in agreement with those obtained from the current sheet model.<sup>11</sup> This agreement occurs, first of all, because the approximately Helmholtz coil configuration of the flux pickup loops makes them insensitive to details of ring geometry, and, second, because the current sheet model properly takes into account the magnetic effect of plasma drift currents (which are self consistently included in the MHD approach). The previous derivation<sup>12</sup> of the drift currents for the current sheet model made no connection to the MHD equations relating current to tensor pressure. Since alternate modeling of the rings can be based on a pressure model, the following derivation was carried out

to reconcile the two approaches. This derivation shows that the diamagnetic effects of a plasma with a given geometrical current distribution are obtained identically whether considered as a collection of point dipoles with guiding center drifts or as a MHD fluid.

Based on a single particle model, the contribution to the magnetic field from the motion of charged particles in the field can be obtained from the current density due to the particles. (This field component is usually small compared to the field due to external currents.) This current density in turn can be expressed as the sum of currents due to cyclotron motion and drift motion. The current density due to cyclotron motion is  $\nabla \times \bar{M}$  where  $\bar{M}$  is dipole moment density per unit volume.  $\bar{M}$  is in turn related to particle kinetic energy by  $E = \bar{M} \cdot \bar{B}$  where  $E$  is the "perpendicular" energy density - perpendicular meaning due to the velocity component perpendicular to the local total magnetic flux density  $\bar{B}$ . (Contributions of the drift velocity to particle kinetic energy are negligible.)

For a distribution of particles (whether or not a fluid model is valid or in equilibrium) the macroscopic  $\bar{B}$  and  $\bar{H}$  fields then satisfy  $\nabla \times \bar{H} = \bar{J}_d$   $\bar{B} = \mu_0(\bar{H} + \bar{M})$  or  $\nabla \times \bar{B} = \mu_0(\bar{J}_d + \bar{J}_c)$  where  $\bar{J}_c = \nabla \times \bar{M}$  and  $|\bar{M}| = .5nm v_{\perp}^2 / B = p_{\perp} / B$  with  $p_{\perp} = .5nm v_{\perp}^2$ . Thus  $\bar{M} = -\hat{b} p_{\perp} / B$ . (1)  
The value of  $\bar{J}_d$  is obtained by averaging single particle drifts over the distribution. The grad B and curvature drifts, when  $\nabla \times \bar{B} \neq 0$ , are<sup>13</sup>

$$\begin{aligned} \bar{v}_d^g &= - \frac{1}{q} \frac{\mu}{B} \frac{\nabla(B^2/2) \times \bar{B}}{B^2} \\ \bar{v}_d^c &= \frac{m}{q} \frac{v_{\parallel}^2}{B^4} [\bar{B} \times (\bar{B} \cdot \nabla) \bar{B}] \\ \mu &= \frac{1}{2} m v_{\perp}^2 / B \end{aligned} \quad (2)$$

These expressions can be reduced as follows:

$(\bar{B} \cdot \nabla) \bar{B} = B(\hat{b} \cdot \nabla) \bar{B} = B(\hat{b} \cdot \nabla)(B\hat{b}) = B^2(\hat{b} \cdot \nabla)\hat{b} + B(\hat{b} \cdot \nabla B)$   
where  $B = |\bar{B}|$  and  $\hat{b} = \bar{B}/B$ . But  $\bar{B} \times \bar{B} = 0$  and  $(\hat{b} \cdot \nabla)\hat{b} = \bar{K}$ , where  $\bar{K}$  is the curvature vector of field  $\bar{B}$ . Thus

$$\bar{v}_d^c = (m/q)(v_{\parallel}^2/B) (\hat{b} \times \bar{\kappa}) \quad (3)$$

We note that  $\nabla(B^2/2) = B\nabla B$ ,  $\nabla(B^2/2) \times \bar{B} = B^2(\nabla B) \times \hat{b}$   
so that in eq.(2)

$$\bar{v}_d^g = - (1/2q)(mv_{\perp}^2/B^2) \nabla B \times \hat{b} \quad (4)$$

Combining eqs.(3) and (4) yields

$$\bar{v}_d = (m/q)\hat{b} \times [(\nabla B/2B^2)v_{\perp}^2 + (\bar{\kappa}/B)v_{\parallel}^2]$$

The drift current is then given by an average over drift velocity as

$$\bar{J}_d = nq\langle\bar{v}_d\rangle.$$

Noting that  $v_{\perp}^2 = v_1^2 + v_2^2$ ,  $v_{\parallel}^2 = v_3^2$ , where 1,2,3 are Cartesian coordinate directions, we have  $\langle v_{\perp}^2 \rangle = 2\langle v_1^2 \rangle$  since  $\langle v_1^2 \rangle = \langle v_2^2 \rangle$ ; and  $p_{\perp} = nm\langle v_1^2 \rangle$ .

Thus

$$\bar{J}_d = \hat{b} \times [ p_{\perp}(\nabla B/B^2) + p_{\parallel}(\bar{\kappa}/B) ] \quad (5)$$

Using eqs. (1) and (5), we see that the total diamagnetic current density required in  $\nabla \times \bar{B} = \mu_0 \bar{J}$  is

$$\bar{J} = -\nabla \times [ \hat{b}(p_{\perp}/B) ] + \hat{b} \times [ p_{\perp}(\nabla B/B^2) + p_{\parallel}(\bar{\kappa}/B) ] \quad (6)$$

Next eq.(6) is manipulated using vector identities. First use  $\nabla \times (f\bar{T}) = f(\nabla \times \bar{T}) + \nabla f \times \bar{T}$ .

Thus

$$\begin{aligned}\nabla \times \hat{b}(p_{\perp}/B) &= (p_{\perp}/B)(\nabla \times \hat{b}) + \nabla(p_{\perp}/B) \times \hat{b} = \\ &= (p_{\perp}/B)(\nabla \times \hat{b}) + (1/B)(\nabla p_{\perp} \times \hat{b}) - (p_{\perp}/B^2)(\nabla B \times \hat{b}),\end{aligned}$$

and

$$\mathcal{J} = \hat{b} \times [p_{\perp}(\nabla B/B^2) + p_{\parallel}(\bar{\kappa}/B) - p_{\perp}(\nabla B/B^2) + (\nabla p_{\perp}/B)] - (p_{\perp}/B)(\nabla \times \hat{b}) \quad (7)$$

Using  $\nabla(\bar{a} \cdot \bar{b}) = (\bar{a} \cdot \nabla)\bar{b} + (\bar{b} \cdot \nabla)\bar{a} + \bar{a} \times (\nabla \times \bar{b}) + \bar{b} \times (\nabla \times \bar{a})$

with  $\bar{a} = \bar{b} = \hat{b}$ , one obtains

$$(\hat{b} \cdot \nabla)\hat{b} = \bar{\kappa} = -\hat{b} \times (\nabla \times \hat{b}). \quad (8)$$

With  $\bar{A} \times (\bar{B} \times \bar{C}) = (\bar{A} \cdot \bar{C})\bar{B} - (\bar{A} \cdot \bar{B})\bar{C}$ , eq.(8) gives

$$\nabla \times \hat{b} = \hat{b}(\hat{b} \cdot \nabla \times \hat{b}) + \hat{b} \times \bar{\kappa}. \quad (9)$$

Using eq.(9) in eq.(7) yields

$$\mathcal{J} = \hat{b} \times [(\nabla p_{\perp}/B) + (p_{\parallel} - p_{\perp})\bar{\kappa}/B] - \hat{b}(p_{\perp}/B)[\hat{b} \cdot \nabla \times \hat{b}].$$

Noting that  $\hat{b} \times \nabla p_{\perp} = \hat{b} \times \nabla_{\perp} p_{\perp}$ , we see that the component of  $\mathcal{J}$  perpendicular to  $\bar{B}$  is

$$\mathcal{J}_{\perp} = \hat{b} \times [\nabla_{\perp} p_{\perp} - (p_{\perp} - p_{\parallel})\bar{\kappa}]/B \quad (10)$$

which is identical to the equation which would result from a tensor pressure equilibrium.<sup>14</sup>

We note that the term proportional to the curvature  $\bar{\kappa}$  in eq.(10) is in the opposite direction to the drift current of the current sheet model. This sign difference is due to the fact that in eq.(10) only the pressure is acted upon by the gradient operator while in eq.(6) the quantity subject to the differential operator is pressure divided by field, i.e., dipole moment density. Thus modeling the ring plasma in terms of a dipole moment density plus single particle drift currents is equivalent to modeling in terms of pressure as a function of position.

### Generalized computer simulation for a current sheet model

Previous computer code implementations of the current sheet model have assumed a pair of concentric cylindrical current sheets of equal length and constant surface current density with length. These current sheets representing the rings were assumed to be present in one or more EBT cavities with identical geometry but possibly different total currents. The assumption of constant surface current density with length is adequate for flux pickup loop signal calibration in terms of energy due to the lack of sensitivity of the calibration to assumed toroidal length for the sheets. However for comparisons of current sheet model results with other diagnostics for ring geometry (such as the 5 channel hard x-ray diagnostic)<sup>15</sup> it is desirable to be able to model a variation of surface current density with length. A new ring simulation computer code has been written for this purpose, and a FORTRAN listing of the code, titled WPCSM is given in Appendix C. This code implements Gaussian and quadratic surface current distributions with toroidal length as well as a constant one. The code also allows the two cylindrical sheets to be non-concentric provided their axes are parallel. The code will calculate the magnetic field due to these current sheets at any arbitrary position in toroidal coordinates. The earlier code, WPERB<sup>16</sup>, was limited to calculation of magnetic field in planes of symmetry in cylindrical coordinates. The generality of the code makes it computationally slower than WPERB, which assumes constant current density with length, so WPERB should be used when the additional generalities of WPCSM are not needed. A listing of subroutine SOLBA, which is used by WPERB (but not WPCSM, which is why WPCSM is slower), is also given in Appendix C. This listing of SOLBA contains the correction of a sign error that affected some diamagnetic field (but not flux) calculations. This corrected version of SOLBA should be loaded with any future use of WPERB. An example of the output of the generalized code, WPCSM, is in Fig. 5 in Section III above.

### Correction to values calculated for ring center offset

After the printing and distribution of the report on the previous year's work, ORNL/Sub-7676/3,<sup>3</sup> had been completed, it was discovered that the computer code SOLBA, used to calculate the magnetic field components due to an ideal solenoid, contained an error which caused the value of the radial magnetic field component returned to have the opposite algebraic sign from the one it should have (relative to the sign of the axial component). This code was used as a subroutine by the program that generated the plots of field ratios versus ring center offsets shown as Figures 9-12 in the report. The sign error was corrected (the listing in Appendix C contains the correction), the programs rerun, and corrected plots produced. The pages in the report where the text was affected by the changes in the plots were rewritten, and revised copies of all pages affected (text and plots) were sent to known recipients of the report. Copies of these revised pages are included here in Appendix D. Note that the numbers on the upper left of pages in Appendix D are the page numbers for the previous year's report. Page numbers for this report (for Appendix D only) are in the lower right corner.

### Limitations of diamagnetic measurements

The goal of diamagnetic field measurements about EBT is to determine the geometry of the electron rings. If the electrons' diamagnetism is represented as a dipole moment distribution then the goal is to determine the geometry of this distribution. Such a determination is fundamentally model dependent due to the impossibility of uniquely specifying a dipole moment distribution solely from external field measurements. This lack of uniqueness is analogous to that in the case of determining a charge distribution in electrostatics from external field measurements; however, the demonstration is more complicated due to the involvement of dipoles and the nonexistence of free magnetic charges.

If all the sources of a magnetic field are contained inside a

finite, simply connected, 3-dimensional region,  $R$ , then the field external to that region can be expressed in terms of a scalar potential:  $H = -\nabla\phi$ . Thus  $\nabla^2\phi = 0$  external to  $R$  and by Green's theorem<sup>17</sup> one has

$$\phi(\bar{x}) = \frac{1}{4\pi} \int_{\substack{\text{Sur} \\ \text{of } R}} \left\{ \frac{1}{|\bar{x} - \bar{x}'|} \frac{\partial\phi(\bar{x}')}{\partial n'} - \phi(\bar{x}') \frac{\partial}{\partial n'} \frac{1}{|\bar{x} - \bar{x}'|} \right\} dS' \quad (11)$$

where  $\partial/\partial n'$  means normal derivative at the surface. Thus  $\phi(\bar{x})$  outside  $R$  can be expressed as due only to a surface magnetic charge distribution  $\partial\phi/\partial n'$  and a dipole layer  $-\phi(\bar{x})$  on the surface of any closed surface containing  $R$  for points external to this closed surface.

If magnetic charges are not allowed, they can be replaced by the normal component of a dipole moment per unit volume,  $\bar{M}$ , at the boundary. We can assume  $\nabla \cdot \bar{M} = 0$  inside  $R$  and get  $\bar{M} = -\nabla\psi$ ,  $\nabla^2\psi = 0$ , and  $\partial\psi/\partial n' = \partial\phi/\partial n'$  to have a unique  $\bar{M}$ . But a different  $\bar{M}(\bar{x})$  distribution will be obtained for each choice of surface  $R$  - hence external field measurements cannot uniquely determine  $\bar{M}$  unless it is known a priori the region over which  $\bar{M} \neq 0$  and that  $\nabla \cdot \bar{M} = 0$  within the region.

Thus, interpretation of diamagnetic field measurements in terms of ring geometry requires use of a parameterized model where parameters are fit to the data. (Note that a truncated multipole expansion is, in fact, such a model.) The model that we have used, for reasons of simplicity, is that of two cylindrical current sheets, which is equivalent to confining all the dipole moment to the region between the sheets.

## V. USE OF A FERROMAGNETIC RESONANCE MAGNETOMETER FOR OBSERVATION OF HIGH FREQUENCY FIELD FLUCTUATIONS

The YIG magnetometer<sup>18</sup> instrumentation developed earlier<sup>2,3</sup> for observation of ring diamagnetic fields was intentionally limited in frequency response. Since the instrumentation used a carrier frequency in the gigahertz range it was anticipated that it could be used to observe high frequency magnetic field fluctuations in the presence of a large, constant background field such as would be encountered in plasma diagnostics. This was demonstrated in a simple test on EBT.<sup>19</sup> A detailed investigation of the limitations of such high frequency measurements formed the basis for a Master's thesis at UMR,<sup>5</sup> and the abstract of this thesis is given in Appendix E.

We note here that the fundamental limitation of frequency response for the YIG magnetometer is not the carrier frequency but the resonance line width of the ferromagnetic material. While the YIG crystals used for EBT measurements would allow a 3 MHz bandwidth, the eddy currents in the cavity walls would act as a low-pass filter with much lower cutoff frequency. Thus plasma fluctuations would be more easily observed and interpreted by non-magnetic methods.

## REFERENCES

1. Kenneth H. Carpenter, "Research Support for Plasma Diagnostics on Elmo Bumpy Torus - Investigation of Diamagnetic Diagnostics for the Electron Rings," ORNL/Sub-7676/1, Department of Electrical Engineering, University of Missouri-Rolla, February 1981.
2. Kenneth H. Carpenter and Marcus K. daSilva, "Research Support for Plasma Diagnostics on Elmo Bumpy Torus - Study of Diamagnetic Measurements for the Electron Rings and Development of a Ferromagnetic Resonance Magnetometer," ORNL/Sub-7676/2, Department of Electrical Engineering, University of Missouri-Rolla, October 1981.
3. Kenneth H. Carpenter and Robert H. Booker, "Research Support for Plasma Diagnostics on Elmo Bumpy Torus - Observations of EBT Ring Geometry by Means of Diamagnetic Field Measurements Using a Compensated Ferromagnetic Resonance Magnetometer, and a Preliminary Numerical Study of EBT Flux Penetration Dynamics," ORNL/Sub-7676/3, Department of Electrical Engineering, University of Missouri-Rolla, October 1982.
4. K. H. Carpenter, R. A. Dandl, M. W. McGuffin, "Calibration of a Diamagnetic Diagnostic for Stored Energy of High Temperature Electron Annuli in Elmo Bumpy Torus (EBT)," ORNL/TM-7076, Oak Ridge National Laboratory, Oak Ridge, TN, May 1982.
5. Robert Howard Booker, "The Development of a Ferromagnetic Resonance Magnetometer for Observation of Minute High Frequency Fluctuations on Large Average Fields," Master's Thesis, Department of Electrical Engineering, University of Missouri - Rolla, 1983.
6. See Reference 3, Section IV. Plasma conditions cannot be repeated precisely, so moving a single probe to different locations provides an unreliable and slow method to obtain field values at multiple points.
7. K. H. Carpenter, "Diamagnetic Measurements for Experimental Determination of EBT Ring Parameters, in N. A. Uckan, ed., Proceedings of the Workshop on EBT Ring Physics: Dec. 3-5, 1979: Oak Ridge, Tenn., Oak Ridge National Laboratory, CONF-791228, April 1980, p. 147.
8. Brian Peterson, "FAST" family of computer codes running on the ORNL EBT data acquisition PDP11/34 and VAX computers.
9. Reference 3, and Appendix D of this report.
10. Reference 1, Section IV, and Reference 2, Section II.
11. Reference 2, pp. 5-8.

12. Reference 4 and Reference 2, pp. 9-11.
13. Lyman Spitzer, Jr., Physics of Fully Ionized Gases, Interscience Publishers, Inc., 1956, Sec. 2.4.
14. C. L. Hedrick, Oak Ridge National Laboratory.
15. O. E. Hankins and D. L. Hillis, "The Axial Electron Temperature and Density Distribution of the Hot Electron Rings in EBT-S," Bulletin of the American Physical Society, Vol. 28, No. 8, October 1983, p.1224.
16. Reference 2, Appendix E.
17. John David Jackson, Classical Electrodynamics, John Wiley & Sons, Inc., 1962, p.15.
18. Kenneth H. Carpenter and Marcus K. daSilva, "Phase-locked Yttrium Iron Garnet Magnetometer for Remote Measurement of Small Field Changes in a Fluctuating Background," Review of Scientific Instruments, Vol. 53, No. 9, September 1982, pp. 1414-1417.
19. Reference 3, p. 18.

## APPENDIX A

UMR HALL EFFECT DIAMAGNETIC DIAGNOSTIC INSTRUMENT  
REFERENCE MANUAL AND OPERATING INSTRUCTIONSOPERATING INSTRUCTIONS

The UMR Hall Effect Diamagnetic Diagnostic instrument is a versatile device which contains Gaussmeters to measure magnetic fields at up to 6 separate locations simultaneously. Both incremental and total field measurements are output continuously. The sensitivity ranges from 20 to 1000 Gauss per volt for the total field. The sensitivity must be chosen so that the total field output level remains less than 2.1 volts (to maintain linearity and hence calibration). The incremental output has 100 times the sensitivity of the total field output, and has a zero offset from the total field. The offset control is used to center the output between  $\pm 10$  volts. An additional feature of the instrument is the generator fluctuation amplifier. The generator shunt signals are multiplied by 20 and level shifted using the generator offset control. Indicators are provided to show when the generator outputs lie within  $\pm 3$  volts. The range of the incremental generator output signal is  $\pm 10$  volts.

Instrument installation

First the main instrument chassis is placed in the EBT control room in a convenient location to data acquisition electronics. Signals from the incremental output jacks are connected to the data acquisition electronics and the incremental field signals are also fed to strip chart recorder channels for real time monitoring. The signals from generator shunts for EBT generators 9 through 12 are connected to their respective BNC connectors on the rear of the instrument chassis. The current input and Hall signal output connectors on the probe isolation

transformer boxes are connected to their respective connectors on the rear of the chassis using cables of the length needed to reach the probe locations. The Hall probes are also connected to the jacks on the isolation boxes, but the probes are not mounted on EBT until after calibration.

### Calibration

Since Hall probes can have different characteristics, each channel of the Gaussmeter must be calibrated with its respective probe. A reference magnet and zero Gauss chamber are required for calibration. Begin by setting the RANGE switch to the most sensitive position which will result in a total output of less than 2 volts when the field of the reference magnet is measured. (I.e., if a 500 Gauss reference magnet is available, the Gaussmeter would be calibrated on the 500 Gauss per volt range since the 200 Gauss per volt range would yield an output of 2.5 volts.) Insert the probe into the reference magnet and set the POLARITY switch to achieve a positive output voltage at the total field output connector on the front of the instrument. Adjust the PHASE PEAK control for maximum output at the total field connector. Alternately insert the probe into the zero Gauss chamber and reference magnet and note the voltage change at the total field output connector. Adjust the RANGE CAL. control to achieve the proper voltage shift based upon the strength of the reference magnet and the range switch position. This completes the calibration of the instrument. A recheck of each channel should now be made to verify the calibration and quantify the repeatability of reference magnet readings. A recheck of calibration at the conclusion of data taking is recommended.

### Probe mounting

With the cables run from the instrument chassis to the probe isolation transformer boxes near EBT the probes are physically attached to the EBT cavity surface at the locations where magnetic field measurements are to be made. A 1/4 inch styrofoam thermal insulation should be provided between the Hall probe surface and the surface to

which it is mounted. The mount must be rigid enough to prevent significant vibration of the probe with respect to the vacuum magnetic field.

### Operation

To measure a magnetic field, the RANGE switch is set to a position which will not result in more than +2.1 volts at the output of the total field connector. The POLARITY switch is set to the position giving a positive output voltage at the total field connector. The total field in Gauss is computed by multiplying the RANGE switch setting by the change in total field (volts) output which occurs when the probe is taken from the zero Gauss chamber and placed in the unknown field. The Gaussmeter output with the probe in the zero Gauss chamber needs to be noted only once for each range and polarity switch position. (This is done during calibration.) Incremental field changes are measured by setting up the Gaussmeter as above and adjusting the offset control to obtain a signal near zero volts at the INC. FIELD x 100 connector. A change in the magnetic field will produce a voltage change at this connector which is 100 times that shown on the range switch. The limit of this incremental output is  $\pm 10$  volts. NOTE THAT IT IS STILL MANDATORY THAT THE THE TOTAL FIELD OUTPUT VOLTAGE BE LESS THAN +2.1 VOLTS.

The generator shunt amplifier and level shifter provide a means to observe minute fluctuations in generator current. Operation is simple. Adjust the GEN OFFSET control until all of the NULL indicators are off. The voltage at each GEN output is within  $\pm 3$  volts when its respective NULL indicator is off. Changes in generator shunt voltage are multiplied by 20 and appear at the output connectors on the front panel. In order to utilize the data from the generator fluctuation signal, data needs to be acquired from all Hall probes while each generator current is incremented separately by an amount near 10 A. The resulting Hall probe signals when ratioed to the generator fluctuation signals then give a matrix of coefficients to multiply into generator fluctuation signals during plasma field measurements to subtract as

corrections from the Hall probe values. Plasma diamagnetic data taking then proceeds by setting the offset controls to give all incremental signals near zero, starting data acquisition, and changing plasma conditions and observing field changes.

## REFERENCE MANUAL

The UMR Hall Effect Diamagnetic Diagnostic instrument consists of a six channel AC carrier Hall effect incremental Gaussmeter and a four-channel generator fluctuation amplifier. The circuits comprising this instrument are described and schematic diagrams for each and a component parts list are given in the following.

### Gaussmeter principles of operation

Figure R1 shows a block diagram of one of the six channels comprising the Gaussmeter. (A six channel Gaussmeter is implemented by duplicating all of the circuitry except the crystal oscillator, divider, and low-pass filter.) The circuits of the subsystems shown on the block diagram function in the the following manner. The Hall probes require an extremely stable source of excitation to achieve the desired resolution for an incremental Gaussmeter. For this reason, a crystal oscillator was chosen over free running types. The oscillator operates at 3.58 MHz, and its output is divided by 2048 and amplitude limited by digital circuitry. The resulting square wave at 1.75 KHz is low-pass filtered to produce a sine wave. This is used to drive a constant current source which provides 50 mA RMS excitation to the Hall probe. The output of the Hall probe contains a large common mode signal because the probe is driven with respect to ground (unbalanced). A transformer is used to remove this component and provide a better impedance match. It also provides a voltage gain of 28. This signal is applied to a variable gain amplifier which determines the range of the instrument. The output of this stage is applied to an amplifier having a gain of 10, but with selectable polarity. This allows one to electrically reverse the direction of the Hall probe. A synchronous detector is used to recover a DC voltage proportional to the total magnetic field. (A synchronous detector will average disturbances that are not correlated with the desired signal. This provides noise immunity.) A signal proportional to minute incremental field deviations is obtained by level shifting and amplifying the total field signal by 100. The circuit

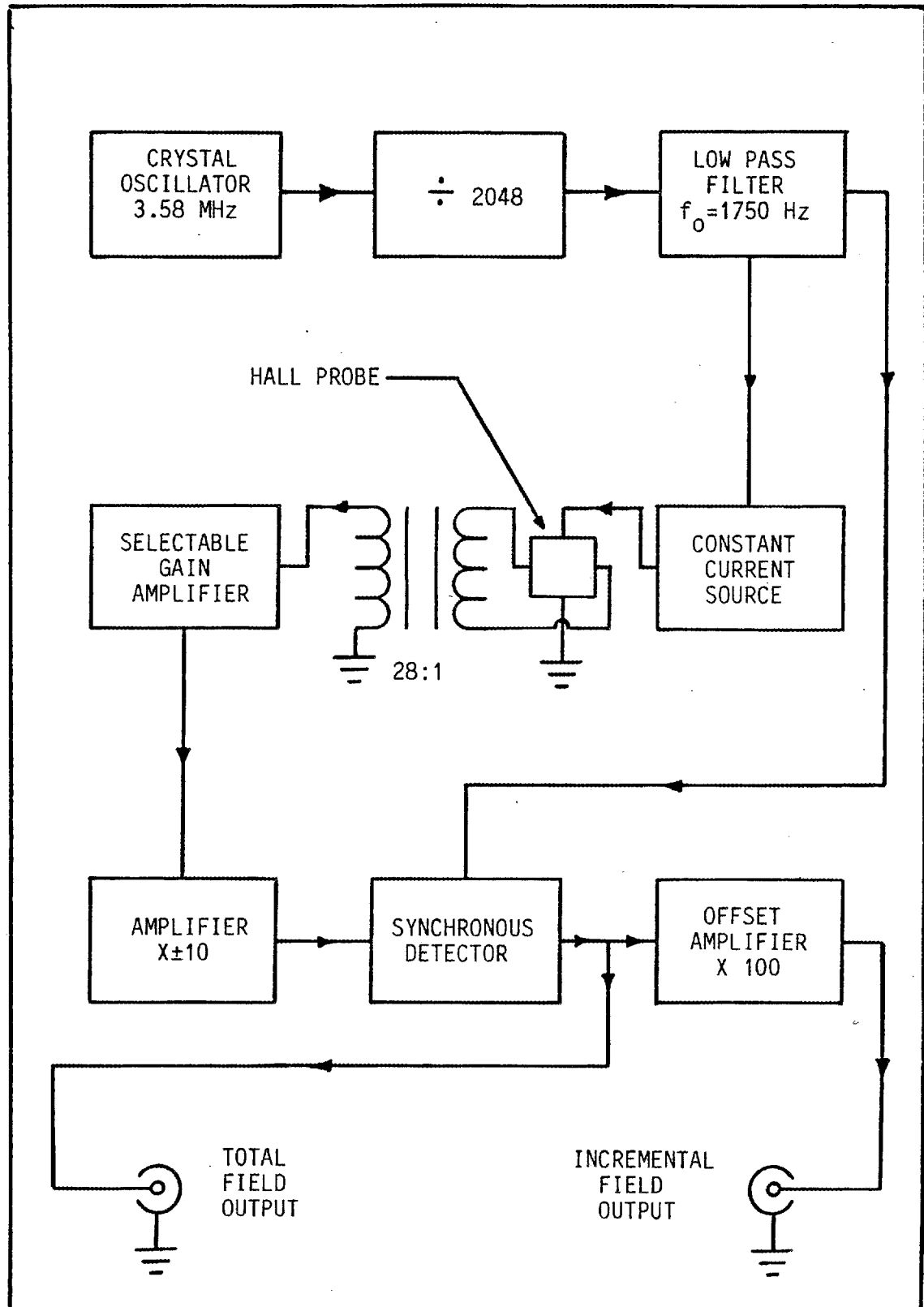


Fig. R1. Block diagram for Hall effect Gaussmeter.

designs for the subsystems (and the generator fluctuation amplifiers not shown on the block diagram) are discussed in the following paragraphs.

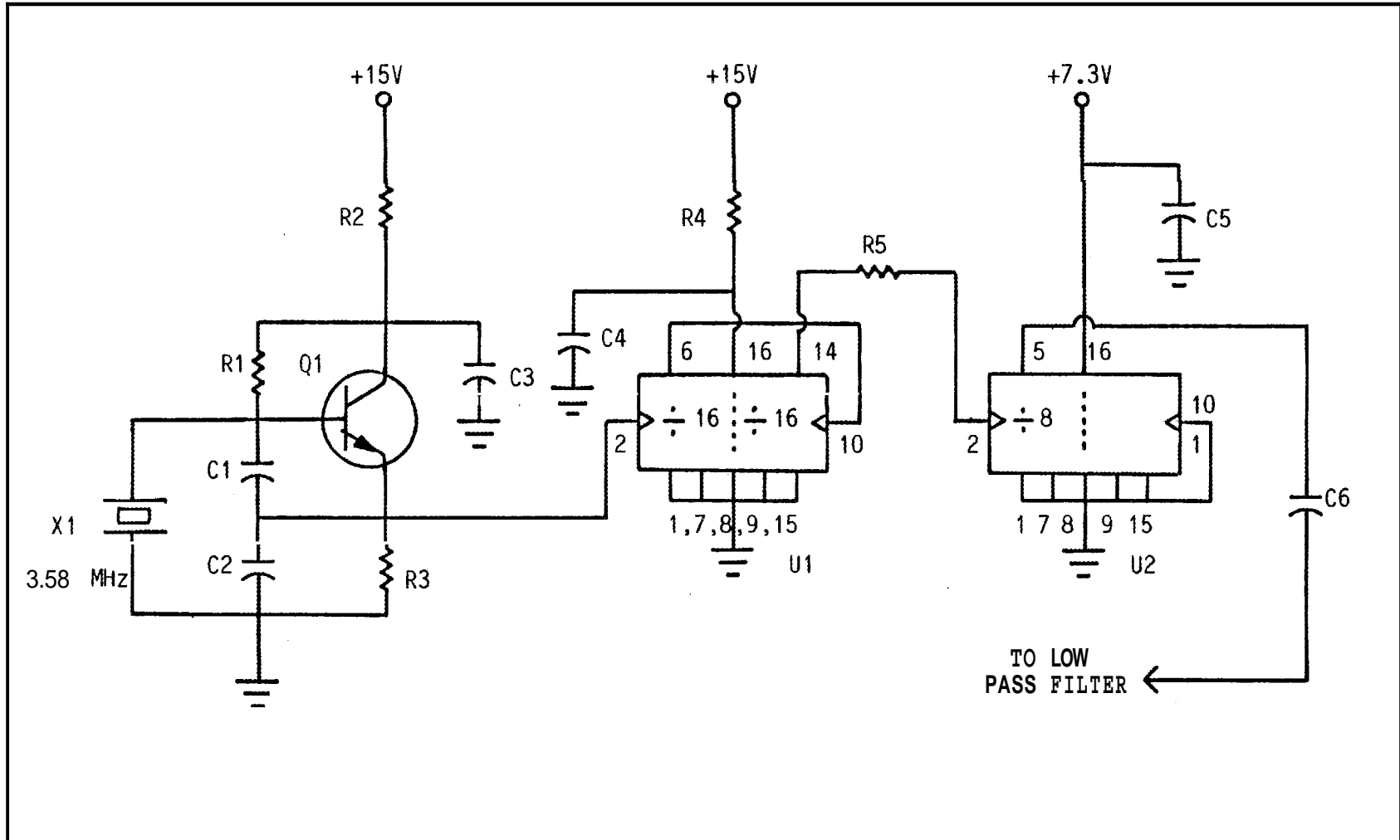
### Oscillator

Schematic 1 shows the crystal oscillator and divider. Transistor Q1 operates as a Colpitts oscillator. A frequency of 3.58 MHz was chosen because of the availability of color subcarrier crystals, and the fact that CMOS digital circuitry will operate at this frequency. The output of the oscillator is divided by 256 using the two CMOS four bit binary counters contained in U1. This signal is divided by 8 and amplitude limited by U2. The result is a very stable 1.75 KHz square wave.

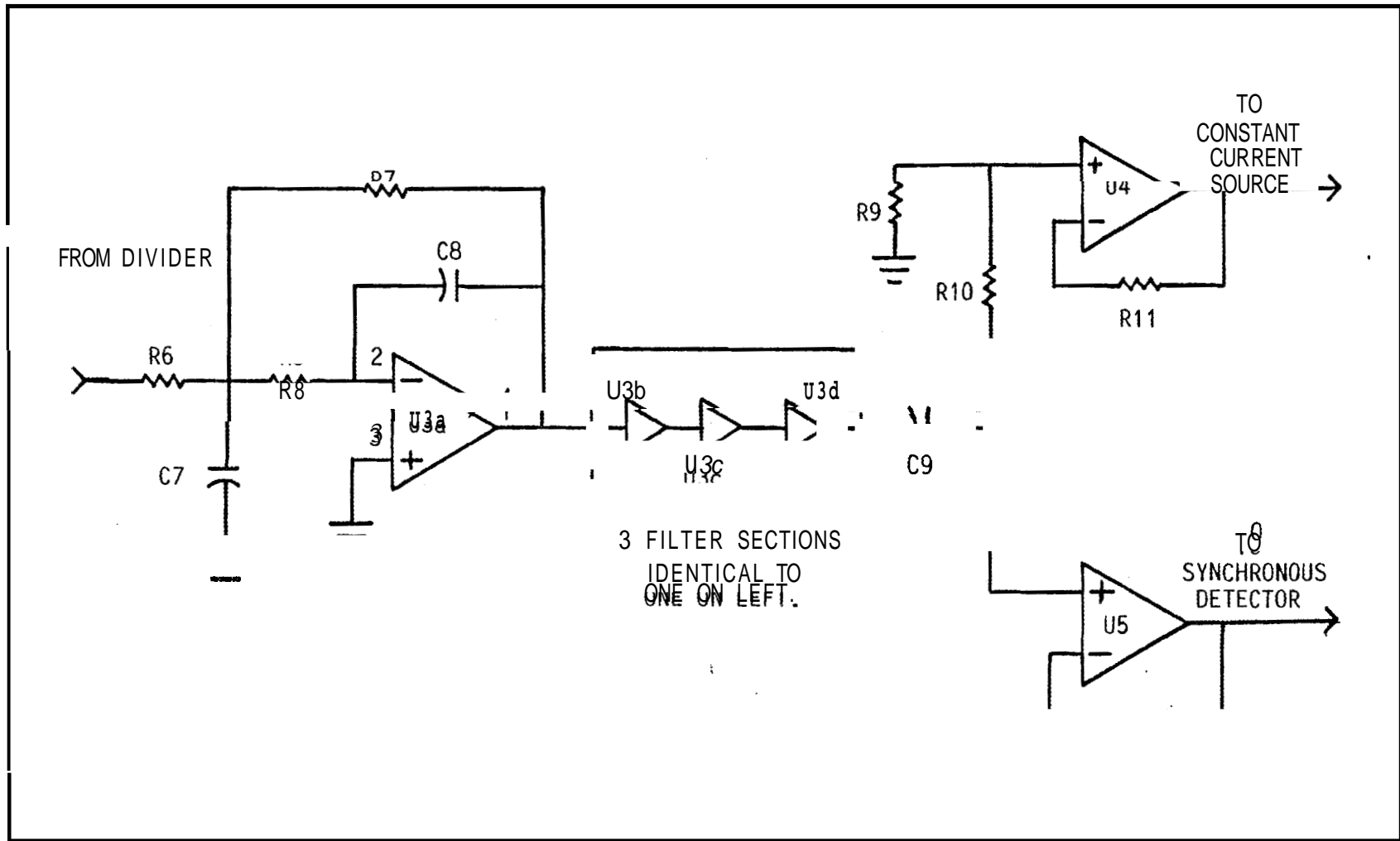
A sine wave is obtained by low-pass filtering the square wave using the circuit shown in Schematic 2. A good operational amplifier is used to implement the four-stage, eight-pole, low-pass filter. One of the four stages is shown in detail. The three other stages are constructed identically to the one shown, and are cascaded to give the eighth order filter. The output of the filter is AC coupled to the buffer amplifiers, U4 and U5, which supply the necessary amount of drive to the six constant current sources and synchronous detectors.

### Constant current source

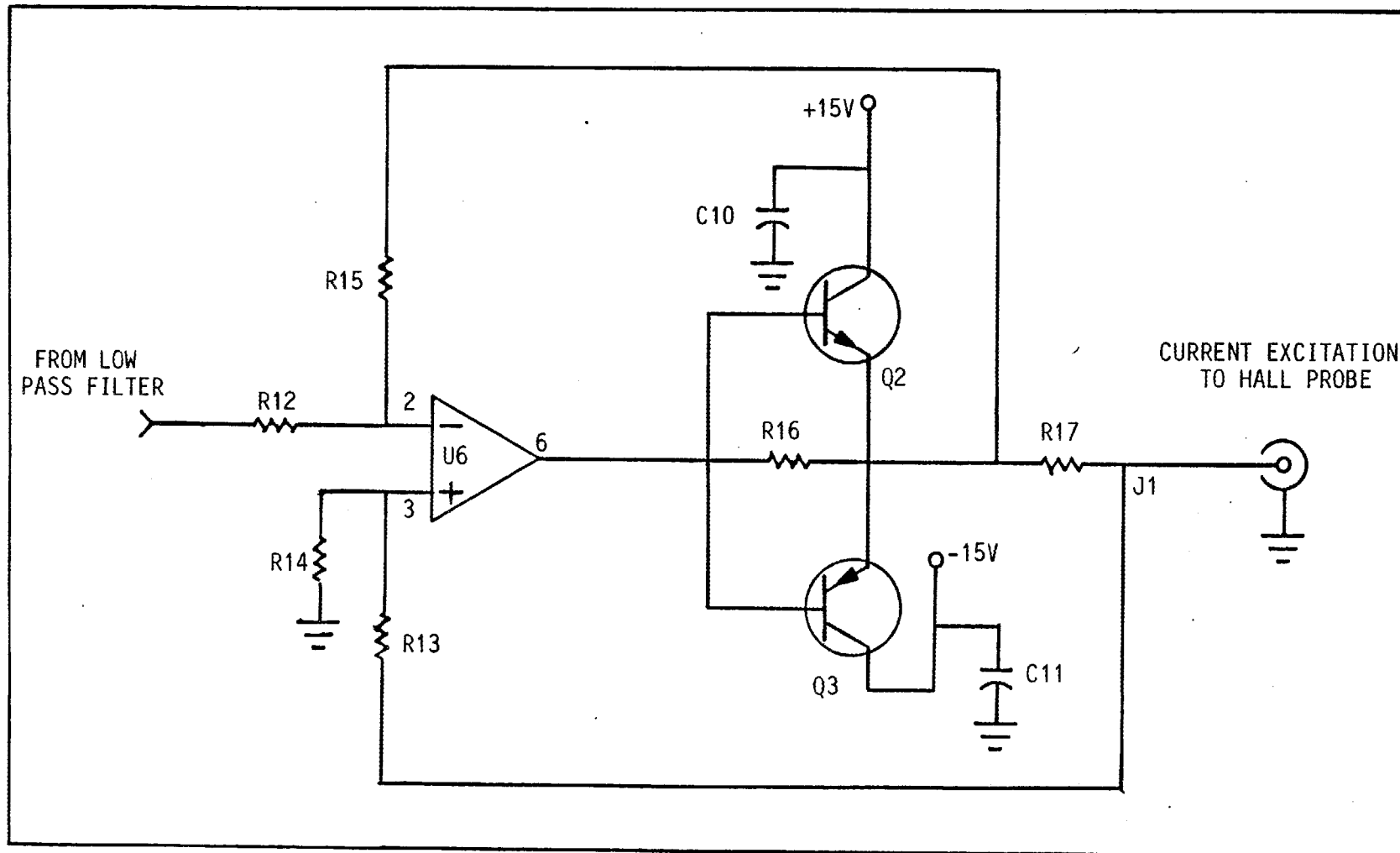
Schematic 3 shows a diagram of the 50 mA RMS constant current source. The circuit operates by maintaining a constant voltage across R17. Transistors Q2 and Q3 operate as a class C push-pull amplifier and supply the portion of the output current that is in excess of a few milliamperes. Currents below this level are supplied by the operational amplifier through R16. The transistors turn on gradually as the voltage across R16 increases above 0.6 volts. This eliminates crossover distortion. The output of the current source is connected via coaxial cable to the remotely located transformer box.



Schematic 1. Oscillator and divider circuit for Hall effect Gaussmeter.



Schematic 2. Low pass filter and buffer amplifiers for Hall effect Gaussmeter.



Schematic 3. Constant current source for Hall effect Gaussmeter.

### Transformer box

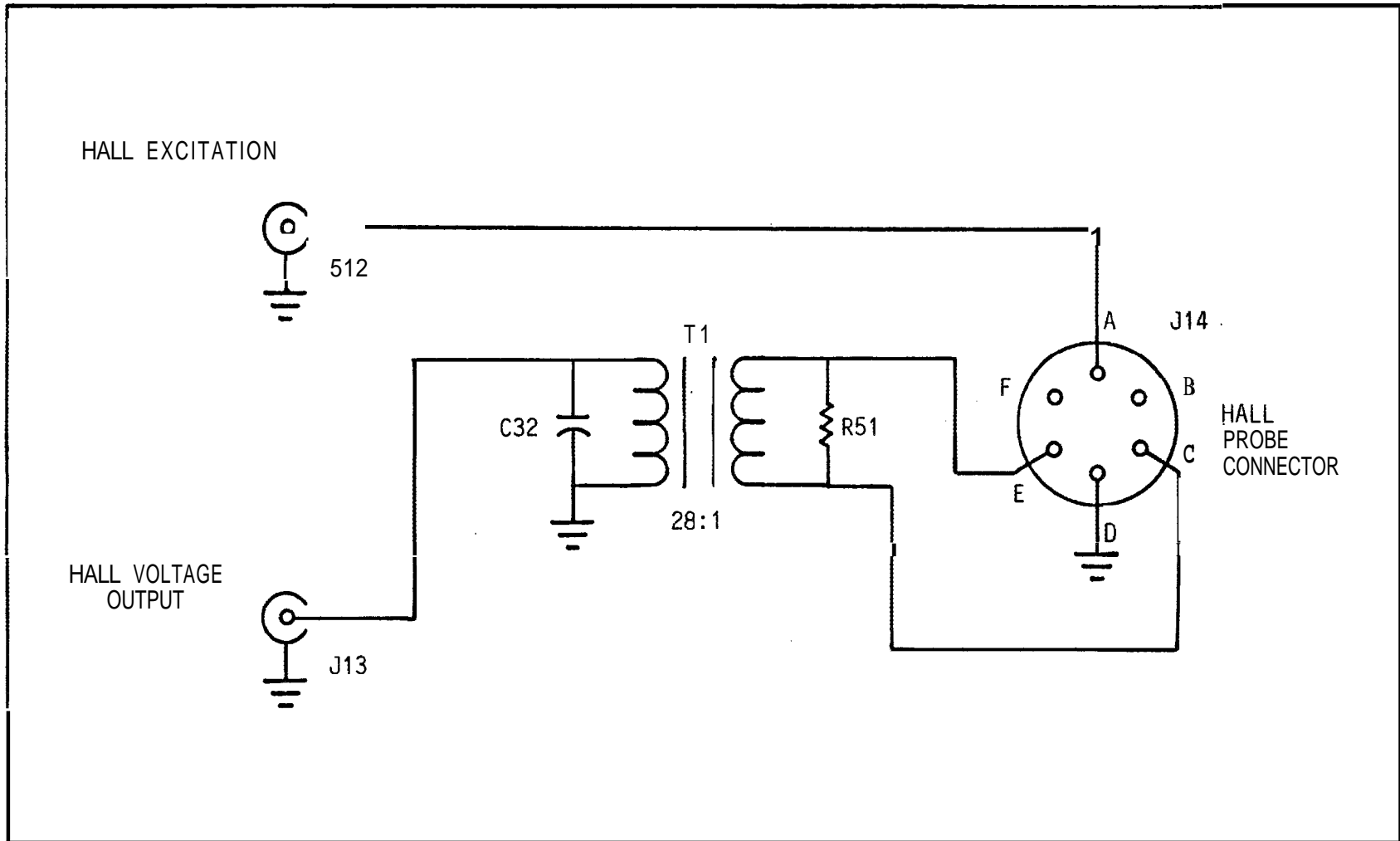
Details of the transformer box are shown in Schematic 4. The output of the current source is connected to pins A and D of J14 and provide the excitation to the Hall probe. The Hall voltage appears across pins C and E. Transformer T1 provides a voltage gain of 28 and removes the common mode component that is present in the output which results because the input is driven with respect to ground. R51 provides the correct load for optimum linearity of the Hall probe. The Hall voltage is connected via coax to the first amplifier. C32 reduces the effect of coax line length (i.e., cable capacitance is small compared to C32).

### AC amplifiers

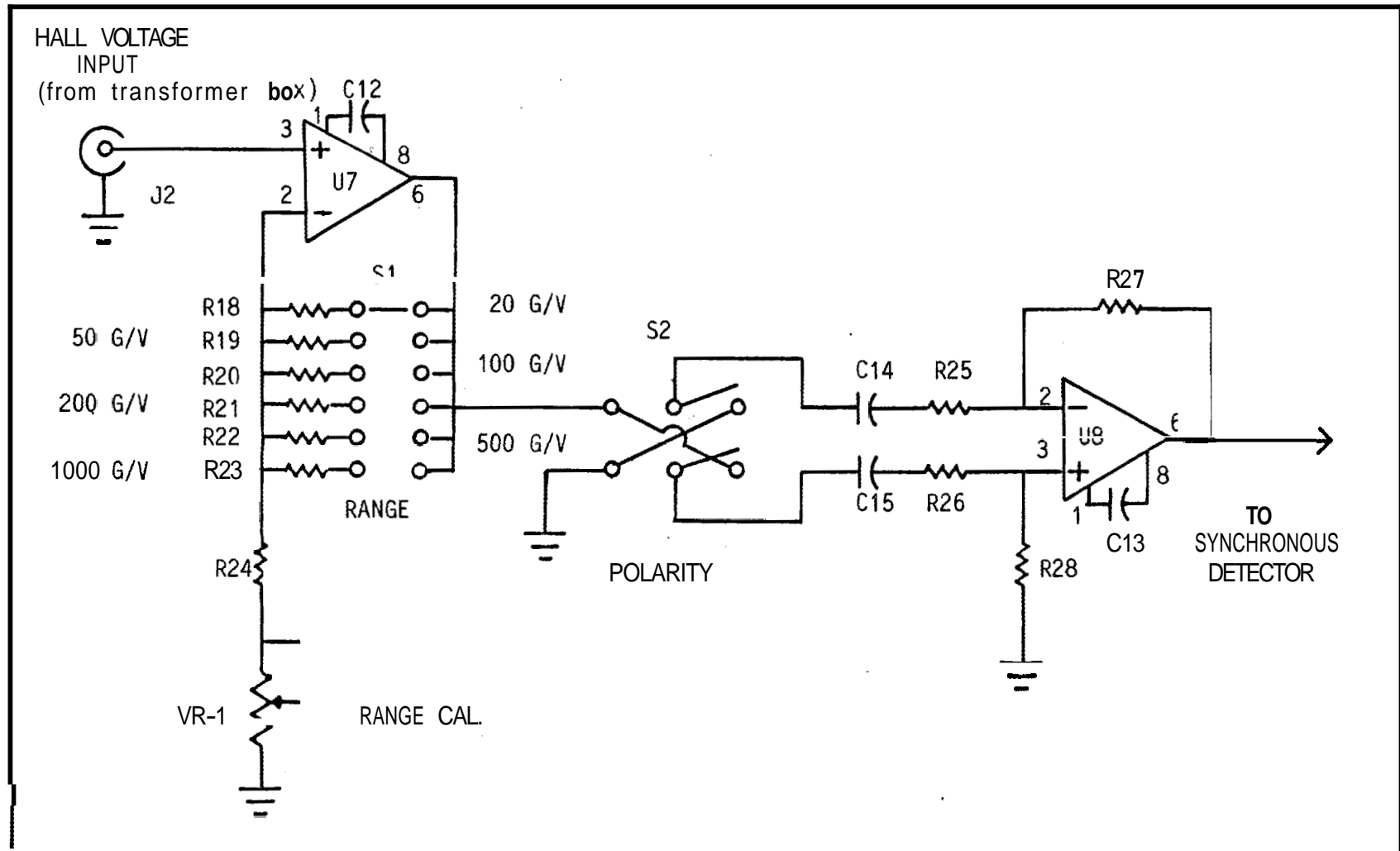
The first and second amplifiers are shown in Schematic 5. Operational amplifier U7 is connected as a selectable gain, non-inverting amplifier. Resistors R18 - R23 are chosen to give the required gain for a particular sensitivity. (The gain of the first amplifier is approximately 6.1 for the 500 G/V range.) Variable resistor VR1 is used to calibrate the magnetometer. S1 serves as a polarity switch selecting a gain of 10 for the second amplifier. The DC offset of first stage is eliminated by AC coupling capacitors C14 and C15. The output of the second amplifier is fed to the synchronous detector.

### Synchronous detector

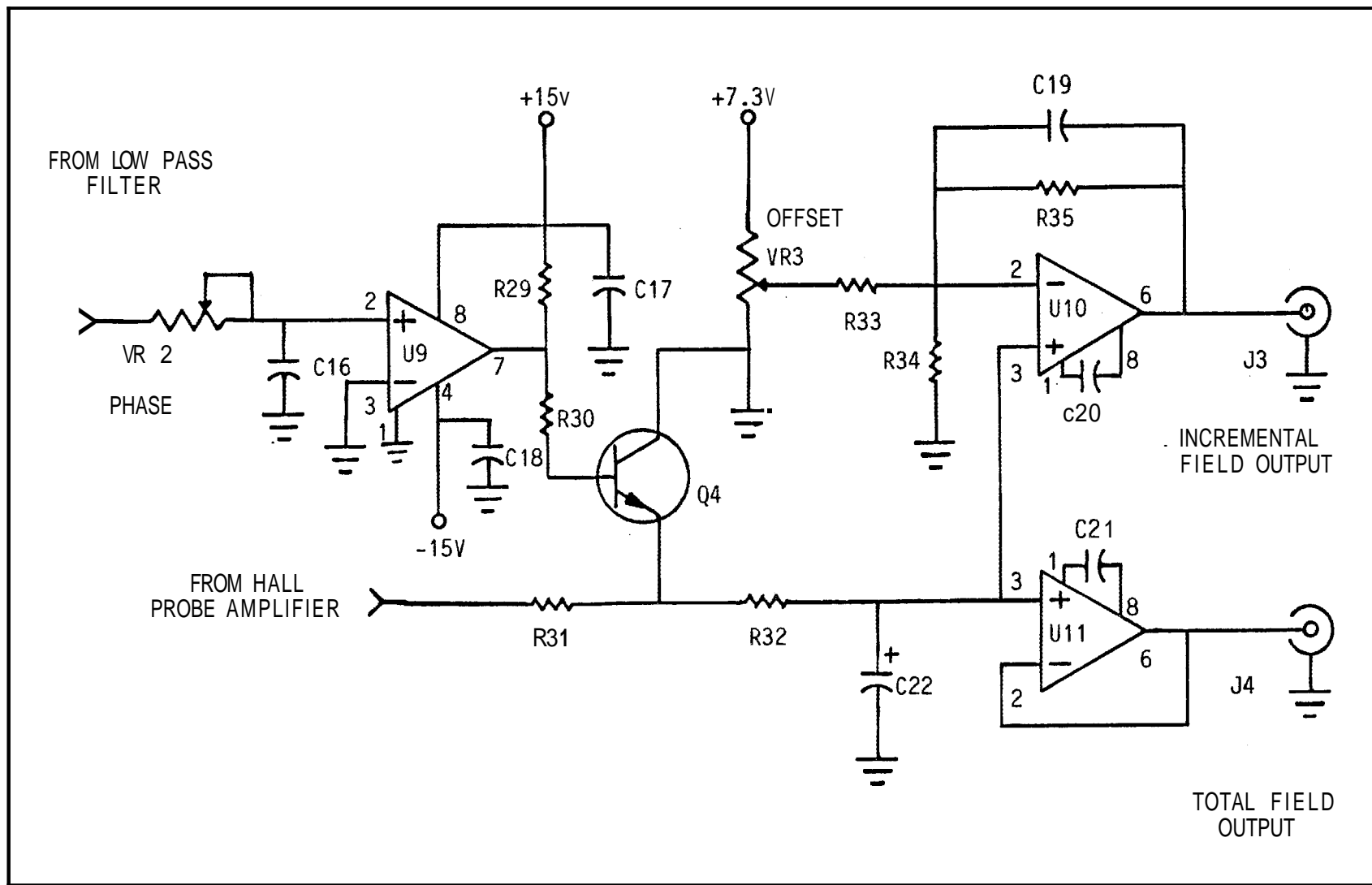
Schematic 6 shows a schematic diagram of the synchronous detector and offset amplifier. Transistor Q4 is used as a switch which synchronously shorts the negative portion of the second amplifier's signal to ground. Thus, the AC signal is synchronously detected or rectified. The proper time to trigger Q4 is obtained from the output of the low-pass filter which also feeds the constant current source providing the Hall probe excitation. A phase shift network consisting of VR2 and C16 is used to adjust the phase of the trigger, which depends upon the phase shift through the cables connecting the Hall probe.



schematic 4. Transformer box.



Schematic 5. First and second amplifiers for Hall effect Gaussmeter.



Schematic 6. Synchronous detector and offset amplifier for Hall effect Gaussmeter.

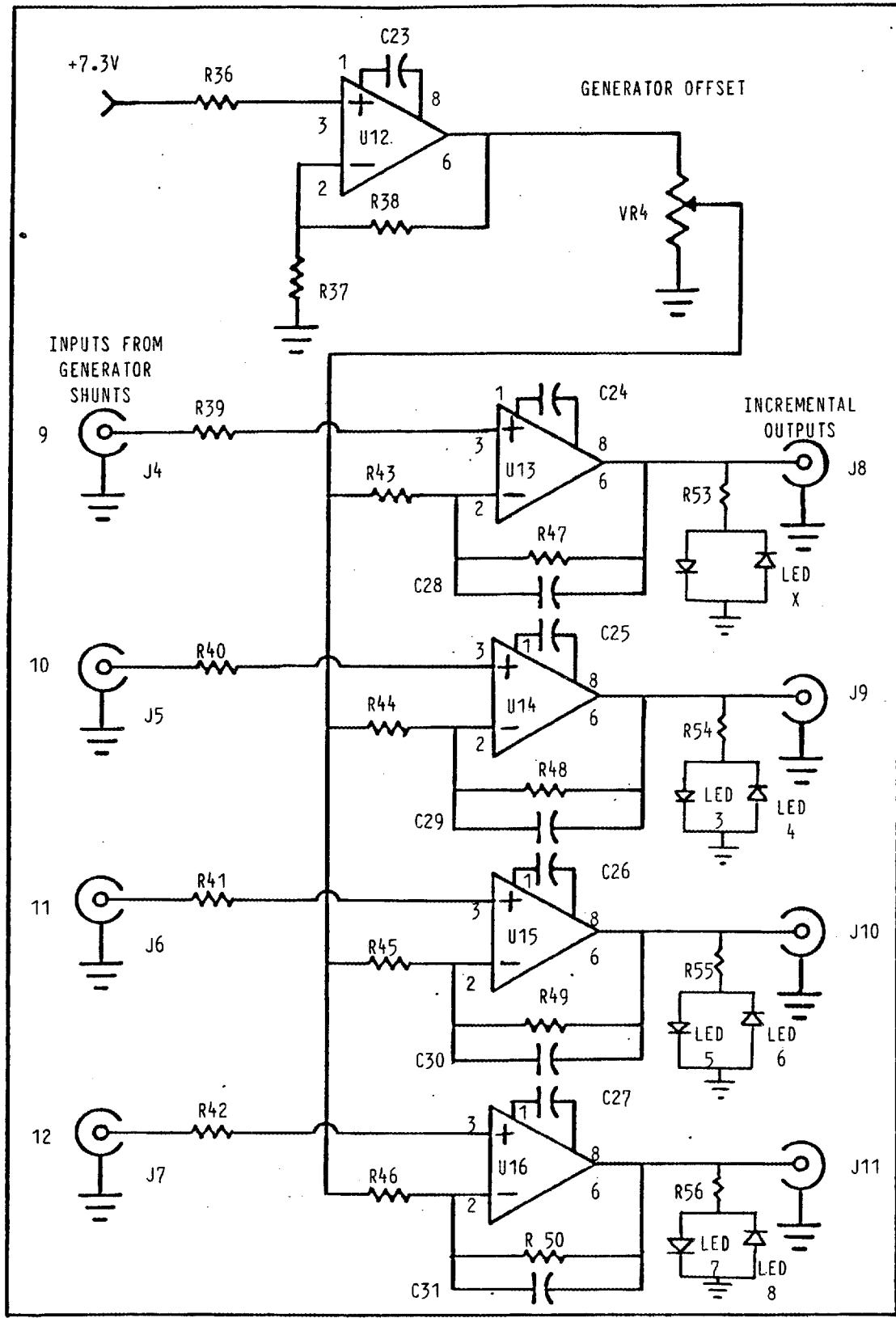
Comparator U9 functions as a zero crossing detector and produces the square wave to drive Q4. The output of the synchronous detector is filtered (i.e., averaged) by R32 and C22. The average voltage at this point must not exceed 2.1 volts for linear operation. This limit occurs because the emitter-base junction appears as a zener diode for  $V_{EB}$  greater than approximately 7 volts. (Note: 2.1 volts is the average value of a half rectified sine wave with a peak value of 7 volts.) The filtered output of the synchronous detector is buffered by U11 and represents the Total Field Output. The Incremental Field Output is obtained from this signal by level shifting and multiplying by 100. Operational amplifier U10 performs this function; the amount of level shifting is determined by the OFFSET potentiometer VR3.

#### Generator fluctuation amplifier

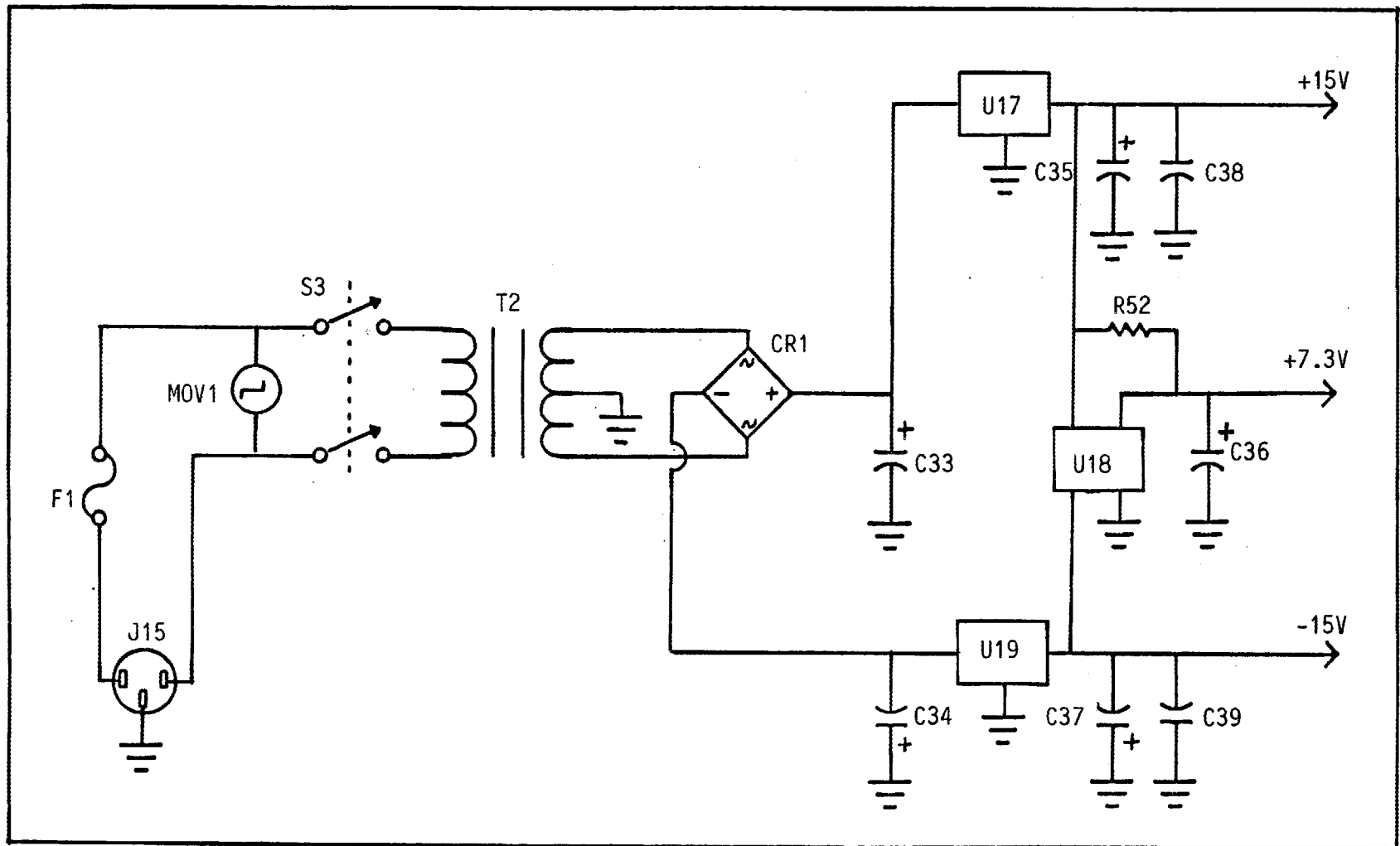
The UMR Hall Effect Diamagnetic Diagnostic instrument provides for level shifting and amplifying the signals obtained from the four generator shunts. This circuit is shown in Schematic 7. Operational amplifier U12 produces a very stable source of 11.3 volts using the precision 7.3 volt source as a reference. This is supplied to VR4 to adjust the offset of amplifiers U13 - U16, which are configured to a non-inverting gain of 20.

#### Power supply

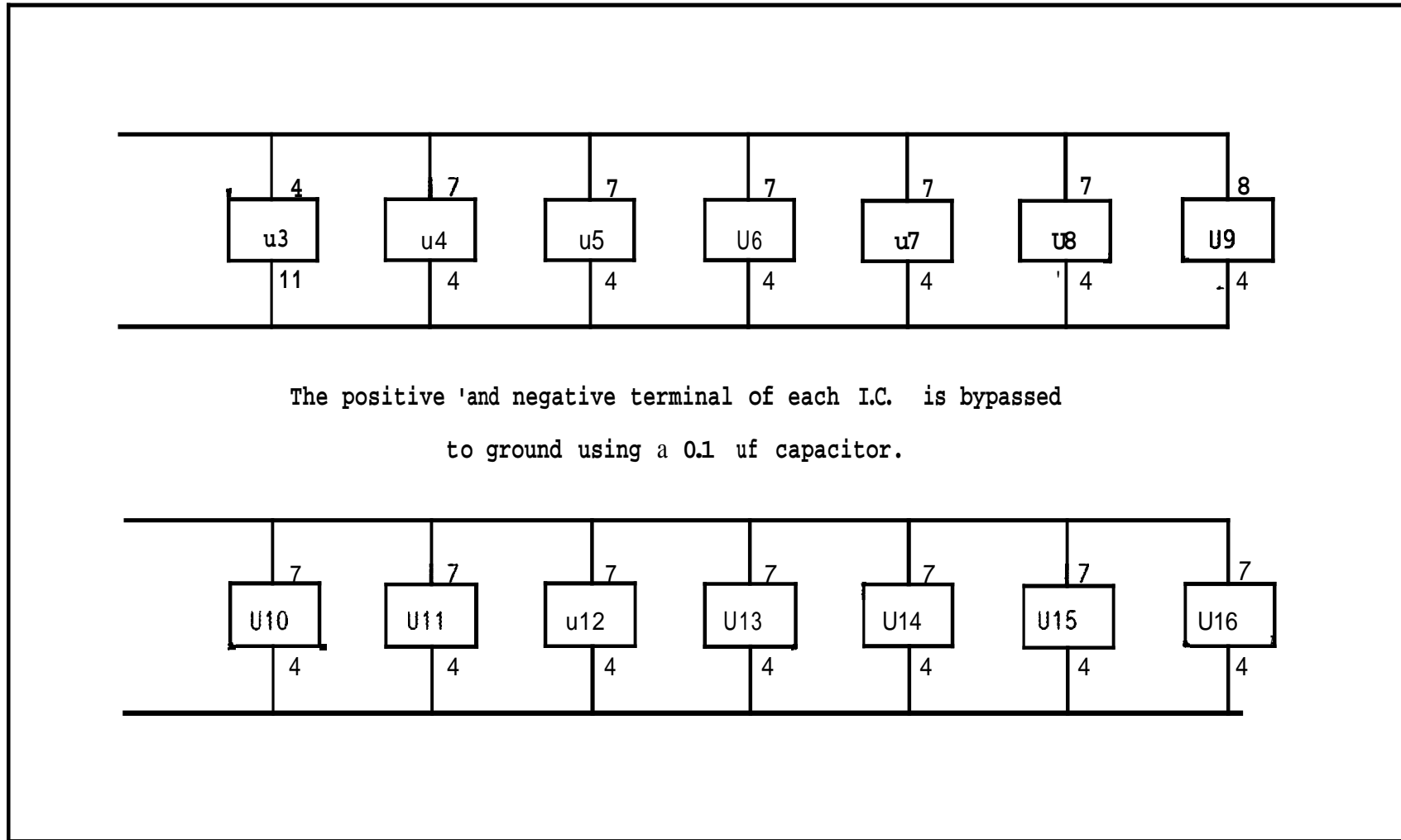
The power supply for both the Gaussmeter and generator offset channels is shown in Schematic 8. The transient suppressor, MOV1, is a must due to the harsh operating environment (i.e., voltage spikes in the A.C. supply would destroy the I.C.'s otherwise). Conventional three terminal regulators are used in the + 15 volt supplies. A stable source of 7.3 volts is provided to critical stages by the National Semiconductor LM399AH integrated circuit designated as U18. The temperature stability of this reference is better than 10 P.P.M. per degree centigrade. The distribution of power to the various integrated circuits is shown in Schematic 9.



Schematic 7. Circuits for generator current fluctuation amplifiers.



Schematic 8. Power supply for Hall Effect Diamagnetic Diagnostic instrument.



Schematic 9. Power distribution to integrated circuits.

Component parts list

## Integrated circuits

U1-U2	National Semiconductor Type	CD4520BC
U3	National Semiconductor Type	LF347N
U4-U6	National Semiconductor Type	LF351N
U7-U8	National Semiconductor Type	LM201
U9	National Semiconductor Type	LM311N
U10	National Semiconductor Type	LM201
U11-U16	National Semiconductor Type	LM301AN
U17	National Semiconductor Type	LM7815K
U18	National Semiconductor Type	LM399AH
U19	National Semiconductor Type	LM7915K

## Transistors

Q1	2N3904
Q2	TIP-31
Q3	TIP-32
Q4	2N3904

## Diodes

CR1	4 Amp 200 PIV Bridge Rectifier
LED1-LED8	T-1 3/4 size yellow light emitting diode

## Capacitors

C1	470 pf	500 V	Silver Mica
C2	33 pf	500 V	Silver Mica
C3-C5	0.1 uf	50 V	Disc Ceramic
C6	1 uf	50 V	Mylar
C7	4700 pf	100 V	Polystyrene - 2%
C8	1000 pf	100 V	Polystyrene - 2%

C9	1 uf	50 V	Mylar
C10-C11	470 uf	25 V	Electrolytic
C12-C13	30 pf	50 V	Polyester
C14-C15	1 uf	50 V	Mylar
C16	4700 pf	100 V	Polystyrene
C17-C18	0.1 uf	50 V	Disc Ceramic
C19	470 pf	100 V	Polystyrene
C20-C21	30 pf	50 V	Polyester
C22	10 uf	25 V	Electrolytic
C23-C27	30 pf	50 V	Polyester
C28-C31	2700 pf	100 V	Polystyrene
C32	7400 pf	100 V	Silver Mica
C33-C34	2000 uf	35 V	Electrolytic
C35-C37	10 uf	35 V	Electrolytic
C38-C39	0.1 uf	50 V	Disc Ceramic

## Variable Resistors

VR1	1 K	2 Watt	Range Calibrate
VR2	50 K	2 watt	PHASE
VR3	10 K 10 Turn	2 watt	OFFSET
VR4	10 K 10 Turn	2 watt	Generator OFFSET

## Fixed resistors

R1	75 K	1/4 watt	5%
R2	100	1/4 watt	5%
R3	470	1/4 watt	5%
R4	100	1/4 watt	5%
R5	4.7 K	1/4 watt	5%
R6-R7	24 K	1/2 watt	2%
R8	12 K	1/2 watt	2%
R9	2500	1/2 watt	1%
R10	8860	1/2 watt	1%
R11	2.2 K	1/2 watt	2%
R12-R13	51 K	1/4 watt	5%

R14-R14	91 K	1/4 watt	5%
R16	270	1/4 watt	5%
R17	27	2 watt	2%
R18	820 K	1/4 watt	5%
R19	330 K	1/4 watt	5%
R20	160 K	1/4 watt	5%
R21	75 K	1/4 watt	5%
R22	27 K	1/4 watt	5%
R23	11 K	1/4 watt	5%
R24	4.7 K	1/4 watt	5%
R25-R26	9.1 K	1/4 watt	5%
R27-R28	91 K	1/4 watt	5%
R29	9.1 K	1/4 watt	5%
R30	47 K	1/4 watt	5%
R31	4.7 K	1/4 watt	5%
R32	51 K	1/4 watt	5%
R33	215 K	1/2 watt	1%
R34	105.5 K	1/2 watt	1%
R35	8.94 M	1/2 watt	1/2%
R36	15 K	1/4 watt	5%
R37	43 K	1/4 watt	5%
R38	24 K	1/4 watt	5%
R39-R42	91 K	1/4 watt	5%
R43-R46	91 K	1/4 watt	5%
R47-R50	1.8 M	1/4 watt	5%
R51	10	1/4 watt	5%
R52	750	1 watt	1%
R53-R56	470	1/4 watt	5%

### Crystals

X1 3.58 MHz Crystal, Type used for color subcarrier in TV sets.

## Switches

S1 6 position rotary switch  
S2 DPDT Toggle Switch  
S3 DPST Toggle Switch

## Connectors

J1-J13 BNC UG-88C/U  
J14 6 pin cannon connector to fit Hall Probe  
J15 3 prong 120 VAC Socket, Chassis Mount

## Transformers and miscellaneous

T1 28:1 Transformer  
T2 36VCT 2 Amp  
MOV1 Metal Oxide Varister GE #V130LA10A  
F1 1 amp 250 V Fuse

APPENDIX B  
FORTRAN SOURCES FOR FWP AND FPR DATA ANALYSIS

The following FORTRAN program, FWPRDN, with subroutine GFWPR, runs on the FED PDP-10 computer and accesses the files in the EBT data base containing the diamagnetic data from ring turn-downs. The comments in the program provide all the instructions needed to load and run it for one familiar with the EBT data base and the earlier "RUNDOWN" program.

```

PROGRAM FWPRDN !K.H.CARPENTER 04OCT84
C
C Program used to process diamagnetic raw data files Annnn.FWP
C and Ammmmm.FPR from the EBT data base into partially reduced
C format files Annnn.FDN.
C Program is similar to RUNDWN except that resulting WPER values
C are not calibrated or corrected for cavity cross talk.
C Instead, output files are written to disk containing the average
C WPER signals, average Hall probe signals, and average generator
C signals and ion gauge pressure signals for further processing
C by other programs.
C One line of comments is added.
C Output files written to UNIT=7 with names
C Annnn.FDN if both .FWP and .FPR data files found,
C AnnnnW.FDN if only .FWP data file found,
C AmmmmmP.FDN if only .FPR data file found.
C
C
C TO RUN: LOAD FWPRDN,GFWPPR,@PUB:AG2TEK
C SAVE
C START
C
C THIS PROGRAM IS A MODIFIED VERSION OF FWPD2 - 23JUL83,
C FWPDWN - 16MAY83, AND KENDWN - 23JUN82.
C
C COMMON/CFWPPR/FWPR(0:1024,64),HFWP(817),HFPR(817)
C DIMENSIONS IN COMMON ARE THOSE NEEDED FOR DESCRIPTOR VERSIONS
C 005 FOR FWP AND 005 FOR FPR.
C DOUBLE PRECISION SFDN,WPDAT,PRDAT,WPTIM,PRTIM,FILT
C LOGICAL WP,PR,LDIF,NPLT,SAMET
C DIMENSION FWP(0:1024,32),FPR(0:1024,32)
C DIMENSION XPLT(4),RPLT(1024)
C DIMENSION IGOOD(64),IGCH(64),IGPR(64),WPMV(64)
C DIMENSION TSWP(6),TSPR(6),WPCOM(16),PRCOM(16),COM2(16),FIL2(2)
C EQUIVALENCE (FWP,FWPR),(FPR,FWPR(0,33))
C EQUIVALENCE (WPDAT,HFWP(4)),(WPTIM,HFWP(6)),(PRDAT,HFPR(4))
C EQUIVALENCE (PRTIM,HFPR(6)),(TSWP,HFWP(28)),(TSPR,HFPR(28))
C EQUIVALENCE (WPCOM,HFWP(34)),(PRCOM,HFPR(34))
C EQUIVALENCE (FILT,FIL2)

```

```

DATA IGOOD/64*1/,INI/0/,I1/1/,I2/1024/,IB/1/
C BEGIN MAIN LOOP:
10 WP=.TRUE.
PR=.TRUE.
TYPE 20
20 FORMAT(' Enter nnnn for Annnn.FWP file (0 for none, -1 to stop)'
1 ,': '$)
ACCEPT 30,NFWP
30 FORMAT(G)
IF(NFWP.LT.0)STOP
TYPE 40
40 FORMAT(' Enter mmmm for Ammmm.FPR file (0 for none): '$)
ACCEPT 30,NFPR
IF(NFPR.LT.0)STOP
IF(NFWP.EQ.0.AND.NFPR.EQ.0)GO TO 10
TYPE 50
50 FORMAT(' Enter SFD where .FWP and .FPR files located (return'
1 ,' for none. E.g., 830816')
ACCEPT 60,SFDN
60 FORMAT(A6)
C NEXT, GET DATA INTO COMMON FOR THESE FILES
CALL GFWPPR(NFWP,NFPR,SFDN,IFLWP,IFLPR)
IF(IFLWP.NE.0.AND.IFLPR.NE.0)GO TO 10
IF(NFPR.EQ.0.OR.IFLPR.NE.0)PR=.FALSE.
IF(NFWP.EQ.0.OR.IFLWP.NE.0)WP=.FALSE.
IF(.NOT.WP.AND..NOT.PR)GO TO 10
C TEST THAT .FWP AND .FPR DATA FOR SAME TURN-DOWN
SAMET=(WPDAT.NE.PRDAT.OR.WPTIM.NE.PRTIM)
IF(SAMET.AND.PR.AND.WP)TYPE 70
70 FORMAT(' WARNING: Check times below. .FWP and .FPR files'
1 /' may not be for same event.')
IF(WP)TYPE 80,WPDAT,WPTIM,TSWP,WPCOM
80 FORMAT(1X,2A10,6A5/1X,16A5)
IF(PR)TYPE 80,PRDAT,PRTIM,TSPPR,PRCOM
C IF(INI.EQ.0)TYPE 90
90 FORMAT(' NCH = channel, 0 to quit, -1 to abort;'
1 /' I1 = 1st sample, I2 = 2nd sample for plot; IB = baud/10')
INI=1
100 WRITE(5,110)
110 FORMAT('// ' Enter NCH,I1,I2,IB: '$)
READ(5,*)NS,I1,I2,IB
IF(NS)10,180,120
120 IF((.NOT.WP.AND.NS.LT.33).OR.(.NOT.PR.AND.NS.GT.32).OR.NS.GT.64)
1 GO TO 100
DO 130 K=I1,I2
130 RPLT(K-I1+2)=FWPR(K,NS)
CALL INITT(IB)
CALL BINITT
XPLT(1)=-1.
XPLT(2)=I2-I1+1
XPLT(3)=I1
XPLT(4)=1.
RPLT(1)=XPLT(2)

```

```

CALL CHECK(XPLT,RPLT)
CALL DSPLAY(XPLT,RPLT)
CALL MOVABS(0,50)
C   WRITE CHANNEL ID ON PLOT ACCORDING TO DSC VERSION
CALL ANMODE
   IF(NS.GT.32)GO TO 170
   IF(HFWP(3).EQ.'005 ')GO TO 140
   K1=28+NS*23
   K2=K1+2
140  GO TO 150
      K1=NS*24+27
      K2=K1+2
150  WRITE(5,160)(HFWP(K),K=K1,K2)
160  FORMAT(1X,3A5)
      GO TO 100
170  IF(HFPR(3).NE.'005 ')GO TO 100
      K1=(NS-32)*24+27
      K2=K1+2
      WRITE(5,160)(HFPR(K),K=K1,K2)
      GO TO 100
180  CALL MOVABS(0,720)
CALL ANMODE
WRITE(5,190)
190  FORMAT(' Enter limits of "BEFORE" then "AFTER" intervals:')
READ(5,*)IT1,IT2,IT3,IT4
C   Note: Only "BEFORE" limits used for pressure channels 33-56
C   and for all channels when "AFTER" time earlier than "BEFORE"
LDIF=IT1+IT2.GE.IT3+IT4
C   BAD CHANNEL IF DATA AT ADC LIMITS
RLOW=HFWP(16)
RHI=HFWP(15)
IF(WP)GO TO 195
RLOW=HFPR(16)
RHI=HFPR(15)
195  DO 220 I=1,64
      BEF=0.
      AFT=0.
      DO 200 J=IT1,IT2
         IF(FWPR(J,I).LE.RLOW.OR.FWPR(J,I).GE.RHI)IGOOD(I)=0
200  BEF=BEF+FWPR(J,I)
         IF(LDIF.OR.(I.GT.32.AND.I.LE.56))GO TO 215
      DO 210 J=IT3,IT4
         IF(FWPR(J,I).LE.RLOW.OR.FWPR(J,I).GE.RHI)IGOOD(I)=0
210  AFT=AFT+FWPR(J,I)
         IF(IT4.GT.IT3)AFT=AFT/(IT4-IT3+1)
215  IF(IT2.GT.IT1)BEF=BEF/(IT2-IT1+1)
220  WPMV(I)=(BEF-AFT)
C   OPTIONAL DISPLAY OF RAW TURNDOWN
CALL NEWPAG
   IF(.NOT.WP)GO TO 300
WRITE(5,270)
270  FORMAT(' Plot turn-down?(1=yes,0=no)')
READ(5,*)IP
IF(IP.NE.1)GO TO 300

```

```

CALL NEWPAG
XPLT(2)=32.
XPLT(3)=1.
RPLT(1)=32.
DO 280 K=1,32
280 RPLT(K+1)=WPMV(K)
CALL BINITT
CALL CHECK(XPLT,RPLT)
CALL DSPLAY(XPLT,RPLT)
CALL MOVABS(0,750)
CALL ANMODE
300 WRITE(5,305)
305 FORMAT(' BAD CHANNELS ARE:')
DO 310 I=1,64
310 IF(IGOOD(I).EQ.0)WRITE(5,*)I
WRITE(5,320)
320 FORMAT(' Enter channel nos. to change (end /,-1 clear,-2 rep.):')
DO 330 I=1,64
330 IGCH(I)=0
NPLT=.TRUE.
READ(5,*)IGCH
DO 340 I=1,64
IF(IGCH(I).LT.1.OR.IGCH(I).GT.64)GO TO 340
IGOOD(IGCH(I))=IGOOD(IGCH(I))-1
IGOOD(IGCH(I))=-IGOOD(IGCH(I))
340 IF(IGCH(I).EQ.-1)NPLT=.FALSE.
IF(NPLT)GO TO 360
DO 350 I=1,64
350 IGOOD(I)=1
360 DO 370 I=1,64
370 IF(IGCH(I).LE.-2)GO TO 100
C ASK FOR ENTRY OF DATA NOT IN DATA BASE:
CALL NEWPAG
WRITE(5,450)WPCOM,PRCOM
450 FORMAT(1X,16A5/1X,16A5/' Enter one line of additional comments:')
READ(5,460)COM2
460 FORMAT(16A5)
C WRITE DATA TO DISK FILE:
FIL2(1)=HFWP(2)
FIL2(2)='.DWN '
IF(.NOT.PR)FIL2(2)='W.DWN'
IF(WP)GO TO 490
FIL2(2)='P.DWN'
FIL2(1)=HFPR(2)
490 OPEN(UNIT=7,FILE=FILT,ACCESS='SEQOUT')
WRITE(7,500)(HFWP(K),K=1,14),WPCOM
500 FORMAT(14A5/(16A5))
WRITE(7,500)(HFPR(K),K=1,14),PRCOM,COM2
WRITE(7,510)(WPMV(K),K=1,64)
510 FORMAT(11F7.4/11F7.4/10F7.4/11F7.4/11F7.4/10F7.4)
DO 515 K=1,64
IGPR(K)=0
IF(WP.AND.(K.LE.32))IGPR(K)=IGOOD(K)
515 IF(PR.AND.(K.GT.32))IGPR(K)=IGOOD(K)

```

```

WRITE(7,520)IGPR,IT1,IT2,IT3,IT4
520 FORMAT(64I1,4I4)
CLOSE(UNIT=7)
WRITE(5,530)
530 FORMAT(' Write header files? (Y or N):'$)
READ(5,540)IAN
540 FORMAT(A1)
IF(IAN.NE.'Y'.AND.IAN.NE.'y')GO TO 10
IF(.NOT.WP)GO TO 550
FIL2(1)=HFWP(2)
FIL2(2)='W.HDR'
OPEN(UNIT=7,FILE=FILT,ACCESS='SEQOUT',MODE='IMAGE')
WRITE(7)HFWP
CLOSE(UNIT=7)
550 IF(.NOT.PR)GO TO 10
FIL2(1)=HFPR(2)
FIL2(2)='P.HDR'
OPEN(UNIT=7,FILE=FILT,ACCESS='SEQOUT',MODE='IMAGE')
WRITE(7)HFPR
GO TO 10
END

```

```

SUBROUTINE GFWPPR(NFWP,NFPR,SFDN,IFLWP,IFLPR)
C
C K.H.CARPENTER 04OCT83
C Routine to read data from .FWP and .FPR files in EBT data base
C into COMMON/CFWPPR/.
C Arguments on call:
C NFWP - INTEGER file sequence number for .FWP file
C NFPR - INTEGER file sequence number for .FPR file
C (zero for either means that file not wanted)
C SFDN - CHARACTER SFD name where .FWP and .FPR files
C are found (left justified, 6 characters max.)
C Must be blanks if no SFD.
C Path used is DSK:[210,2000,SFD].
C On return:
C IFLWP = 0 if no error in .FWP file input
C 1 if OPEN error
C -1 if data reading error
C IFLPR = 0 if no error in .FPR file input
C 1 if OPEN error
C -1 if data reading error
C Variables in COMMON copied from .FWP and .FPR files or
C set to zero if file not available or not wanted.
C
COMMON/CFWPPR/FWPR(0:1024,64),HFWP(817),HFPR(817)
C DIMENSIONS IN COMMON ARE THOSE NEEDED FOR DESCRIPTOR VERSIONS
C 005 FOR FWP AND 004 FOR FPR.
DOUBLE PRECISION SFDN
DIMENSION FSPEC(7),FWP(0:1024,32),FPR(0:1024,32),ICL(67234)
EQUIVALENCE (FWP,FWPR),(FPR(0,1),FWPR(0,33)),(ICL,FWPR(0,1))
EQUIVALENCE (NSW,HFWP(26)),(NSP,HFPR(26))
DATA FSPEC(7)/' '/'/
DO 5 K=1,67234

```

```

5      ICL(K)=0
      IFLWP=0
      IFLPR=0
      IF(NFWP.LE.0)GO TO 500
C      ENCODE FILESPEC AND OPEN .FWP FILE
      ENCODE(5,10,FWP)NFWP
10     FORMAT('A',I4)
C      CHANGE BLANKS IN NAME TO ZEROS
      FWP=FWP.OR."402010040
      ENCODE(30,20,FSPEC)FWP,SFDN
20     FORMAT('DSK:',A5,'.FWP[210,2000,','A6,']')
      TYPE 30,FSPEC
30     FORMAT(1X,7A5)
      OPEN(UNIT=50,ACCESS='SEQIN',MODE='IMAGE',DIALOG=FSPEC,ERR=1000)
C      READ IN HEADER FROM FILE
      READ(50,END=1010,ERR=1010)HFWP
C      CHECK THAT CORRECT FILE WAS FOUND
      IF((HFWP(1).NE.'03FWP').OR.(HFWP(2).NE.FWP))GO TO 1010
C      BRANCH ACCORDING TO DESCRIPTOR VERSION
      IF(HFWP(3).NE.'005 ')GO TO 100
C      CHECK THE NUMBER OF SAMPLES PER CHANNEL
      IF(NSW.GT.1024)GO TO 1010
      IF(NSW.LT.1024)GO TO 40
C      READ IN DATA
      READ(50,END=2020,ERR=1010)FWP
      CLOSE(UNIT=50)
      GO TO 500
40     DO 50 K=1,32
50     READ(50,END=2020,ERR=1010)(FWP(L,K),L=0,NSW)
      CLOSE(UNIT=50)
      GO TO 500
100    IF(HFWP(3).NE.'003 ')GO TO 200
      IF(HFWP(26).NE.HFWP(786).OR.NSW.GT.1024)GO TO 1010
C      TRANSFER DATA FROM HFWP INTO FWP
      DO 110 K=787,817
110    FWP(1,K-786)=HFWP(K)
      READ(50,END=1010,ERR=1010)FWP(1,32)
      READ(50,END=2020,ERR=1010)((FWP(K,L),L=1,32),K=2,NSW)
      DO 120 K=1,32
120    FWP(0,K)=HFWP(26)
      CLOSE(UNIT=50)
      GO TO 500
C      HANDLE OTHER DESCRIPTOR VERSIONS HERE
200    TYPE 210,FSPEC,HFWP(3)
210    FORMAT(1X,7A5,' uses DSC version ',A5,' not yet supported')
      IFLWP=-1
      GO TO 500
C
C      NEXT GET .FPR FILE AND DATA IN SAME MANNER AS FOR .FWP
500    IF(NFPR.LE.0)RETURN
C      ENCODE FILESPEC AND OPEN .FPR FILE
      ENCODE(5,10,FPR)NFPR
C      CHANGE BLANKS IN NAME TO ZEROS
      FPR=FPR.OR."402010040

```

```

ENCODE(30,520,FSPEC)FPRN,SFDN
520  FORMAT('DSK:',A5,'.FPR[210,2000],'A6,']')
      TYPE 30,FSPEC
      OPEN(UNIT=50,ACCESS='SEQIN',MODE='IMAGE',DIALOG=FSPEC,ERR=2000)
C     READ IN HEADER FROM FILE
      READ(50,END=2010,ERR=2010)HFPR
C     CHECK THAT CORRECT FILE WAS FOUND
      IF((HFPR(1).NE.'03FPR').OR.(HFPR(2).NE.FPRN))GO TO 2010
C     BRANCH ACCORDING TO DESCRIPTOR VERSION
      IF(HFPR(3).NE.'005 ')GO TO 600
C     CHECK THE NUMBER OF SAMPLES PER CHANNEL
      IF(NSP.NE.1024)GO TO 2010
C     READ IN DATA
      READ(50,END=2020,ERR=2010)FPR
      CLOSE(UNIT=50)
      RETURN
600  TYPE 210,FSPEC,HFPR(3)
      IFLPR=-1
      RETURN
C     ERROR MESSAGES AND RETURNS HERE
1000  TYPE 1005,FSPEC
1005  FORMAT(' OPEN ERROR FOR ',7A5)
      IFLWP=1
      GO TO 500
1010  TYPE 1015,FSPEC
1015  FORMAT(' DATA ERROR WITH ',7A5)
      IFLWP=-1
      GO TO 500
2000  TYPE 1005,FSPEC
      IFLPR=-1
      RETURN
2010  TYPE 1015,FSPEC
      IFLPR=-1
      RETURN
2020  TYPE 2030,FSPEC
2030  FORMAT(' WARNING: End of file reading ',7A5)
      RETURN
      END

```

APPENDIX C  
FORTRAN SOURCE CODES FOR EBT RING CURRENT SHEET MODELS

This appendix contains the FORTRAN sources for all the routines used to calculate magnetic fields and flux from the generalized current sheet model for the EBT electron rings. The primary routine is WPCSM, which is written as a subroutine to allow calls from other programs needing field or flux values. WPCSM is more general than the earlier code, WPERB, in that WPCSM allows the surface current distribution to vary with distance along the sheet. Extensive comments in the listing of the main subroutine, WPCSM, explain how to call it and interpret the results. The listing below includes the additional subroutines that WPCSM calls, and also includes a sample driver program, TPWCSM, which allows interactive entry of model parameters. Subroutine SOLBA, which is included in the listing, is not used by WPCSM as presently written, but could be substituted (with proper adjustment of normalization) when a constant surface current density is specified.

Subroutine SOLBA is included below to provide a corrected version and should be used in place of any version of earlier date. In particular, it should be used with the simpler current sheet code, WPERB, the listing for which was included in Appendix E of the corresponding report for 1981, ORNL/Sub-7676/2.

The following listing is in the form of a compressed file for the IBM 4341 VM/CMS computer, and includes command files to ease use. The FORTRAN should compile with few, if any, changes on the PDP-10 computer.

```
:READ WPCSM EXEC A1 TEMP 10/18/83 10:47:05
*Files for EBT ring field and flux modeling - most general version.
*K.H.Carpenter 18OCT83
&1 &2 COMPWPC EXEC A1
&1 &2 WPCSM FORTRAN A1
&1 &2 LOOPBA FORTRAN A1
&1 &2 SOLBAJ FORTRAN A1
&1 &2 DCEIB FORTRAN A1
&1 &2 SOLFBM FORTRAN A1
&1 &2 SOLBA FORTRAN A1
```

```

&1 &2 SGAUS8   FORTRAN  A1
&1 &2 ZEROIN   FORTRAN  A1
&1 &2 TWPCSM   FORTRAN  A1
* Files for EBT ring diamagnetic simulation
* using current sheet model with different
* possible surface current distributions.
* To load test program TWPCSM, first
* EXEC COMPWPC, then FORTVS TWPCSM,
* then GLOBAL TXTLIB VFORTLIB,
* then LOAD TWPCSM SOLFBM.
:READ COMPWPC EXEC      A1 TEMP  10/18/83 09:33:18
FORTVS WPCSM ( NOPRINT NOTERM
FORTVS LOOPBA ( NOPRINT NOTERM
FORTVS SOLBAJ ( NOPRINT NOTERM
FORTVS DCEIB ( NOPRINT NOTERM
FORTVS SOLFBM ( NOPRINT NOTERM
FORTVS SGAUS8 ( NOPRINT NOTERM
FORTVS ZEROIN ( NOPRINT NOTERM
:READ WPCSM   FORTRAN  A1 TEMP  10/18/83 09:33:19
SUBROUTINE WPCSM(WP,BTO,BRA,BPO,PHI,RHO,PSI,VMCL,VMCR,GA,AL,
1  RT,RSM,RC,AOFOC,AOFOL,AOFOR,DF,BF,RF,MODEL,IERR,IERF,IERB,IERN)
C   K.H.CARPENTER 02FEB83 - 08JUN83
C   K.H.C. 03JUN83 - Add additional offsets for outer sheets.
C
C   When MODEL = 1,
C       this subroutine calculates the "perpendicular energy"
C       in one annulus in one EBT cavity based on
C       the current sheet model described in ORNL/TM-7076,
C       and outputs the corresponding B field at a specified point.
C
C   When MODEL = 2,
C       the surface current distribution along the length of the
C       current sheet is changed from uniform to quadratic.
C
C   When MODEL = 3,
C       the surface current distribution is changed to Gaussian.
C
C   ARGUMENTS TO SET ON CALL:
C
C       MODEL =      1 - for uniform surface current
C                   2 - for quadratic surface current
C                   3 - for Gaussian surface current
C
C       PHI =        toroidal location at which to evaluate B
C                   (in degrees), zero is at midplane,
C                   positive to right (toward lower cav.no.)
C
C       RHO =         minor radius for B field calculation
C
C       PSI =         poloidal angle for B field cal.
C                   (in degrees) zero toward large
C                   major radius
C

```



C WP = perpendicular energy of annulus  
 C (in Joules)  
 C  
 C BTO = toroidal field component (in Gauss)  
 C (at PHI,RHO,PSI)  
 C  
 C BRA = radial field component (in Gauss)  
 C  
 C BPO = poloidal field component (in Gauss)  
 C  
 C RSM = ring mean radius (cm)  
 C  
 C RC = ring center offset towards larger  
 C major radius (cm)  
 C  
 C DF = unchanged if > 0 on call; set to  
 C calculated value if = 0 on call  
 C  
 C IERR = 0, if accuracy OK; 1, if subtraction  
 C caused WP to be lost in noise;  
 C -1, if argument in error on call;  
 C  
 C IERF = 10 if less than 8 digits accuracy  
 C from integration in SOLBAJ during  
 C flux linkage calculation;  
 C 20 if less than 3 digits accuracy  
 C possible.  
 C  
 C IERB = same as IERF but for calculation  
 C of fields due to central ring  
 C  
 C IERN = same as IERB but for neighbors  
 C

EXTERNAL ZERFUN  
 DOUBLE PRECISION RSD,SLD,RFD,ZFD,BRD,BZD,APD,DPI,RFD2  
 COMMON/CISOL/RSD,SLD,RFD,ZFD,BRD,BZD,APD  
 COMMON/CWPCSM/BZ,AMC  
 COMMON/CSOLFB/MOD,IEM  
 COMMON/CSOLF/FL,BL,XB,ZB,ADEG,CX,SX,XBR,BSX,BCX

C  
 C CONSTANTS PERTAINING TO EBT:  
 C ZB0 = Distance of pickup loop from midplane (cm)  
 C RB = Radius of pickup loop (cm)  
 C RM = Major radius (cm)  
 C ANC = No. of cavities  
 C AME = 2\*PI\*(electron mass)/(electron charge) in (Gauss/GHz)  
 C ATC = Total no. turns in series in pickup coils on one cavity  
 C TAU = Pickup loop voltage integration time constant (seconds).  
 C

DATA ZB0/9.5/,RB/30.0/,RM/150.0/,ANC/24.0/,AME/357.22/  
 DATA ATC/200.0/,TAU/0.1/  
 DATA DPI/3.141592653589793D0/

C ACCURACY LEVELS:  
 C ACC1 for loss of precision due to subtraction  
 C

```

C      NG      order of Gaussian integration
C      NSUB    no. of subdivisions over which to apply Gaussian int.
DATA ACC1/1.E-3/,NG/8/,NSUB/1/

C
C      COORDINATE TRANSFORMATIONS FOR ADJACENT CAVITIES:
DATA INI/0/,BOLD/0./,PHILD/0./
IF(INI.EQ.1.AND.PHI.EQ.PHILD)GO TO 10
INI=1
PHILD=PHI
ANR=2.*DPI/ANC
PH=PHI*DPI/180.
CNO=COS(PH)
SNO=SIN(PH)
CNL=COS(PH-ANR)
SNL=SIN(PH-ANR)
CNR=COS(PH+ANR)
SNR=SIN(PH+ANR)

C
C      TEST INPUT ARGUMENTS FOR RANGE:
10  IERR=0
IF(BF.LE.0..OR.GA.LE.0..OR.AL.LT.0..OR.RT.LE.0.)GO TO 100
IF(RF.LE.0.0)GO TO 100

C
C      IF RSM = 0:
C      FIND RING MEAN RADIUS AND CENTER FROM RESONANCE AT RF
C      (9GHZ for EBT-I) AND COLESTOCK FIELD MODEL
C      (WARNING - FIELD MODEL VALID ONLY FOR EBT-I/S)
C
IF(RSM.GT.0.)GO TO 15
RC=XR
RSM=RR
IF(BOLD.EQ.GA*BF/RF)GO TO 20
BOLD=GA*BF/RF
BZ=AME/BOLD
C
C      ZEROIN is zero finding routine by R. Brent
C      XOUT=ZEROIN(-2.,30.,ZERFUN,0.1)
C      XIN =ZEROIN(-30.,-2.,ZERFUN,0.1)
C      XR=0.5*(XOUT+XIN)
C      RC=XR
C      RR=0.5*(XOUT-XIN)
C      RSM=RR
C      GO TO 20

C
C      USE INPUT VALUES IF RSM 0:
15  BOLD=0.
XR=RC
RR=RSM
XOUT=RR+XR
XIN=-RR+XR

C
C      IF DF 0, CALCULATE DF FROM COLESTOCK FIELD MODEL AND FORMULA
C      DF=1.+0.5*LN(Bin/Bout)
C
C      20  IF(DF.LE.0)DF=1.+0.5*ALOG(PAT(XOUT-0.5*RT)/PAT(XOUT+0.5*RT))

```

```

DFM2=DF-2.
C
C   CALCULATE FLUX LINKAGE FOR 1 TURN DUE TO ANNULUS IN SAME CAVITY
RSD=RR-Ø.5*RT
  IF(RSD.LE.Ø.DØ)GO TO 1ØØ
SLD=AL
BL=RB
  ADEG=Ø.
  XB=XR
  ZB=ZBØ
CALL SOLFM(NG,NSUB,MODEL)
IERF=IEM
  FS1T=FL*DFM2
RSD=RSD+RT
XB=XR-AOFOC*RT
CALL SOLFM(NG,NSUB,MODEL)
IERF=MAXØ(IERF,IEM)
  FS1T=FS1T+FL*DF
  IF(FS1T/FL.LT.ACC1)GO TO 2ØØ
C
C
C   CALCULATE SURFACE CURRENTS FOR USE IN FIELD CALCULATIONS AS
C   AL * muØ * M/4PI in Gauss (times length unit squared)
AMØ=5.E+4*TAU/(ATC*FS1T*BL)
AMC=AMØ*VMC
AML=AMØ*VMCL
AMR=AMØ*VMCR
C   Note: If AOFOC, AOFOL, and AOFOR are not all the same value then
C   the 1 turn flux linkage should be recalculated for each neighbor
C   and the separate values used to find surface currents for each of
C   the three rings. However, if changing AOFOC (or AOFOL or AOFOR)
C   causes a significant change in the 1 turn flux linkage then the
C   routine used to decouple the flux loop signals must be modified to
C   take this into account. By test runs, observing AMØ for various
C   AOFOC, we find that AMØ is insensitive to AOFOC for all reasonable
C   choices of ring parameters. For a typical case AMC changed from
C   82.792 to 82.327 to 81.645 when AOFOC changed from Ø to .5 to 1.
C
C   CALCULATE FIELDS DUE TO CENTRAL ANNULUS:
C   FIRST FOR OUTER CURRENT SHEET -
C
C   GET COORDINATES IN ANNULUS FRAME FROM TOROIDAL
PS=DPI*PSI/18Ø.
SPS=SIN(PS)
CPS=COS(PS)
RFS=RHO*SPS
RSR=RM+RHO*CPS
RFC=RSR*CNO-RM-RC+AOFOC*RT
RFD2=RFS*RFS+RFC*RFC
RFD=DSQRT(RFD2)
ZFD=-RSR*SNO
CALL SOLBM(MODEL)
IERB=IEM
BRØ=BRD*DF

```

```

BZØ=BZD*DF
C  TRANSFORM FIELDS TO TOROIDAL COORDINATES:
   CPHS=RFC/RFD
   SPHS=RFS/RFD
   BRAC=BRØ*(CPHS*CPS*CNO+SPHS*SPS)-BZØ*CPS*SNO
   BTOC=-BRØ*CPHS*SNO-BZØ*CNO
   BPOC=BRØ*(-CPHS*SPS*CNO+SPHS*CPS)+BZØ*SPS*SNO
C
C  NEXT FOR INNER CURRENT SHEET -
   RFC=RFC-AOFOC*RT
   RFD2=RFS*RFS+RFC*RFC
   RFD=DSQRT(RFD2)
   RSD=RSD-RT
   CALL SOLBM(MODEL)
   IERB=MAXØ(IERB,IEM)
   BRØ=BRD*DFM2
   BZØ=BZD*DFM2
C  TRANSFORM FIELDS TO TOROIDAL COORDINAGES:
   CPHS=RFC/RFD
   SPHS=RFS/RFD
   BRAC=BRAC+BRØ*(CPHS*CPS*CNO+SPHS*SPS)-BZØ*CPS*SNO
   BTOC=BTOC-BRØ*CPHS*SNO-BZØ*CNO
   BPOC=BPOC+BRØ*(-CPHS*SPS*CNO+SPHS*CPS)+BZØ*SPS*SNO
C
C  CALCULATE FIELDS DUE TO ADJACENT CAVITIES' ANNULI:
C  CAVITY ON RIGHT - INNER CURRENT SHEET
   RFC=RSR*CNR-RM-RC
   RFD2=RFS*RFS+RFC*RFC
   RFD=DSQRT(RFD2)
   ZFD=-RSR*SNR
   CALL SOLBM(MODEL)
   IERN=IEM
   BR1=BRD*DFM2
   BZ1=BZD*DFM2
C  TRANSFORM FIELDS TO TOROIDAL COORD.:
   CPHS=RFC/RFD
   SPHS=RFS/RFD
   BRAR=BR1*(CPHS*CPS*CNR+SPHS*SPS)-BZ1*CPS*SNR
   BTOR=-BR1*CPHS*SNR-BZ1*CNR
   BPOR=BR1*(-CPHS*SPS*CNR+SPHS*CPS)+BZ1*SPS*SNR
C
C  OUTER CURRENT SHEET -
   RSD=RSD+RT
   RFC=RFC+AOFOR*RT
   RFD2=RFS*RFS+RFC*RFC
   RFD=DSQRT(RFD2)
   CALL SOLBM(MODEL)
   IERN=MAXØ(IERN,IEM)
   BR1=BRD*DF
   BZ1=BZD*DF
C  TRANSFORM FIELDS TO TOROIDAL COORD.:
   CPHS=RFC/RFD
   SPHS=RFS/RFD
   BRAR=BRAR+BR1*(CPHS*CPS*CNR+SPHS*SPS)-BZ1*CPS*SNR

```

```

BTOR=BTOR-BR1*CPHS*SNR-BZ1*CNR
BPOR=BPOR+BR1*(-CPHS*SPS*CNR+SPHS*CPS)+BZ1*SPS*SNR
C   CAVITY ON LEFT - OUTER CURRENT SHEET
RFC=RSR*CNL-RM-RC+AOFOL*RT
RFD2=RFS*RFS+RFC*RFC
RFD=DSQRT(RFD2)
ZFD=-RSR*SNL
CALL SOLBM(MODEL)
IERN=MAX0(IERN,IEM)
BR2=BRD*DF
BZ2=BZD*DF
C   TRANSFORM TO TOROIDAL COORD.:
CPHS=RFC/RFD
SPHS=RFS/RFD
BRAL=BR2*(CPHS*CPS*CNL+SPHS*SPS)-BZ2*CPS*SNL
BTOL=-BR2*CPHS*SNL-BZ2*CNL
BPOL=BR2*(-CPHS*SPS*CNL+SPHS*CPS)+BZ2*SPS*SNL
C
C   INNER CURRENT SHEET -
RSD=RSD-RT
RFC=RFC-AOFOL*RT
RFD2=RFS*RFS+RFC*RFC
RFD=DSQRT(RFD2)
CALL SOLBM(MODEL)
IERN=MAX0(IERN,IEM)
BR2=BRD*DFM2
BZ2=BZD*DFM2
C   TRANSFORM TO TOROIDAL COORD.:
CPHS=RFC/RFD
SPHS=RFS/RFD
BRAL=BRAL+BR2*(CPHS*CPS*CNL+SPHS*SPS)-BZ2*CPS*SNL
BTOL=BTOL-BR2*CPHS*SNL-BZ2*CNL
BPOL=BPOL+BR2*(-CPHS*SPS*CNL+SPHS*CPS)+BZ2*SPS*SNL
C
C   COMBINE RESULTS AND APPLY SCALE FACTORS:
C   NUMERICAL FACTOR IN NEXT LINE TAKES INTO ACCOUNT LENGTHS IN CM NOT
C   M, AND VMC IN MILLIVOLTS NOT VOLTS.
WP=1.E-2*DPI*VMC*AME*TAU*ABS(RF)*RT*RR/(ATC*FS1T*BL)
C   If not a constant current distribution, WP must be multiplied by
C   the area under the actual distribution (ratioed to that under a
C   constant one).
IF(MODEL.EQ.2)WP=WP*0.942809041D0
IF(MODEL.EQ.3)WP=WP*1.04474065965D0
BRA=BRAC*AMC+BRAL*AML+BRAR*AMR
BTO=BTOC*AMC+BTOL*AML+BTOR*AMR
BPO=BPOC*AMC+BPOL*AML+BPOR*AMR
RETURN
C
C   ERROR RETURNS:
100 IERR=-1
RETURN
200 IERR=1
RETURN
END

```

```

FUNCTION ZERFUN(X)
COMMON/CWPCSM/BZ,AMC
ZERFUN=BZ-PAT(X)
RETURN
END

FUNCTION PAT(X)
C Colestock fit to midplane field in EBT-I/S restricted to zero
C angle.
T2=0.
R=X
IF(X.GE.0.)GO TO 10
T2=3.14159**2
10 R=-X
PT=T2*(1.-3.724E-2*T2)
C1=(PT+20.81)*1.046E-4
C2=C1-2.04158E-3
C3=(PT+12.43)*.5966
AL=C1+C2*SIN((R-13.8)/C3)
PAT=EXP(-AL*((X+2.90281)**2))
RETURN
END
:READ LOOPBA FORTRAN A1 TEMP 10/18/83 09:33:21
SUBROUTINE LOOPBA
IMPLICIT REAL*8 (A-H,O-Z)
COMMON/CLOOP/A,R,Z,BR,BZ,AP
C K.H.Carpenter 14FEB83
C LOOPBA calculates magnetic field and vector potential
C for a circular loop.
C Cylindrical coordinates are used with loop having
C radius A, lying in Z=0 plane, center at origin.
C Field point is R, Z.
C A, R, Z must be set in COMMON/CLOOP/ on call.
C On return field values are set in COMMON:
C BR = flux density radial component
C BZ = flux density axial component
C AP = vector potential azimuthal component.
C
C All output values are normalized to the loop current
C and to permeability. To obtain dimensional values
C multiply all output values by current times permeability
C divided by 4*PI.
C
C A, R, and Z must be input in the same units of length as
C those used in the (SI) units for permeability.
C (I.,e., if I is in Amperes and A, R, Z in meters, to
C get BR, BZ in Tesla and AP in Weber/m, multiply values
C returned by I*10**-7.
C If A, R, Z are in cm and I in Amp, to get BR, BZ in Gauss
C and AP in Gauss-cm, multiply values returned by I/10.)
C
C No test is made on input arguments.
C Accuracy will be reduced if R is near A and Z is near zero

```

```

C      so that the argument to the elliptic integral routine is
C      near one.
C      If R=A and Z=0, OVERFLOW will occur.
C
      IF(R.EQ.0.D0)GO TO 10
      AK2=4.D0*A*R/((A+R)*(A+R)+Z*Z)
      CALL DCEIB(RK,RE,AK2)
      AK=DSQRT(AK2)
      OMK2=1.D0-.5D0*AK2
      AP=4.D0*DSQRT(A/R)*(OMK2*RK-RE)/AK
      DR=AK/DSQRT(4.D0*A*R)
      BR=2.D0*Z*DR*(OMK2*RE/(1.D0-AK2)-RK)/R
      BZ=2.D0*DR*(RK+RE*(A*A-R*R-Z*Z)/((A-R)*(A-R)+Z*Z))
      RETURN
10    BR=0.D0
      AP=0.D0
      DN=DSQRT(Z*Z+A*A)
      BZ=6.2831 85307 17958 64769 25287 D0 *A*A/(DN*DN*DN)
      RETURN
      END
:READ  SOLBAJ  FORTRAN  A1  TEMP  10/18/83 09:33:22
SUBROUTINE SOLBAJ(AJ,A,B,IER1)
C      K.H.Carpenter 25FEB83 - 08JUN83
      IMPLICIT REAL*8 (A-H,O-Z)
      COMMON/CISOL/RSD,SLD,RFD,ZFD,BRD,BZD,APD
      COMMON/CISOLE/ABSERR
      COMMON/CLOOP/AR,R,Z,BR,BZ,AP
C
C      SOLBAJ calculates the B-field and A-field components for
C      a solenoidal current sheet with surface current distribution
C      given by DOUBLE PRECISION FUNCTION AJ(ZN).
C      Field components are calculated by numerical integration of
C      the corresponding components due to a one-turn circular loop.
C      One-turn components are calculated by routine LOOPBA.
C      Integration is carried out using the 21 point Gauss-Kronrod rule
C      as implemented in the adaptive integration routine QAGS.
C      The integration routine used below is a version, modified to
C      allow simultaneous integration of all three field components,
C      of SUBROUTINE QUARUL, which is called by QAGS and is contained
C      in the source listing of QAGS. QAGS is from "QUADPACK",
C      IBM/370, DOUBLE PRECISION version, dated 15May79, developed by
C      Technische Universitat Wien and Katholieke Uniwersiteit Leuven.
C      See comments in the source listing of QUARUL, and P.W.Gaffney,
C      "Information and Advice on Numerical Software," ORNL/CSD/TM-147,
C      May 1981, for more details on the numerical method.
C      Comment lines headed "CQ" below are taken from the routine QUARUL.
C
C      Before call to SOLBAJ the calling program must set variables
C      RSD,SLD,RFD,ZFD in COMMON/CISOL. On return the field component
C      values are found in BRD,BZD, and APD in COMMON/CISOL.
C****
C      SOLBAJ AND SOLBA GIVE IDENTICAL RESULTS
C      WHEN AJ(ZN)=1 FOR ALL ZN AND A=-.5, B=.5,
C      E X C E P T that BRD and BZD as returned by SOLBAJ must be

```

```

C      multiplied by SLD to obtain the values returned by SOLBA.
C****
C      Input values:
C
C      RSD - RADIUS OF SOLENOID CURRENT SHEET
C      SLD - LENGTH OF SOLENOID CURRENT SHEET BETWEEN HALF-MAXIMUMS
C            OF CURRENT DISTRIBUTION AJ
C      RFD - FIELD POINT RADIAL DISTANCE FROM SOLENOID AXIS
C      ZFD - FIELD POINT AXIAL DISTANCE FROM CENTER OF SOLENOID
C      (Input values can be in any unit of length, but all four must
C        be in the same units. Choice of units will affect normalization
C        of results.)
C
C      ARGUMENTS:
C      AJ      - FUNCTION SUBPROGRAM DEFINING SURFACE CURRENT
C                DENSITY FUNCTION AJ(ZN). THE ACTUAL NAME FOR AJ
C                NEEDS TO BE DECLARED E X T E R N A L IN THE
C                CALLING PROGRAM. ARGUMENT ZN IS DISTANCE ALONG
C                SOLENOID AXIS DIVIDED BY SLD. (THUS IF MAXIMUM
C                OF AJ IS AT ZN=0 THEN AJ(0.5)=0.5*AJ(0).)
C
C      A      - LOWER LIMIT OF INTEGRATION DIVIDED BY SLD
C
C      B      - UPPER LIMIT OF INTEGRATION DIVIDED BY SLD
C
C****
C      Output values:
C
C      BRD - NORMALIZED RADIAL FIELD COMPONENT
C      BZD - NORMALIZED AXIAL FIELD COMPONENT
C      APD - NORMALIZED ANGULAR VECTOR POTENTIAL COMPONENT
C      IER1- PRECISION INDICATOR
C      To obtain dimensional values for components:
C      Multiply all components by surface current density at Z=0
C      (in Amps per unit of length used to input SLD),
C      and divide by AJ(0). (If AJ(0)=0, use another Z.)
C      Multiply all components by permeability divided by 4 times pi.
C      Multiply all components by SLD.
C      See comments in LOOPBA for examples.
C
C      BRD, BZD, and APD are the results of approximating the
C      integrals of the one-turn loop components over the
C      normalized interval A to B
C      BY APPLYING THE 21-POINT
C      GAUSS-KRONROD RULE (RESK), OBTAINED BY OPTIMAL
C      ADDITION OF ABSCISSAE TO THE 10-POINT GAUSS
C      RULE (RESG).
C
C      Internal values calculated:
C      ABSERR(K) - ESTIMATE OF THE MODULI OF THE ABSOLUTE ERRORS
C                WHICH SHOULD NOT EXCEED ABS(I-RESULT)
C
C      RESABS(K) - APPROXIMATIONS TO THE INTEGRALS OF THE
C                ABSOLUTE VALUES OF THE FIELD COMPONENTS

```

C  
C  
C Argument IER1 is set on output by testing of ABSERR(K).  
C IER1=0 for 8 digits or better precision  
C IER1=10 for 3 to 8 digits precision  
C IER1=20 for less than 3 digits precision for least precise  
C component  
C

CQ

DIMENSION FV1(3,10),FV2(3,10),XGK(11),WGK(11),WG(10)  
DIMENSION RESG(3),RESK(3),RESKH(3),RESASC(3),FC(3)  
DIMENSION RESABS(3),RESULT(3),ABSERR(3)

CQ THE ABCISSAE AND WEIGHTS ARE GIVEN FOR THE INTERVAL (-1,1).  
CQ BECAUSE OF SYMMETRY ONLY THE POSITIVE ABCISSAE AND THEIR  
CQ CORRESPONDING WEIGHTS ARE GIVEN.

CQ

CQ XGK - ABCISSAE OF THE 21-POINT GAUSS-KRONROD RULE :  
CQ XGK(2), XGK(4), ... ABCISSAE OF THE 10-POINT  
CQ GAUSS RULE  
CQ XGK(1), XGK(3), ... ABCISSAE WHICH ARE OPTIMALLY  
CQ ADDED TO THE 10-POINT GAUSS RULE

CQ

CQ WGK - WEIGHTS OF THE 21-POINT GAUSS-KRONROD RULE

CQ

CQ WG - WEIGHTS OF THE 10-POINT GAUSS RULE, CORRESPONDING  
CQ TO THE ABCISSAE XGK(2), XGK(4), ...  
CQ WG(1), WG(3), ... ARE SET TO ZERO.  
CQ

CQ

DATA XGK(1),XGK(2),XGK(3),XGK(4),XGK(5),XGK(6),XGK(7),  
\* XGK(8),XGK(9),XGK(10),XGK(11)/  
\* 0.9956571630258081D+00, 0.9739065285171717D+00,  
\* 0.9301574913557082D+00, 0.8650633666889845D+00,  
\* 0.7808177265864169D+00, 0.6794095682990244D+00,  
\* 0.5627571346686047D+00, 0.4333953941292472D+00,  
\* 0.2943928627014602D+00, 0.1488743389816312D+00,  
\* 0.0000000000000000D+00/

CQ

DATA WGK(1),WGK(2),WGK(3),WGK(4),WGK(5),WGK(6),WGK(7),  
\* WGK(8),WGK(9),WGK(10),WGK(11)/  
\* 0.1169463886737187D-01, 0.3255816230796473D-01,  
\* 0.5475589657435200D-01, 0.7503967481091995D-01,  
\* 0.9312545458369761D-01, 0.1093871588022976D+00,  
\* 0.1234919762620659D+00, 0.1347092173114733D+00,  
\* 0.1427759385770601D+00, 0.1477391049013385D+00,  
\* 0.1494455540029169D+00/

CQ

DATA WG(1),WG(2),WG(3),WG(4),WG(5),WG(6),WG(7),WG(8),  
\* WG(9),WG(10)/  
\* 0.0000000000000000D+00, 0.6667134430868814D-01,  
\* 0.0000000000000000D+00, 0.1494513491505806D+00,  
\* 0.0000000000000000D+00, 0.2190863625159820D+00,  
\* 0.0000000000000000D+00, 0.2692667193099964D+00,  
\* 0.0000000000000000D+00, 0.2955242247147529D+00/

CQ

CQ

```

CQ          MACHINE DEPENDENT CONSTANT
CQ          -----
CQ          "EPMACH" IS THE RELATIVE MACHINE ACCURACY
CQ          (ABOUT 0.3D-15 FOR A 56-BIT MACHINE)
CQ
CQ          DATA EPMACH/0.3D-15/
CQ
CQ          LIST OF MAJOR VARIABLES
CQ          -----
CQ          CENTRE - MID POINT OF THE INTERVAL
CQ          HLGTH - HALF LENGTH OF THE INTERVAL
CQ          ABSC - ABSCISSA
CQ          FV* - FUNCTION VALUE
CQ          RESG - 10-POINT GAUSS FORMULA
CQ          RESK - 21-POINT GAUSS-KRONROD FORMULA
CQ          RESKH - APPROXIMATION TO MEAN VALUE OF F OVER (A,B), I.E.
CQ                  TO I/(B-A)
CQ          RESASC - APPROXIMATION TO INTEGRAL OF ABS(F-RESKH) OVER
CQ                  (A,B)
CQ
CQ          IER1=0
CQ          CENTRE = 0.5D+00*(A+B)
CQ          HLGTH = 0.5D+00*(B-A)
CQ          DHLGTH = DABS(HLGTH)
CQ
CQ          COMPUTE THE 21-POINT GAUSS-KRONROD APPROXIMATION TO
CQ          THE INTEGRAL, AND ESTIMATE THE ABSOLUTE ERROR
CQ
CQ          DO 2 K=1,3
2          RESG(K) = 0.0D+00
          AR=RSD
          R=RFD
          Z=ZFD
          CALL LOOPBA
          AJ1=AJ(CENTRE)
          FC(1)=BR*AJ1
          FC(2)=BZ*AJ1
          FC(3)=AP*AJ1
          DO 3 K=1,3
3          RESK(K)=WGK(11)*FC(K)
          RESABS(K)=DABS(RESK(K))
          DO 10 J=1,10
            ABSC = HLGTH*XGK(J)
            Z=ZFD-(CENTRE-ABSC)*SLD
            CALL LOOPBA
            AJ1=AJ(CENTRE-ABSC)
            FV1(1,J)=BR*AJ1
            FV1(2,J)=BZ*AJ1
            FV1(3,J)=AP*AJ1
            Z=ZFD-(CENTRE+ABSC)*SLD
            CALL LOOPBA
            AJ1=AJ(CENTRE+ABSC)
            FV2(1,J)=BR*AJ1
            FV2(2,J)=BZ*AJ1

```

```

FV2(3,J)=AP*AJ1
DO 5 K=1,3
FSUM=FV1(K,J)+FV2(K,J)
RESG(K)=RESG(K)+WG(J)*FSUM
RESK(K)=RESK(K)+WGK(J)*FSUM
5 RESABS(K)=RESABS(K)+WGK(J)*(DABS(FV1(K,J))+DABS(FV2(K,J)))
10 CONTINUE
DO 25 K=1,3
RESKH(K) = RESK(K)*0.5D+00
RESASC(K) = WGK(11)*DABS(FC(K)-RESKH(K))
DO 20 J=1,10
RESASC(K) = RESASC(K)+WGK(J)*(DABS(FV1(K,J)-RESKH(K))
1 +DABS(FV2(K,J)-RESKH(K)))
20 CONTINUE
RESULT(K) = RESK(K)*HLGTH
RESABS(K) = RESABS(K)*DHLGTH
RESASC(K) = RESASC(K)*DHLGTH
ABSERR(K) = DABS((RESK(K)-RESG(K))*HLGTH)
IF(RESASC(K).NE.0.D+00) ABSERR(K) = DMAX1(EPMACH*RESABS(K)*0.5D+02
*,RESASC(K)*DMIN1(0.1D+01,DSQRT((0.2D+03*ABSERR(K)/RESASC(K))**3)))
C
C Now set IER1
C IF(RESULT(K).NE.0.D0)ABSERR(K)=ABSERR(K)/DABS(RESULT(K))
C IF(IER1.EQ.0.AND.ABSERR(K).GT.1.D-8)IER1=10
C IF(ABSERR(K).GT.1.D-3)IER1=20
25 CONTINUE
C Calculate final results and return
BRD=RESULT(1)
BZD=RESULT(2)
APD=RESULT(3)
RETURN
END
:READ DCEIB FORTRAN A1 TEMP 10/18/83 09:33:23
SUBROUTINE DCEIB(RK,RE,AK2)
IMPLICIT REAL*8 (A-H,O-Z)
C K.H.Carpenter 11FEB83
C Calculates complete elliptic integrals of 1st and 2nd kind.
C AK2 is input argument,
C RK is resultant value of elliptic integral of 1st kind,
C RE is resultant value of elliptic integral of 2nd kind.
C RK = int. 0 to PI/2 of (1 - AK2*SIN(TH)**2)**-.5 dTH
C RE = int. 0 to PI/2 of (1 - AK2*SIN(TH)**2)**+.5 dTH
C
C ALL VARIABLES ARE REAL*8.
C
C Precision of result depends on value of AK2.
C For AK.LT..99, precision is 16 decimal digits.
C For AK2=.9999999999999999, precision is 4 digits.
C
C Maximum iterations required is 8;
C not over 6 iterations required when AK2.LE..99.
C
C DIVIDE CHECK is forced for RK when AK2=1.
C

```

```

DATA PI2/1.570796326794897D0/, P/0.D0/
A=1.D0
B=DSQRT(1.D0-AK2)
IF(B.LE.P)GO TO 30
C=0.5D0*AK2
CM=0.25D0
10 T=A-B
IF(T.LE.P)GO TO 20
A1=A
A=0.5D0*(A+B)
B=DSQRT(A1*B)
C=C+CM*T*T
CM=CM*2.D0
GO TO 10
20 RK=PI2/A
RE=RK-RK*C
RETURN
30 RE=1.D0
A1=0.D0
RK=RE/A1
RETURN
END
:READ SOLFBM FORTRAN A1 TEMP 10/18/83 09:33:23
SUBROUTINE SOLFM(NG,NSUB,MODEL)
C K.H.Carpenter 08JUN83
C If MODEL=1, SOLFM is identical to SOLF(NG,NSUB);
C if MODEL=2, SOLBAJ with a quadratic distribution is substituted
C for SOLBA; if MODEL=3, a Gaussian distribution is substituted.
C SUBROUTINE SOLF(NG,NSUB)
C K.H.CARPENTER 28JUL81
C COPIED FROM VERSION OF 07JUL81 ON PDP-10
C USES GAUSSIAN INTEGRATION TO PERFORM (NORMALIZED) INTEGRAL
C OF EQ(26), ORNL/TM-7076.
C NG IS ORDER OF GAUSSIAN INTEGRATION; NSUB IS NUMBER OF
C SUBDIVISIONS OF THE CIRCLE OVER WHICH GAUSSIAN INTEGRATION IS
C APPLIED.
C RETURNS NORMALIZED FLUX LINKAGE IN A CIRCULAR LOOP DUE TO A
C CYLINDRICAL CURRENT SHEET.
C ARGUMENTS PASSED IN COMMONS /CSOLF/ AND /CISOL/.
C CALLING PROGRAM MUST SET CURRENT SHEET PARAMETERS IN /CISOL/:
C RADIUS RSD, LENGTH SLD
C CALLING PROGRAM MUST SET LOOP PARAMETERS IN /CSOLF/:
C RADIUS BL, CENTER IN SHEET COORDINATES XB,ZB,
C ANGLE IN DEGREES OF LOOP NORMAL TO SHEET AXIS, ADEG
C NORMALIZED FLUX LINKAGE IS RETURNED AS FL IN /CSOLF/.
C FL=FLUX*2*PI/MU0/BL/SLD/CURDEN
C
DOUBLE PRECISION DPI
EXTERNAL SOFUN
COMMON/CSOLF/FL,BL,XB,ZB,ADEG,CX,SX,XBR,BSX,BCX
COMMON/CSOLFB/MOD,IEM
DATA DPI/3.141592653589793D0/
MOD=MODEL
IEM=0

```

```

ANX=DPI*ADEG/180.
CX=COS(ANX)
SX=SIN(ANX)
XBR=SB/BL
BSX=BL*SX
BCX=BL*CX
C   IF INTEGRATION NOT REQUIRED DUE TO SYMMETRY, SKIP IT.
   IF((ADEG.EQ.0..OR.ADEG.EQ.180.).AND.(XB.EQ.0.))GO TO 10
   CALL SGAUS8(0.D0,DPI,NSUB,ANSWER,SOFUN,NG)
   FL=ANSWER
   RETURN
10  FL=DPI*SOFUN(0.)
   RETURN
   END
   FUNCTION SOFUN(ALP)
   DOUBLE PRECISION RSD,SLD,RFD,ZFD,BRD,BZD,APD
   EXTERNAL AJQUAD,AJGAUS,AJONE
   COMMON/CISOL/RSD,SLD,RFD,ZFD,BRD,BZD,APD
   COMMON/CSOLF/FL,BL,XB,ZB,ADEG,CX,SX,XBR,BSX,BCX
   COMMON/CSOLFB/MOD,IEM
   A=ALP
   SA=SIN(A)
   CA=COS(A)
   ZFD=ZB-BSX*CA
   RFD=SQRT((BL*SA)**2+(XB+BCX*CA)**2)
   IF(MOD-2)20,30,40
20  CALL SOLBAJ(AJONE,-0.5D0,0.5D0,IE)
   GO TO 50
30  CALL SOLBAJ(AJQUAD,-0.707106781D0,+0.707106781D0,IE)
   GO TO 50
40  CALL SOLBAJ(AJGAUS,-1.D0,1.D0,IE)
50  IF(IE.NE.0)IEM=MAX0(IE,IEM)
   SOFUN=APD*(BCX+XB*CA)/RFD
   RETURN
   END
   FUNCTION AJONE(X)
   IMPLICIT REAL*8 (A-H,0-Z)
C   Constant distribution function. K.H.Carpenter 07JUN83
   AJONE=1.D0
   RETURN
   END
   FUNCTION AJQUAD(X)
   IMPLICIT REAL*8 (A-H,0-Z)
C   Quadratic distribution function. K.H.Carpenter 07JUN83
C   Yields max. of 1 for zero argument, .5 for + or - .5 .
   AJQUAD=1.D0-2.D0*X*X
   RETURN
   END
   FUNCTION AJGAUS(X)
C   Gaussian distribution function. K.H.Carpenter 07JUN83
C   Yields max. of 1 for zero argument, .5 for + or - .5 .
   IMPLICIT REAL*8 (A-H,0-Z)
   DATA FTLN2/2.772588722D0/
   AJGAUS=DEXP(-X*X*FTLN2)

```

```

RETURN
END
SUBROUTINE SOLBM(MODEL)
C   K.H.Carpenter 07JUN83
C   Routine called by WPCSM to calculate B field.
  IMPLICIT REAL*8 (A-H,O-Z)
  EXTERNAL AJQUAD,AJGAUS,AJONE
  COMMON/CSOLFB/MOD,IEM
  IEM=0
  IE=0
  MOD=MODEL
  IF(MODEL-2)20,30,40
20  CALL SOLBAJ(AJONE,-0.5D0,0.5D0,IE)
    GO TO 50
30  CALL SOLBAJ(AJQUAD,-0.707106781D0,0.707106781D0,IE)
    GO TO 50
40  CALL SOLBAJ(AJGAUS,-1.D0,1.D0,IE)
50  IF(IE.NE.0)IEM=IE
RETURN
END
:READ SOLBA   FORTRAN  A1 TEMP   10/18/83 09:33:24
SUBROUTINE SOLBA
  IMPLICIT REAL*8 (A-H,O-Z)
  COMMON/CISOL/RS,SL,RF,ZF,BR,BZ,AP
C   K.H.CARPENTER 29SEP80  UMR DEPT. OF EE.
C   KHC:06JAN82: MODIFIED TO ALLOW NEGATIVE RF.
C   KHC:26FEB83: CHANGED TO GIVE CORRECT SIGN TO BR FOR RIGHT
C   HANDED COORDINATES
C****
C   Calculates the B-field and A-field components for an ideal
C   solenoid using the method of M.W.Garrett, JAP Vol.34 p2567 (1963).
C   This version is an adaption of the BIDSOL subroutine written by
C   Tommy Tucker of Oak Ridge Nat. Lab., Computer Sciences Div.
C   (BIDSOL converted to double precision, normalization changed, and
C   calculation of vector potential added.)
C****
C   Input values:
C   RS - RADIUS OF SOLENOID CURRENT SHEET
C   SL - LENGTH OF SOLENOID CURRENT SHEET
C   RF - FIELD POINT RADIAL DISTANCE FROM SOLENOID AXIS
C   (IF RF 0, ABSOLUTE VALUE USED AND RESULT FOR BR NEGATED.)
C   ZF - FIELD POINT AXIAL DISTANCE FROM CENTER OF SOLENOID
C   (Input values can be in any unit of length, but all four must
C   be in the same units.)
C   Output values:
C   BR - NORMALIZED RADIAL FIELD COMPONENT
C   BZ - NORMALIZED AXIAL FIELD COMPONENT
C   AP - NORMALIZED ANGULAR VECTOR POTENTIAL COMPONENT
C   To obtain dimensional values for components:
C   Multiply all components by surface current density and
C   multiply all components by permeability divided by 4 times pi.
C   In addition, multiply AP by the dimensional length of the
C   solenoid current sheet.
C****

```

```

DATA PI/3.14159 265389 793238 D0/
DATA TOL/1.D-12/, CUT/5.D-4/, CUTSQ/25.D-8/
ABRF=DABS(RF)
RSMRF=RS-ABRF
RSPRF=ABRF+RS
RSPFSQ=RSPRF**2
DZ1=ZF-0.5D0*SL
DZ2=DZ1+SL
DZ1SQ=DZ1*DZ1
R1SQ=RSPFSQ+DZ1SQ
R1=DSQRT(R1SQ)
DZ2SQ=DZ2*DZ2
R2SQ=RSPFSQ+DZ2SQ
R2=DSQRT(R2SQ)
IF(ABRF.GT.1.0D-6)GO TO 20
C ON AXIS THE CALCULATION SIMPLIFIES TO
BZ=2.D0*PI*(DZ2/R2-DZ1/R1)
BR=0.D0
AP=0.D0
RETURN
20 CONTINUE
RSRFT4=RS*ABRF*4.D0
PAR1=RSRFT4/R1SQ
CMOD1=DSQRT(1.D0-PAR1)
A1=1.D0
B1=CMOD1
CPRIME=RSMRF/RSPRF
CCHAR=CPRIME**2
IF(CCHAR.GE.CUTSQ)GO TO 30
C TO CALCULATE BZ AT OR NEAR THE RADIUS OF THE CURRENT SHEET,
C MODIFY CCHAR TO ALLOW THE ITERATION TO PROCEED WITHOUT
C ZERO DIVIDED OR OVERFLOW. THE BZ CALCULATION IS CORRECTED
C FOR THE SMALL ERROR INTRODUCED AT THE END OF THE ROUTINE.
CPRIMA=CUT
IF(RSMRF.LT.0.D0)CPRIMA=-CPRIMA
CCHAR=CUTSQ
30 CONTINUE
D1=CCHAR/CMOD1
CHAR=1.D0-CCHAR
E1=CHAR/CCHAR
F1=0.D0
S1=0.D0
PAR2=RSRFT4/R2SQ
CMOD2=DSQRT(1.D0-PAR2)
A2=1.D0
B2=CMOD2
D2=CCHAR/CMOD2
E2=E1
F2=0.D0
S2=0.D0
TWOP=1.D0
100 CONTINUE
TWOP=TWOP*2.D0
C=A1

```

```

A1=(A1+B1)*.5D0
B1=DSQRT(C*B1)
CSQ1=(C-A1)**2
S1=S1+CSQ1*TWOP
C=A2
A2=(A2+B2)*.5D0
B2=DSQRT(C*B2)
CSQ2=(C-A2)**2
S2=S2+CSQ2*TWOP
C=F1
F1=(E1+F1)*.5D0
DPONE=D1+1.D0
E1=(D1*E1+C)/DPONE
D1=B1*.25D0*DPONE*DPONE/(A1*D1)
C=F2
F2=(E2+F2)*.5D0
DPONE=D2+1.D0
E2=(D2*E2+C)/DPONE
D2=B2*.25D0*DPONE*DPONE/(A2*D2)
IF((CSQ1.GT.TOL).OR.(CSQ2.GT.TOL))GO TO 100
C ONE ADDITIONAL 'A' STEP WILL HALVE THE ERROR
A1=(A1+B1)*.5D0
A2=(A2+B2)*.5D0
C BR CAN NOW BE CALCULATED FROM ELLIPTIC INTEGRAL VALUES
C26F BR=.5D0*PI*(R2*S2/A2-R1*S1/A1)/RF
BR=-.5D0*PI*(R2*S2/A2-R1*S1/A1)/RF
C CONTINUE ITERATIONS TO IMPROVE ACCURACY OF 3RD COMPLETE ELL. INTEGRAL
200 CONTINUE
C=F1
F1=(E1+F1)*.5D0
DPONE=D1+1.D0
E1=(D1*E1+C)/DPONE
D1=.25D0*DPONE*DPONE/D1
C=F2
F2=(E2+F2)*.5D0
DPONE=D2+1.D0
E2=(D2*E2+C)/DPONE
D2=.25D0*DPONE*DPONE/D2
IF((D1*D2-1.D0).GT.TOL)GO TO 200
F1=(E1+F1)*.5D0
F2=(E2+F2)*.5D0
C BZ AND AP CAN NOW BE CALCULATED
BZ=PI*(DZ2*(RS+RS+RSMRF*F2)/(RSPRF*R2*A2)-
      DZ1*(RS+RS+RSMRF*F1)/(RSPRF*R1*A1))
IF((CCHAR.EQ.CUTSQ).AND.(CPRIME.NE.0.D0))BZ=BZ+PI*
  DABS(CPRIMA-CPRIME)/CPRIMA*(DZ2/(R2*CMOD2)-DZ1/(R1*CMOD1))
RSMRFS=RSMRF**2
AP=(DZ2*(R2*.5D0*(PAR2+S2)-RSMRFS*F2/R2)/A2 -
     DZ1*(R1*.5D0*(PAR1+S1)-RSMRFS*F1/R1)/A1)*.5D0*PI/(ABRF*SL)
RETURN
END
:READ SGAUS8 FORTRAN A1 TEMP 10/18/83 09:33:24
SUBROUTINE SGAUS8(XL,XU,NFOLD2,ANSW,FUN,NPT2)
CC MODIFIED 1MAY79 BY KHC TO HAVE MAX NPT2=8

```

```

CC
C      THIS IS A SINGLE PRECISION VERSION TO RUN ON THE 7600.
C.....
C PROGRAM AUTHOR E. B. HARRIS
C GASEOUS DIFFUSION DEVELOPMENT DIVISION, UNION CARBIDE CORP.,
C NUCLEAR DIV.,
C OAK RIDGE, TENN.
C
C XL=LOWER LIMIT OF INTEGRAL
C XU=UPPER LIMIT OF INTEGRAL
C NFOLD2=NUMBER OF EQUAL SUBINTERVALS THAT (XL,XU) IS TO BE
C SUBDIVIDED INTO
C ANSW=APPROXIMATE VALUE OF THE INTEGRAL AS EVALUATED BY THIS
C SUBROUTINE
C FUN=THE NAME OF THE SINGLE PRECISION FUNCTION SUBPROGRAM THAT
C DEFINES THE INTEGRAND FUNCTION. FUN HAS ONE SINGLE PRECISION
C VARIABLE, SAY X, AS AN ARGUMENT AND RETURNS THE VALUE OF THE
C INTEGRAND AT X (WHERE X IS THE VARIABLE OF INTEGRATION). THE
C NAME PASSED TO FUN MUST BE DECLARED EXTERNAL IN THE CALLING
C PROGRAM.
C NPT2=NUMBER OF POINTS (ORDER) AT WHICH THE INTEGRAND IS TO BE
C EVALUATED IN EACH SUBINTERVAL, I.E., TOTAL NUMBER OF
C EVALUATIONS = NPT2*NFOLD2. PERMISSABLE VALUES OF NPT2 ARE
C 2, 3, 4, 5, 6, 7, 8, 9, 10, 12, 16, 20, 24, 32, 40, 48, 64,
C 80, AND 96. IF NPT2 IS .LT. 2, 2 POINTS ARE USED. IF NPT2 IS
C .GT. 96, 96 POINTS ARE USED. WITHIN THE RANGE OF 2-96, IF NPT2
C IS NOT ONE OF THE PERMISSABLE VALUES, THE NEXT HIGHER
C PERMISSABLE VALUE IS USED.
C
C THE DATA STATEMENTS BEGINNING WITH AN2 AND ENDING WITH AN96D
C ARE THE ABSCISSAS AND WEIGHT FACTORS FOR THE GAUSSIAN INTEGRATION
C AND ARE TAKEN FROM THE HANDBOOK OF MATHEMATICAL FUNCTIONS EDITED
C BY MILTON ABRAMOWITZ AND IRENE A. STEGUN, APPLIED MATHEMATICS
C SERIES 55, U. S. DEPARTMENT OF COMMERCE, NATIONAL BUREAU OF
C STANDARDS, 1964, PAGES 916-919.
C.....
C LOGICAL EVEN,READY
C DIMENSION AN2(2),AN3(4),AN4(4),AN5(6),AN6(6),AN7(8),AN8(8)
C DIMENSION CONST(38),JSTART(7)
C EQUIVALENCE (CONST(1),AN2(1)),(CONST(3),AN3(1)), (CONST(7),AN4(1))
C & ,(CONST(11),AN5(1)),(CONST(17),AN6(1)), (CONST(23),AN7(1)),
C & (CONST(31),AN8(1))
C DATA JSTART/4,8,12,18,24,32,40/
C & ,READY/.FALSE./
C DATA AN2/ 0.577350269189626, 1.0000000000000000/
C DATA AN3/ 0.0000000000000000, 0.8888888888888889, 0.774596669241483,
C & 0.5555555555555556/
C DATA AN4/ 0.339981043584856, 0.652145154862546, 0.861136311594053,
C & 0.347854845137454/
C DATA AN5/ 0.0000000000000000, 0.5688888888888889, 0.538469310105683,
C & 0.478628670499366, 0.906179845938664, 0.236926885056189/
C DATA AN6/ 0.238619186083197, 0.467913934572691, 0.661209386466265,
C & 0.360761573048139, 0.932469514203152, 0.171324492379170/
C DATA AN7/ 0.0000000000000000, 0.417959183673469, 0.405845151377397,

```

```

& 0.381830050505119, 0.741531185599394, 0.279705391489277,
& 0.949107912342759, 0.129484966168870/
DATA AN8/ 0.183434642495650, 0.362683783378362, 0.525532409916329,
& 0.313706645877887, 0.796666477413627, 0.222381034453374,
& 0.960289856497536, 0.101228536290376/
C.....
C   ON FIRST TIME PROGRAM IS INVOKED, TAKE ONE-HALF OF THE CONSTANTS
C   IN ARRAY CONST.
C.....
      IF (READY) GO TO 20
      DO 10 I=1,38
          CONST(I)=0.5D+00*CONST(I)
10     CONTINUE
      READY=.TRUE.
20    NPT=IABS(NPT2)
      NFOLDS=IABS(NFOLD2)
C.....
C   DETERMINE THE PERMISSABLE NUMBER OF POINTS TO USE IN EACH
C   SUBINTERVAL AND THE STARTING POINT IN ARRAY CONST FOR THAT
C   NUMBER OF POINTS.
C.....
      IF (NPT.LT.2) NPT=2
      IF (NPT.GT.8) NPT=8

      JHOLD=JSTART(NPT-1)
      EVEN=.FALSE.
      IF (MOD(NPT,2).EQ.0) EVEN=.TRUE.
      H=(XU-XL)/DBLE(FLOAT(NFOLDS))
      A=XL-0.5D+00*H
      ANSW=0.D+00
      KSTOP=NPT/2
      DO 60 I=1,NFOLDS
          J=JHOLD
          A=A+H
          DO 50 K=1,KSTOP
              J=J-3
              C=CONST(J)*H
              J=J+1
              ANSW=ANSW+CONST(J)*(FUN(A+C)+FUN(A-C))
50     CONTINUE
          IF (EVEN) GO TO 60
          ANSW=ANSW+CONST(J-2)*FUN(A)
60    CONTINUE
      ANSW=ANSW*H
      RETURN
      END
:READ ZEROIN  FORTRAN  A1 TEMP  10/18/83 09:33:25
      REAL FUNCTION ZEROIN(AX,BX,F,TOL)
      REAL AX,BX,F,TOL
C
C   A ZERO OF THE FUNCTION F(X) IS COMPUTED IN THE INTERVAL AX,BX .
C
C INPUT..
C

```

```

C AX   LEFT ENDPOINT OF INITIAL INTERVAL
C BX   RIGHT ENDPOINT OF INITIAL INTERVAL
C F    FUNCTION SUBPROGRAM WHICH EVALUATES F(X) FOR ANY X IN
C      THE INTERVAL AX,BX
C TOL  DESIRED LENGTH OF THE INTERVAL OF UNCERTAINTY OF THE
C      FINAL RESULT ( .GE. 0.0)
C
C
C      OUTPUT..
C
C      ZEROIN ABCISSA APPROXIMATING A ZERO OF F IN THE INTERVAL AX,BX
C
C      IT IS ASSUMED THAT F(AX) AND F(BX) HAVE OPPOSITE SIGNS
C      WITHOUT A CHECK. ZEROIN RETURNS A ZERO X IN THE GIVEN INTERVAL
C      AX,BX TO WITHIN A TOLERANCE 4*MACHEPS*ABS(X) + TOL, WHERE MACHEPS
C      IS THE RELATIVE MACHINE PRECISION.
C      THIS FUNCTION SUBPROGRAM IS A SLIGHTLY MODIFIED TRANSLATION OF
C      THE ALGOL 60 PROCEDURE ZERO GIVEN IN RICHARD BRENT, ALGORITHMS FOR
C      MINIMIZATION WITHOUT DERIVATIVES, PRENTICE - HALL, INC. (1973).
C
C      REAL A,B,C,D,E,EPS,FA,FB,FC,TOL1,XM,P,Q,R,S
C
C      COMPUTE EPS, THE RELATIVE MACHINE PRECISION
C
C      EPS = 1.0
C      10 EPS = EPS/2.0
C      TOL1 = 1.0 + EPS
C      IF (TOL1 .GT. 1.0) GO TO 10
C
C      INITIALIZATION
C
C      A = AX
C      B = BX
C      FA = F(A)
C      FB = F(B)
C
C      BEGIN STEP
C
C      20 C = A
C      FC = FA
C      D = B - A
C      E = D
C      30 IF (ABS(FC) .GE. ABS(FB)) GO TO 40
C      A = B
C      B = C
C      C = A
C      FA = FB
C      FB = FC
C      FC = FA
C
C      CONVERGENCE TEST
C

```

```

40 TOL1 = 2.0*EPS*ABS(B) + 0.5*TOL
   XM = .5*(C - B)
   IF (ABS(XM) .LE. TOL1) GO TO 90
   IF (FB .EQ. 0.0) GO TO 90
C
C IS BISECTION NECESSARY
C
   IF (ABS(E) .LT. TOL1) GO TO 70
   IF (ABS(FA) .LE. ABS(FB)) GO TO 70
C
C IS QUADRATIC INTERPOLATION POSSIBLE
C
   IF (A .NE. C) GO TO 50
C
C LINEAR INTERPOLATION
C
   S = FB/FA
   P = 2.0*XM*S
   Q = 1.0 - S
   GO TO 60
C
C INVERSE QUADRATIC INTERPOLATION
C
50 Q = FA/FC
   R = FB/FC
   S = FB/FA
   P = S*(2.0*XM*Q*(Q - R) - (B - A)*(R - 1.0))
   Q = (Q - 1.0)*(R - 1.0)*(S - 1.0)
C
C ADJUST SIGNS
C
60 IF (P .GT. 0.0) Q = -Q
   P = ABS(P)
C
C IS INTERPOLATION ACCEPTABLE
C
   IF ((2.0*P) .GE. (3.0*XM*Q - ABS(TOL1*Q))) GO TO 70
   IF (P .GE. ABS(0.5*E*Q)) GO TO 70
   E = D
   D = P/Q
   GO TO 80
C
C BISECTION
C
70 D = XM
   E = D
C
C COMPLETE STEP
C
80 A = B
   FA = FB
   IF (ABS(D) .GT. TOL1) B = B + D
   IF (ABS(D) .LE. TOL1) B = B + SIGN(TOL1, XM)
   FB = F(B)

```

```
IF ((FB*(FC/ABS(FC))) .GT. 0.0) GO TO 20
GO TO 30
C
C DONE
C
90 ZEROIN = B
RETURN
END
:READ TWPCSM FORTRAN A1 TEMP 10/18/83 09:33:26
C TEST DRIVER PROGRAM FOR WPCSM. K.H.CARPENTER 02FEB83 - 07JUN83
COMMON/CWPCSM/BZF,AMC
NAMELIST/TWPCSM/WP,BTO,BRA,BPO,PHI,RHO,PSI,VMC,VMCL,VMCR,AMC,
1 AFOFC,AOFOL,AOFOR,IERF,IERB,IERN,
2 GA,AL,RT,RC,RCI,RSM,RSMI,BZF,DF,DFI,BF,RF,MODEL,IERR
10 WRITE(5,20)
20 FORMAT(' Enter AL,RT,RC,RSM,DF,BF,GA,RF,MODEL,PHI,RHO,PSI,VMC, '
1 , 'VMCL,VMCR,AFOFC,AOFOL,AOFOR: ')
READ(5,*,END=25)AL,RT,RCI,RSMI,DFI,BF,GA,RF,MODEL,PHI,RHO,PSI,
1 VMC,VMCL,VMCR,AFOFC,AOFOL,AOFOR
25 IF(AL.LT.0.)STOP
RSM=RSMI
RC=RCI
DF=DFI
CALL WPCSM(WP,BTO,BRA,BPO,PHI,RHO,PSI,VMC,VMCL,VMCR,GA,AL,
1 RT,RSM,RC,AFOFC,AOFOL,AOFOR,DF,BF,RF,MODEL,IERR,IERF,IERB,IERN)
WRITE(6,TWPCSM)
GO TO 10
END
```

## APPENDIX D

## CORRECTED PAGES FOR ORNL/Sub-7676/3

This appendix contains the revised pages for the previous fiscal year's subcontract report. The revision corrects for a sign error discovered in the SOLBA computer subroutine. (The corrected source code listing for SOLBA is included in Appendix C.) Page numbers on the upper right corner in the revised pages which follow are the numbers in the original report. The page numbers which apply to this report are given in the lower right for this Appendix only.

## ABSTRACT

Studies of the diamagnetism of the hot electron rings in Elmo Bumpy Torus have been carried out by experimental observation and numerical simulation. The ferromagnetic resonance (YIG) magnetometer instrumentation has been improved to include compensation for vacuum field generator current fluctuations, and a detailed reference manual has been written for this instrumentation. Observations of diamagnetic fields, by means of the YIG magnetometer, have been made at the large and small major radius locations just outside the vacuum vessel at the center of the horizontal midplane of an EBT cavity. Ratios of these diamagnetic fields are in good agreement to the values obtained using a current sheet model for the rings, and indicate a small net displacement of the centroid of the electrons' magnetic moments toward the larger major radius from the location anticipated on the basis of vacuum field particle drift surfaces. This effect has been noted over a wide range of EBT-S and EBT-I plasma conditions.

A preliminary numerical study of flux penetration dynamics has been made assuming a "bumpy cylinder" geometry for the EBT vacuum vessel. Estimates made by this study show that the diamagnetic signal from the rings should penetrate the vacuum vessel in a time on the order of 100 mS when the plasma is changed. This penetration time appears qualitatively reasonable.

RESEARCH SUPPORT FOR PLASMA DIAGNOSTICS ON ELMO BUMPY TORUS -  
OBSERVATIONS OF EBT RING GEOMETRY BY MEANS OF DIAMAGNETIC FIELD  
MEASUREMENTS USING A COMPENSATED FERROMAGNETIC RESONANCE MAGNETOMETER,  
AND A PRELIMINARY NUMERICAL STUDY OF EBT FLUX PENETRATION DYNAMICS

I. INTRODUCTION

Experimental characterization of geometry, stored energy, and dynamic behavior of the hot electron rings in EBT-I/S is important to understanding plasma confinement in EBT devices. We have been carrying out diamagnetic observations and calculations directed towards obtaining a better knowledge of the ring parameters. Our work in this area prior to October 1, 1981, has been reported previously.<sup>1</sup> Since that time we have improved the instrumentation for observing ring diamagnetic field intensity, and have used it to observe fields from a wide range of plasma conditions. The data obtained has been compared to a simple current sheet model for the rings, and the comparison shows that the centroids of the rings' magnetic moments are shifted toward the outer (large major radius) toroidal edge of the vacuum vessel by between 0.5 and 1 centimeter from the centers for particle drift orbits in the vacuum field. The improved instrumentation for observing diamagnetic fields is described in section III below, and the detailed operating instructions and circuit schematics for the equipment are included in an appendix. The observations of the EBT plasma are described in section IV, and the analysis of the experimental data using the current sheet model is given in section V.

The ring energy and geometry are steady state properties. One also wishes to observe the dynamics of the change in diamagnetic fields and flux, whether induced by external changes in controlled parameters such as heating power and gas feed, or by plasma instabilities. We have tested the ferromagnetic resonance magnetometer for possible use in observation of high frequency field fluctuations. This is described in section III. We have also carried out a preliminary numerical analysis for the dynamics of the flux penetration of the EBT vacuum vessel. The method and results are described in section II of this report, which follows below.

Of the six parameters of the current sheet model, the ring center offset couples most strongly to the field ratio. Thus we present the results of the calculations with the model as plots of field ratio versus ring center offset with the other model parameters varied to give a family of curves. These curves are given in Figures 9-12. In each figure one parameter is varied to give the family of curves while the others are held at nominal values. We note that the field ratios plotted include the contributions due to the rings in the nearest neighbor cavities. (Otherwise the field ratios would be unity for zero center offset.)

Fig. 9 shows the effect of varying the parameter of ring axial length for the current sheet model on the plot of field ratio versus ring offset from cavity center. The other ring parameters are set at nominal values: ring thickness is 3 cm, ring mean radius is 12.3 cm (corresponding to the distance from the ring center based on vacuum field drift surfaces to the heating resonance position in the vacuum field for 7250 A generator current and 14 Ghz sub-harmonic heating), and ring drift factor as calculated theoretically for the particle drifts in the vacuum field.<sup>18</sup> (This last parameter is not strictly constant but changes slightly with the others.) The remaining parameter of the current sheet model - mean surface current density - is merely a constant multiplier and so cancels in taking field ratios. The horizontal lines on the plots mark the experimental limits of 1.2 and 1.4 for the field ratio. Thus we see that ring center offset values from -1.9 to -0.9 cm are compatible with the experimental field ratios and ring lengths from 1 cm to 20 cm.

Observations using a 5 channel hard x-ray diagnostic indicate that mean ring axial length lies in the range 10 to 15 cm for typical plasma conditions.<sup>19</sup> Thus the reasonable range for center offset based on length variation is reduced from the range corresponding to a 1 to 20 cm variation in length. For calculations varying the other parameters, ring length was fixed at 10 cm.



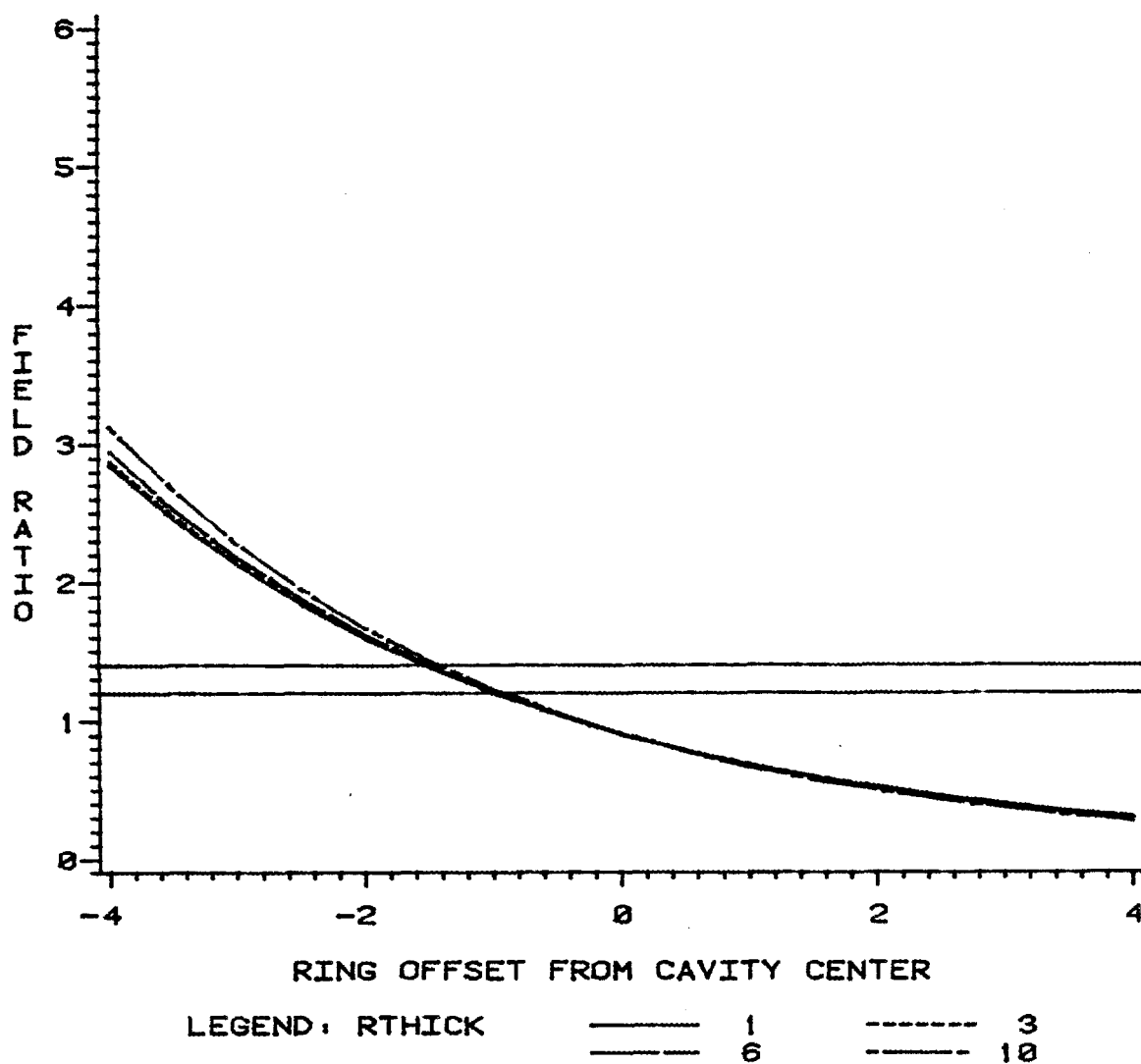


Fig. 10. Current sheet model result for ratio of field at small major radius to field at large major radius YIG probe location versus ring offset from geometrical center of EBT cavity. Ring model radial thickness is parameter varied. Horizontal lines indicated limits of experimentally observed field ratios.



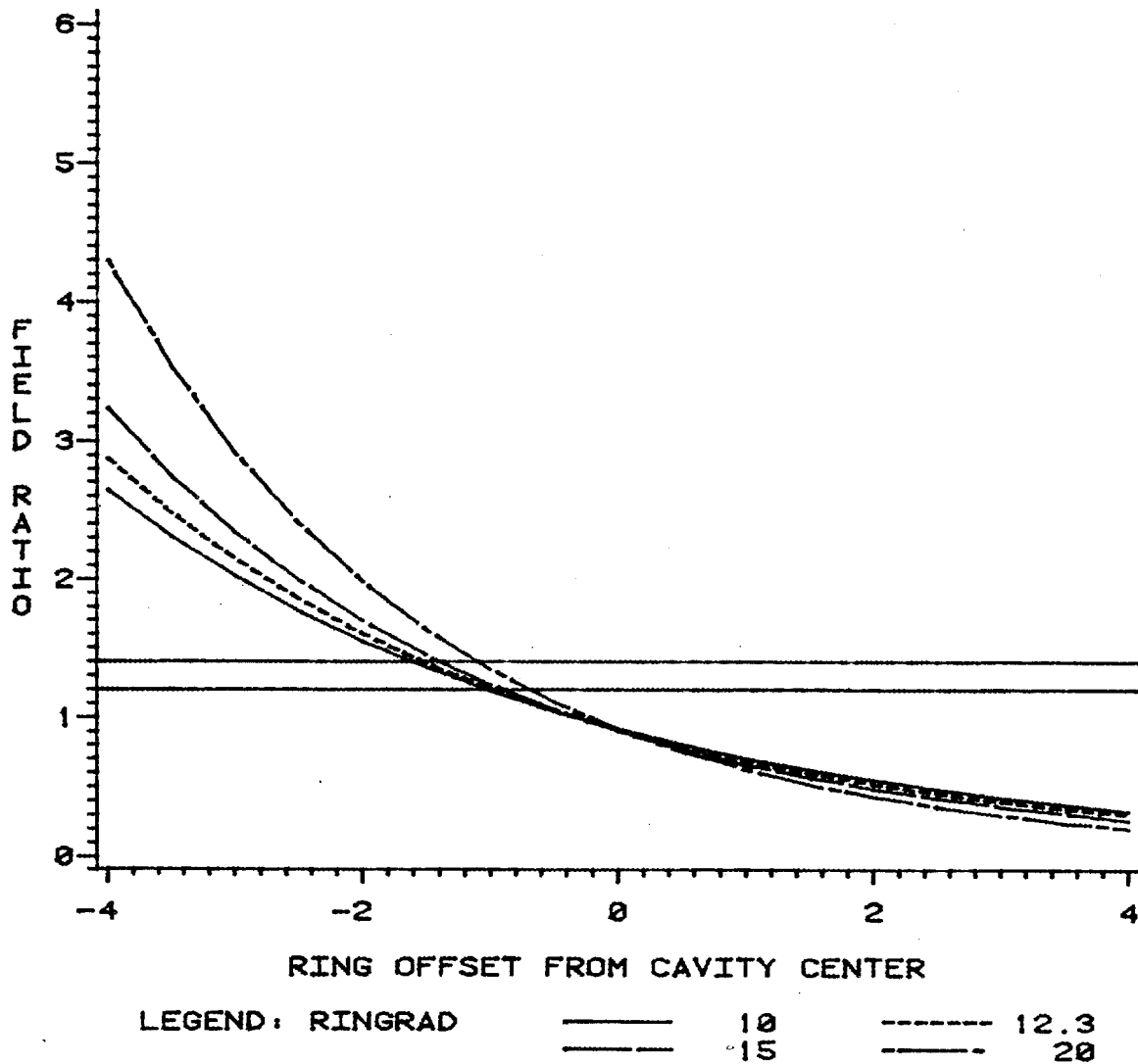


Fig. 12. Current sheet model result for ratio of field at small major radius to field at large major radius YIG probe location versus ring offset from geometrical center of EBT cavity. Ring model mean radius is parameter varied. Horizontal lines indicated limits of experimentally observed field ratios.

We note here that the particle drift surfaces in the vacuum field predict the ring center offset value to be around -2 cm. Thus the data with the current sheet model imply a small radial shift toward the larger major radius position.

Fig. 10 shows the effect of varying ring thickness in the model (with other parameters as for Fig. 9). Clearly, this parameter does not have a significant coupling to the field ratio values.

Fig. 11 shows the effect of changing the ratio of current density on the outer sheet to that on the inner sheet. (The range of values covers all that can be reasonably expected to occur.) This drift current effect has negligible influence on the field ratios calculated with the model (although strongly affecting absolute magnitudes for field).

Fig. 12 shows the effect on the field ratio of changing ring mean radius. Mean radius is the parameter that is most sensitive in terms of shift of predicted ring center offset. Even so, a mean radius value well below that corresponding to the distance between vacuum field heating resonance locations would be required to bring the center offset to the vacuum field value. We note that a high beta ring should have a smaller mean radius than a low beta one due to the heating resonance position moving toward the cavity center in the diamagnetism.

#### Discussion of diamagnetic data analysis

The current sheet model indicates an outward radial shift for the mean diamagnetic activity of the rings from the location predicted from vacuum field drift surfaces. However, the experimental uncertainties in the field ratios are large enough to preclude making any major conclusions based on this observation. We do note that the center shift could be negligibly small if the mean radius became a few centimeters smaller than in the vacuum field case. As this is the

correct tendency for a high beta situation, the experimental results appear to have a reasonable interpretation in terms of the current sheet model.

The current sheet model is, of course, not an accurate representation of the electrons' dipole moment distribution. Better models must be sought in self consistent field modifications, multiple rings, or other approaches, keeping in mind that many of the other possible models could be represented as superpositions of the simple current sheets used here. Any such superposition must retain the same general relationship of field ratio to mean model parameters as the ones we have presented here.

## APPENDIX E

ABSTRACT FROM MASTER'S THESIS  
-----THE DEVELOPMENT OF A FERROMAGNETIC  
RESONANCE MAGNETOMETER FOR OBSERVATION  
OF MINUTE HIGH FREQUENCY FLUCTUATIONS  
ON LARGE AVERAGE FIELDS

By

Robert Howard Booker

A THESIS

Presented to the Faculty of the Graduate School of the  
UNIVERSITY OF MISSOURI-ROLLAIn Partial Fulfillment of the Requirements for the Degree  
MASTER OF SCIENCE IN ELECTRICAL ENGINEERING  
1983

## ABSTRACT

A magnetometer was developed to measure small, high frequency fluctuations on large average fields. The principle of operation is envelope detection of the amplitude modulation induced into the output of a Yttrium Iron Garnet (YIG) tuned filter by field fluctuations. As tested with a YIG filter having a bandwidth of 6.4 MHz, the system will resolve field fluctuations from 0.003 to 0.6 Gauss upon an average field ranging from 200 to 1400 Gauss, provided the fluctuations are bandlimited from DC to 4 MHz. Theoretically, the maximum field fluctuations and frequency response are limited by and are directly proportional to the line width of the ferromagnetic resonance. The differential equations governing this behavior were developed and solved by both quasi-steady-state and numerical methods. These theoretical results have been experimentally verified.

## APPENDIX F

## ABSTRACTS OF PAPERS PRESENTED AT 1982 APS-DPP MEETING

The following abstracts appeared in Bulletin of the American Physical Society, Vol. 27, No. 8, Part II, October 1982, p. 1114.

8V4 The Toroidal Extent of the Hot Electron Rings in EBT-S.\*  
 D. L. Hillis, ORNL, and K. H. Carpenter, Univ. of Missouri-Rolla. --  
 Measurements of the hot electron ring geometry are central to understanding the ring power balance on EBT-S. The hot electron rings on EBT-S are produced via electron-cyclotron resonant heating (ECRH) using a 28-GHz CW gyrotron, at power levels up to 200 kW. The parameters of the hot electron rings are studied via hard x-ray measurement techniques and with YIG magnetometers. A single hot electron ring is viewed with an array of NaI detectors such that the axial distribution of ring temperature and density can be determined and thereby the axial length. Typical values are:  $T_e$  400 to 500 keV,  $n_e$  2 to  $5 \times 10^{11} \text{ cm}^{-3}$ , and annulus length 10 to 12 cm. Finally, by combining the experimental measurements and other diamagnetic measurements, estimates can be obtained for both the stored energy and the volume of a single hot electron ring on EBT-S.

\*Research sponsored by the Office of Fusion Energy, U. S. Department of Energy, under contract W-7405-eng-26 with the Union Carbide Corporation and subcontract 7676/X01 with the University of Missouri.

8V5 Diamagnetic Field and Flux Measurements on EBT and Correlations to Models of Ring Geometry,\* K. H. CARPENTER, R. H. BOOKER, University of Missouri - Rolla, D. L. HILLIS, and G. R. HASTE, ORNL. -- In order to gain information on the geometry of the electron rings in EBT-I/S, the intensity of diamagnetic field strength due to the rings was observed using a YIG incremental magnetometer, and the total diamagnetic flux due to the rings was measured with pickup loops. Field intensity was measured at the outer wall of the vacuum vessel in the horizontal midplane at both the small and large major radius locations. Ratios of these fields, when compared to those from a simple current sheet model, indicate that the rings' centers move out in the major radius under high beta conditions. Comparison of field and flux measurements interrelates ring thickness, radius, and toroidal length. A more detailed ring model allows correlation of the diamagnetic observations with observations from a 5-channel hard x-ray diagnostic.

\*Research sponsored by the Office of Fusion Energy, U. S. Department of Energy under contract with the Union Carbide Corporation and subcontract 7676/X01 with the University of Missouri.

<sup>1</sup>Kenneth H. Carpenter and Marcus K. daSilva, Rev. Sci. Instrum. 53, 1414, (1982).